Photochemical degradation of dissolved organic matter in arctic surface waters

by

Collin Patrick Ward

A dissertation submitted in partial fulfillment
of the requirements for the degree of
Doctor of Philosophy
(Earth and Environmental Sciences)
in the University of Michigan
2015

Doctoral Committee:

Assistant Professor Rose M. Cory, Chair
Professor Joel D. Blum
Associate Professor Gregory J. Dick
Professor George W. Kling
Emeritus Professor Philip A. Meyers

Dedication

To Kiffy, Uncle Pat, and Lebold - thanks for the good times

Acknowledgements

It is practically impossible to acknowledge all the folks and organizations that deserve credit for helping me complete this dissertation, but here it goes. First, thanks to my advisor Rose for the endless patience, insight, and enthusiasm over the years. Despite that the music and food scene does not compare to north cackalacky, moving with your lab to Ann Arbor was one of the best decisions I've made over the past five years. It's been an honor to help establish the aquatic geochemistry lab at UM, and I am excited for the future of your lab. My committees at UNC and UM were very different, each with its strengths that helped me a great deal. At UNC, Drs. Surratt, Weinberg, and Whalen challenged me to focus on the details that comprise a robust experimental design. At UM, Drs. Blum, Dick, and Meyers pushed me to think about my research more broadly, which has changed the way I think about Earth's processes and history. George served on both committees, and consistently went above and beyond the expectations as a committee member. Thank you for teaching me how to stay organized and be critical of my work. Byron didn't serve on either committee, but provided lots of input over the years. He also has an unparalleled passion for baseball, which I admire.

Thanks to all the current and former students and technicians in the Cory, Kling, and Crump Labs. Namely, Harrold and Jason have been there since the beginning and I'm deeply thankful for their friendship and support over the years. Thanks to Rachel Sleighter at ODU for teaching me high resolution mass spectrometry and patiently answering my questions. The same can be said about Sarah Burton at EMSL, who taught me how to acquire and analyze NMR

spectra. The logistical support at Toolik was extremely helpful throughout my three field seasons. Thanks to Anne Hudon for helping me transfer to UM and being an excellent resource.

Thanks to the friends I've made over the past five years and my apologies to the old friends that I've lost touch with. I was very fortunate to be surrounded by a great group of folks in NC. Thanks to everyone at the cradle, the underground, and everlaughter. I'm really happy for you Tracey Jones. Thanks to Will, Tommy, and DC for the bike rides and epic racquetball matches. Thanks to Amanda and Carlos, and Katie and Mike for living in Durham so we could come visit and explore together. Thanks to all my classmates at UNC and UM for talking through all the small, inevitable roadblocks. My soccer teams in NC and MI provided a much needed stress relief after work. Thanks to Yo and Ryan in Columbus for being good friends and mentors.

Many thanks to my parents for their encouragement and support, even though the route I have taken is unfamiliar and probably very confusing for them. Thanks to my brothers for providing different perspectives on life - it's important to hear multiple voices. Thanks to my extended family for being so incredibly supportive and loyal. The same can be said about Katie's family, who has consistently demonstrated their support since the day we met. Finally, thanks to Katie for joining me on this adventure. We've experienced every emotion possible, including many that we didn't want to, but it's fair to say that we've learned a lot about each other and how we think the world works (or should work). I look forward to continuing this adventure with you, and thanks for encouraging me to adopt lenny - he's pretty cool.

Table of Contents

List of Figures

Figure

List of Tables

Table

List of Appendices

Appendix

Abstract

A critical component in the global carbon cycle is the fate of dissolved organic matter (DOM) drained from soil into inland waters. However, we currently lack the information needed to predict the conversion of DOM to carbon dioxide (CO_2) versus partially oxidized or degraded compounds that are exported to the ocean. In arctic freshwaters, complete and partial photo-oxidation dominate DOM processing in the water column. However, the relative importance of these sunlight-driven pathways is likely governed by the chemical composition of DOM, which is expected to change with increasing ecological disturbances in the Arctic (e.g., tundra fires and permafrost thaw). Here, the molecular level controls on the photo-degradation of DOM in arctic freshwaters were investigated. The dominant sink of dissolved black carbon, a byproduct of tundra fires incorporated into the DOM pool, was partial photo-oxidation to compounds that are likely exported to the ocean. DOM draining the shallow organic mat of arctic soils contained higher molecular weight, more oxidized, and more unsaturated aromatic species compared to DOM draining the deeper permafrost layer. Despite differences in chemical composition (i.e., degree of saturation and oxidation), organic mat and permafrost DOM exhibited similar susceptibilities to complete photo-oxidation. Photo-decarboxylation of tannin-like compounds was likely an important mineralization pathway of organic mat and permafrost DOM, suggesting that these compounds may control the photo-mineralization of DOM in arctic surface waters. Permafrost DOM was significantly more susceptible to partial photo-oxidation compared to DOM leached from the organic mat, potentially due to the depletion of phenolic moieties with antioxidant properties in permafrost DOM that may quench the oxidation of DOM by sunlight.

Thus, increased permafrost thaw and increased inputs of permafrost DOM to arctic surface waters may increase the rates of photochemical DOM processing of DOM and shift the dominant DOM degradation pathway from complete to partial photo-oxidation. Measurements of apparent quantum yield spectra for the photo-mineralization of a wide range of DOM sources indicated that yields were largely controlled by the initial DOM composition. This dissertation has demonstrated that the chemical composition of DOM strongly controls its susceptibility to photochemical degradation in arctic surface waters.

Chapter 1

Introduction

1.1 The role of dissolved organic matter in the global C cycle.

Carbon dioxide (CO_2) emissions from inland surface waters to the atmosphere are as large as the net carbon (C) transfer from the atmosphere to Earth's surface (~ 2 Pg C y^{-1}).[1–4] In northern latitudes, C fluxes from freshwaters may account for up to 40% of the net land surface C exchange with the atmosphere.[5] These large fluxes of CO_2 to the atmosphere are supported mainly by the movement of dissolved organic matter (DOM) from land and its subsequent complete oxidation to CO_2 in freshwaters.[1,4,6,7] Globally, the current estimate is that about 50% of organic C that is transferred from land to surface waters is mineralized to CO_2, while the remaining DOM is exported through rivers to the oceans unprocessed or as partially degraded forms.[4] Thus a critical component of the global C cycle is the fate of DOM drained from soils into inland waters, yet we currently don't understand the molecular level controls on DOM degradation, which is needed to predict the conversion of DOM to CO_2 vs. partially oxidized or degraded compounds that remain in the DOM pool (DOM_{OX}) and are exported to the ocean (Fig. 1.1).

The fate of DOM, as either conversion to CO_2 or partially oxidized or degraded compounds (Fig. 1.1), is usually attributed to bacterial respiration. However, a recent study showed that photochemical oxidation of DOM to CO_2 was greater than or equal to bacterial respiration in the water column of streams, rivers, and lakes of the Arctic.[7] Furthermore, we

found that photochemical processing of DOM to CO_2 and partially-oxidized DOM exported to the ocean accounts for 70-95% of total DOM processed in the water column of arctic lakes and rivers.[7]

These recent advances in our understanding of photochemistry in C cycling are especially relevant to understanding the rapid changes in arctic ecosystems in the face of climate change (*discussed below*). The ongoing thawing of permafrost soils, which contain approximately twice the amount of carbon as the atmosphere,[8,9] is the only change on Earth that allows tremendous stores of organic carbon to be converted into CO_2 on relatively short time scales, thus providing an accelerating feedback to global warming.[10,11] However, we can't predict the amount of permafrost DOM that will be oxidized completely to CO_2 versus partially oxidized and exported to oceans because predictions based on bulk or average properties of DOM incompletely describe the susceptibility of DOM to complete or partial oxidation by bacterial or sunlight. Our inability to make these predictions is due in large part to the molecular complexity and diversity of organic molecules within the DOM pool.

1.2 Characterizing the chemical composition of DOM

DOM is operationally defined as the naturally occurring, organic molecules in waters that pass through a ~ 0.45 μm filter.[12] DOM is formed through the breakdown or decay of parent biomolecules, such as lignin, carbohydrates, or tannins, to yield soluble compounds that comprise the DOM pool.[12] These weathered products of once-living organic matter are broadly characterized based on functional group distributions or the number of rings and double bonds. However, the structural arrangement of most compounds within the DOM pool is unknown, which in turn limits our capacity to relate the molecular composition of DOM to its susceptibility

to degradation.[12] In other words, the elemental composition of molecules within the DOM pool can be measured, i.e., the amounts of C, H, O, and N in each molecule, but it is not possible to determine how these atoms are arranged.[12] One of the best emerging tools to characterize the chemical composition of DOM is ultra-high resolution Fourier transform-ion cyclotron resonance mass spectrometry (FT-ICR MS).[13,14] Typical FT-ICR mass spectra of freshwater DOM contain ~10,000 individual ions, each corresponding to a unique molecular formula within the DOM pool.

The distribution of molecules within the DOM pool detected by FT-ICR is commonly organized, classified, and visualized using van Krevelen diagrams (Fig. 1.2).[15] For example, the van Krevelen diagram in Fig. 1.2 shows a typical distribution of the thousands of compounds detected within DOM from freshwaters, each plotted according to their H/C and O/C ratios. Many DOM compounds overlap in H/C and O/C with classes of precursor biomolecules (e.g., lignin), as identified by the colored circles on Fig. 1.2.[13] These DOM compounds that overlap with the bounds of H/C and O/C ratios defined by the precursor biomolecules share chemical properties such as number of double bonds or ring structures, degree of saturation, and oxidization state. Overlap in chemical properties between molecules within the DOM pool and precursor biomolecules shape the expectations for the susceptibility of DOM to degradation. However, basing our expectations of susceptibility to degradation on comparisons to precursor biomolecules has failed to predict DOM conversion to CO_2 by bacteria or sunlight in natural waters.[16–19] Thus, we must revise our approach by classifying compounds as more or less susceptible to degradation based on concurrent measurements of changes to the chemical composition of DOM during degradation and measurements of the susceptibility of DOM to degradation. This is the approach I've taken in my thesis research, which is outlined below

starting with the current understanding of the controls on the photochemical degradation of DOM.

1.3 Controls on the photochemical degradation of DOM

Sunlight exposure stimulates the light-absorbing, aromatic fraction of DOM, and promotes photo-degradation of the wider DOM pool through a range of photochemical reactions.[20] When exposed to light, DOM may be photo-mineralized to CO_2 or CO,[21,22] broken down to lower molecular weight compounds,[23] or incompletely oxidized to stable, recalcitrant material (Fig. 1.1);[24] evidence to date suggests that the amount of these products depends on the direct and indirect photochemical mechanisms at work, which remain poorly understood. Direct photochemical degradation of DOM occurs as light energy translates into the breaking of bonds, while indirect photo-degradation occurs when photo-excited chromophoric DOM interacts with other aqueous constituents such as dissolved oxygen or water to produce reactive transients such as reactive oxygen species and organic radicals, which in turn break down both chromophoric DOM as well as the uncolored pool of DOM not accessible to direct photochemical degradation.[25]

Although the underlying mechanisms of DOM photo-degradation remain poorly characterized, photo-degradation is generally an oxidative process whereby direct or indirect reactions oxidize relatively reduced C (in organic form as DOM) to its highest oxidation state (+IV) as CO_2. Viewed on a van Krevelen diagram (red arrow; Fig, 1.2), photo-degradation is expected to progressively oxidize condensed, unsaturated, aromatic compounds to compounds that contain more oxygen (higher O/C) and are more saturated (higher H/C), producing CO_2. Thus, aromatic carbon is recognized as an important control on DOM photo-degradation in

surface waters.[18] This is because aromatic C is needed to initiate photochemical reactions (there can be no photochemical processes without the absorption of light), and because observations consistently report that aromatic C content decreases following the exposure of DOM to sunlight.[18] However, no study has determined the relative importance of CO_2 vs. other photochemical breakdown products (i.e., oxidized DOM), from the degradation of aromatic C over time scales relevant for DOM degradation in freshwaters (i.e., days to weeks). Instead, it is commonly assumed that all photochemical degradation of aromatic C results in CO_2. For instance, aromatic C content has been strongly, positively correlated to the loss of DOC by sunlight in arctic surface waters, which has been interpreted as evidence for the conversion of aromatic C to CO_2 by sunlight.[27] In addition, many studies relating DOM mineralization by sunlight to aromatic C content have not corrected for differences in the amount or rate of light absorption by DOM.[19,27–30] That is, as aromatic C content increases, so does the rate of light absorption, and the more light absorbed, the more photochemical reactions may take place. Thus, in studies where the measured photo-degradation of DOM was not normalized to the light absorbed by DOM, any conclusion about the susceptibility of DOM to photo-degradation may have been confounded by differences in the amount of light absorbed to initiate photochemical reactions, and may not provide a clear comparison of relative susceptibilities to photo-degradation between multiple DOM sources.[31] In contrast, the few studies that have normalized the measured photo-mineralization of DOM to the amount of light absorbed by DOM have reported no relationship between aromatic C content and the susceptibility of DOM to photo-mineralization,[32,33] suggesting a wide range in the susceptibility of aromatic C to photo-degradation, including the possibility that aromatic C is broken down to other compounds and may not be oxidized completely to CO_2.

It is misleading or at best too simplistic to assume that the susceptibility of DOM to photochemical reactions is governed by the amount of aromatic C present because there are likely many secondary (indirect) photochemical reactions that contribute to DOM photo-degradation, such as those initiated by reactive oxygen species.[25] For example, a recent study proposed that phenolics, a subset of hydroxylated aromatic compounds within the DOM pool, may play an important role in "quenching" the photo-degradation of DOM.[34] Specifically, it was proposed that phenolics act as "antioxidants," quenching the reactive radicals or oxidants produced by photochemical reactions of DOM (e.g., hydroxyl radical or singlet oxygen). Because these reactive radicals and oxidants have been implicated in the partial photochemical oxidation of DOM,[24,26] the antioxidant function of phenolics may protect DOM from oxidation, potentially slowing or preventing the partial oxidation of DOM by sunlight. Phenolics can be abundant within the aromatic fraction of DOM,[35] and are derived from the breakdown of lignin and tannin-like compounds. Thus, while aromatic C is likely broken down in the process of light-absorption, the phenolic subset of aromatic C may slow or prevent the partial photo-oxidation of DOM.

There are additional, indirect lines of evidence that the composition, and not only the content, of aromatic C influence the products of DOM photo-degradation. For example, photo-decarboxylation of DOM, or the photochemical breakdown of organic acids to CO_2, has been proposed as an important pathway for the photo-mineralization of DOM.[29,36–38] This suggests that the composition and reactivity of carboxyl C may control the susceptibility of DOM to photo-mineralization. While several studies have demonstrated that model compounds can undergo photo-decarboxylation to produce CO_2 in controlled laboratory experiments,[39,40] evidence for photo-decarboxylation of the thousands of compounds within the DOM pool is

limited, likely owing to the difficulty of quantifying carboxyl content in complex, heterogeneous mixtures.[36,38] For example, one study estimated the contribution of photo-decarboxylation reaction to the photo-mineralization of DOM using titrations to quantify loss of carboxyl content during photo-degradation of DOM.[38] However, in addition to loss of carboxyl groups during photo-degradation, there is likely some production of carboxyl C (via oxidative reactions), and breakdown or changes in the structural arrangements of organic acids that shift the pK_a values, which make it difficult to quantify the amount of carboxyl C using titrations, and thus the contribution of carboxyl C to CO_2 production. In addition, early work on DOM photo-degradation attempted to convert all carboxyl groups to esters, thereby eliminating the pathway for the photochemical conversion of organic acids to CO_2.[36] While a decrease in photochemical O_2 consumption was observed, CO_2 production was not measured and no analysis was conducted to confirm that carboxyl groups were quantitatively converted to esters. Thus, despite minimal indirect evidence for the photo-decarboxylation of DOM, there is no direct evidence and thus no consensus on the potential breakdown of aromatic acids (such as tannic acids) as a source of CO_2 as DOM is degraded by sunlight in natural waters.

Finally, it has been widely reported that sunlight breaks down high molecular weight, aromatic compounds within the DOM pool into lower molecular weight compounds.[41,42] However, in one study no relationship was observed between the molecular weight of DOM and the susceptibility of DOM to photo-mineralization along a river to ocean continuum.[32] Given that most high molecular weight DOM is aromatic, again these results are consistent with aromatic C having a wide range of susceptibilities to degradation by sunlight.

In summary, no study has determined the specific mechanisms by which DOM is degraded by sunlight into CO_2 or to partially oxidized DOM (DOM_{ox}; Fig. 1.1). Identifying how

the composition of DOM may control the relative importance of these two major classes of photo-products is important because of the different and likely contrasting roles these products play in the C cycle. Photochemical oxidation of DOM to CO_2 is likely a significant source of CO_2 evasion from inland waters.[4,7] In contrast, while some fraction of partially-oxidized DOM likely supports bacterial respiration to CO_2,[4,7,23] the majority of partially oxidized DOM may be compounds that are relatively more recalcitrant to further breakdown to CO_2 by bacteria or sunlight.[7,16,43] Thus, the goal of my thesis was to develop relationships between the chemical composition of DOM, its susceptibility to degradation by sunlight, and the class of products produced (CO_2 vs. DOMox; Fig. 1.1). My approach to achieve this goal was to analyze the chemical composition of DOM using standard and state of the art techniques before and after sunlight exposure, while concurrently quantifying the susceptibility of DOM to complete and partial photo-oxidation. Specifically, my objectives were to test the following hypotheses:

1. *The aromatic fraction of DOM is degraded to CO_2 and to partially oxidized compounds that remain in the DOM pool.*

2. *Carboxylic acids, including aromatic acids, are preferentially mineralized by sunlight to CO_2.*

3. Phenolic C slows the partial oxidation of DOM by sunlight.

To test the above hypotheses on the role of chemical composition on the susceptibility of DOM to complete and partial photo-oxidation, I carried out experiments in the Alaskan Arctic using natural gradients in the composition of DOM (i.e., gradients in aromatic, carboxyl, and phenolic C content). These gradients in DOM composition in surface waters were generated by current or expected disturbances to the land surface (discussed below).

1.4 How will a changing Arctic alter DOM composition and degradation?

Climate warming in the Arctic is increasing the prevalence of ecological disturbances that could change the composition and reactivity of DOM transferred from land to surface waters. Surface air temperatures in the Arctic are increasing twice as fast as global mean temperatures, and from 2005 - 2011 temperatures in this region were the warmest since records began in 1880.[44] This warming is increasing the frequency and intensity of ecological disturbances,[45] which in turn could substantially change the chemical composition of DOM and its susceptibility to degradation in arctic surface waters. For example, fire regime models predict that by the end of the 21st century, 62% of mid- to high-latitude regions will experience increases in wildfire activity.[46] Wildfires produce black carbon (BC), a molecularly diverse organic residue comprised of light-absorbing condensed aromatic ring structures that are formed at high temperatures (Fig. 1). In addition to a changing fire regime, permafrost soils are warming and the depth of the annually thawed, active soil layer is increasing in response to warmer surface air temperatures.[47–49] DOM leached from deeper permafrost layers of arctic soils is enriched in lower molecular weight, less aromatic, less oxidized species compared to DOM leached from the shallower organic mat (Fig. 1.1). Given that transfers of C from soils to surface waters are strong in the Arctic,[6] the easily mobilized or dissolved fraction of wildfire and permafrost-derived organic carbon pools are likely to be flushed from land to surface waters, where their susceptibility to oxidation is poorly characterized. This dissertation tested how ecological disturbances in the Alaskan Arctic, such as increasing fires and permafrost thaw, will change the chemistry of DOM flushed to surface waters, and how these changes to chemical composition may control the susceptibility of DOM to oxidation by sunlight.

While this dissertation is focused on changes to C cycling in arctic surface waters, the findings presented herein have significant implications for the global C cycle. First, temperate zones are also experiencing significant increases in wildfire activity,[50–52] thereby providing new sources of black carbon to temperate watersheds. Given that black carbon is a major component of global riverine DOM export,[53] the processes that govern the oxidation of black carbon likely apply across all surface waters.

Second, northern circumpolar permafrost soils store ~1700 Pg of organic C,[8,9] roughly twice the 800 Pg-C stored in the atmosphere today. As permafrost soils continue to thaw, the organic C they store is being oxidized to greenhouse gases such as CO_2.[10,11,54] In fact, the thawing and oxidation of permafrost soil organic C is considered one of the most likely positive climate feedbacks from terrestrial ecosystems to the atmosphere in the next few decades.[55–57] Thus, determining the susceptibility of newly thawed permafrost C to oxidation will help predict the magnitude of this arctic feedback to the global carbon cycle.

Third, two recent high-profile papers call for a better understanding of (i) how global inland waters process C released from soils, and (ii) what determines whether C ends up in the atmosphere as CO_2 or the oceans as DOM.[4,58] This dissertation directly addressed these knowledge gaps by determining relationships between the chemical composition of DOM and its susceptibility to oxidation in surface waters.

For example, in chapter 2[1], I quantified the complete and partial photo-oxidation of particulate and dissolved black carbon. Concurrently, I quantified shifts in the chemical composition of dissolved black carbon following exposure to sunlight. My findings indicated that dissolved black carbon was more susceptible to photo-oxidation than particulate black carbon, and partial photo-oxidation was a more important degradation pathway of dissolved

[1] C. P. Ward, R. L. Sleighter, P. G. Hatcher, and R. M. Cory, *Environ. Sci. Process. Impacts*, 2014, 721–731.

black carbon than was complete photo-oxidation. Prior to this study, it was assumed that sunlight degraded dissolved black carbon to produce mainly CO_2. However, I found that complete photo-oxidation to CO_2 was the minor dominant degradation pathway. Thus, future work is needed in order to refine the geochemical interpretation of sunlight as a sink for black carbon in natural waters, including characterizing the composition and reactivity of partially photo-oxidized dissolved black carbon.

In chapter 3[2], I characterized the chemical composition of DOM sources leached from different depths in permafrost soils. While the focus of my dissertation is on the photochemical degradation of DOM, I measured rates of bacterial degradation of permafrost DOM in the dark because some have reported that permafrost DOM is very rapidly degraded by bacteria,[59] while other studies have reported no significant differences in rates of permafrost DOM degradation by bacteria (compared to DOM draining the active layer in watersheds with permafrost soils).[60] If permafrost DOM is rapidly degraded by bacteria, then photo-degradation may be relatively less important as thawing soils export more permafrost DOM to surface waters. I found that bacterial production rates and bacterial efficiencies were significantly higher for permafrost compared to organic mat DOM; however, respiration rates were similar between DOM sources. Thus, increased release of permafrost DOM from arctic soils to surface waters may not increase the carbon dioxide produced by bacterial respiration, and photochemical processes will continue to be important for the fate of DOM in arctic surface waters.

The chemical characterization conducted in chapter 3 demonstrated that DOM leached from the shallower organic mat was chemically distinct compared to DOM leached from the deeper permafrost layer. DOM draining the shallow organic mat of arctic soils contained higher molecular weight, more oxidized, and more unsaturated aromatic species compared to DOM

[2] C. P. Ward and R. M. Cory, *Geochim. Cosmochim. Acta*, 2015, In Review.

draining the deeper permafrost layer, suggesting that increased permafrost thaw will change the composition and reactivity of DOM flushed to arctic surface waters compared to DOM currently draining the shallow active layer.

In chapter 4, I tested hypotheses and developed relationships between the chemical composition of DOM leached from the shallower organic mat and deeper permafrost horizon and its susceptibility to complete and partial photo-oxidation. Organic mat and permafrost DOM exhibited similar susceptibilities to complete photo-oxidation. The production of lower molecular weight, less oxidized formulas detected alongside the loss of carboxyl C and the production of CO_2 strongly suggested that photo-decarboxylation is an important pathway for the photo-mineralization of organic mat and permafrost DOM. Permafrost DOM exhibited a higher susceptibility to partial photo-oxidation compared to organic mat DOM, potentially owing to a decreased abundance of phenolic moieties that quench the oxidation of DOM by reactive oxygen species. Increased permafrost thaw may increase photochemical DOM processing rates in surface waters that drain permafrost soils and shift the dominant DOM processing pathway from complete to partial photo-oxidation, thereby increasing the production of compounds with unknown susceptibilities to further oxidation by sunlight or bacteria. In turn, photochemical oxidation processes could become more important in shaping the composition and reactivity of DOM exported downstream to the Arctic Ocean.

In chapter 5,[3] I present results from an inter-lab comparison study of apparent quantum yield spectra for the photo-mineralization of DOM. Here, I validated the method used to quantify the apparent quantum yield spectrum for the photo-mineralization of a wide range of DOM

[3] The comparison study is being coordinated by Birgit Koehler at Uppsala University. Other contributors to this study include: Bill Miller and Leanne Powers (University of Georgia), Anssi Vähätalo (University of Helsinki), Lars Tranvik and Karolina Einarsdottir (Uppsala University), Leena Siitonen and Koistinen Mervi (University of Jyväskylä), and Rose Cory (University of Michigan).

sources from inland waters. This is important because all photochemical reactions are wavelength dependent and understanding this dependence is critical for quantifying rates of photochemical degradation of DOM in the water column. All DOM sources exhibited decreasing yields with increasing wavelength, consistent with the few other measurements of this spectra.[61,62] Differences in yields between modelled spectra (i.e., linear vs. exponential) were significantly less than differences in yields between DOM sources, indicating that yields varied in large part due to the initial chemical composition of the DOM. Finally, my results supported the hypothesis that the chemical composition of DOM, including the chemical composition of aromatic C content, plays a substantial role in the susceptibility of DOM to photo-degradation in sunlit surface waters.

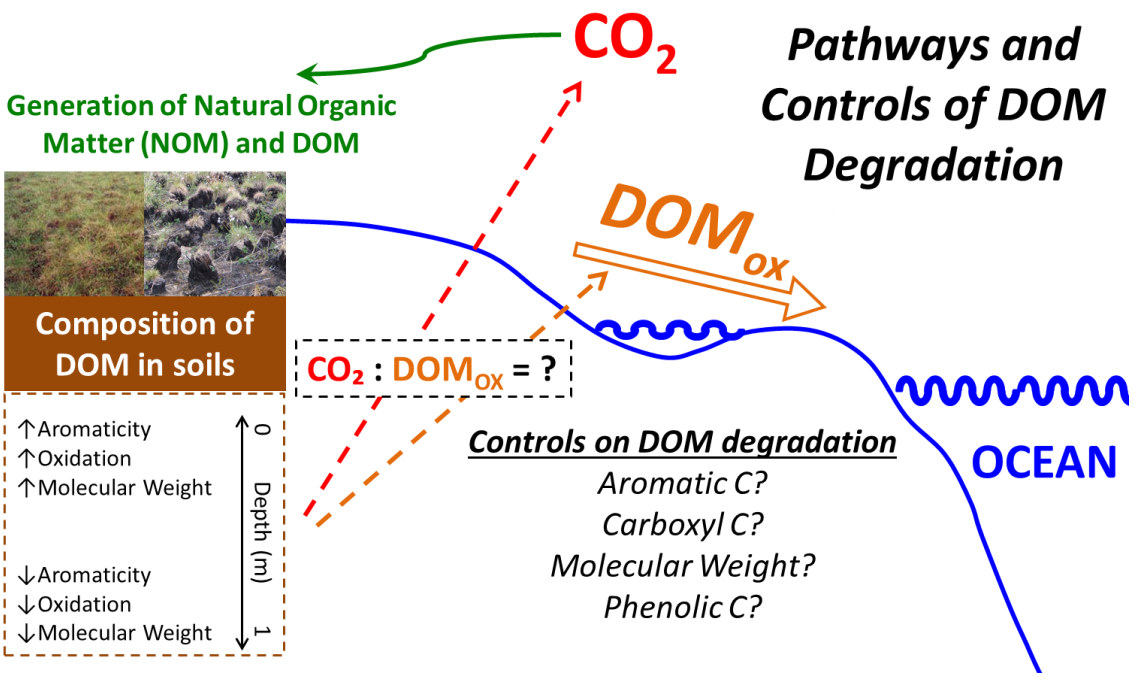

Figure 1.1 Conceptual model for the controls on the composition and degradation of DOM in sunlit surface waters.

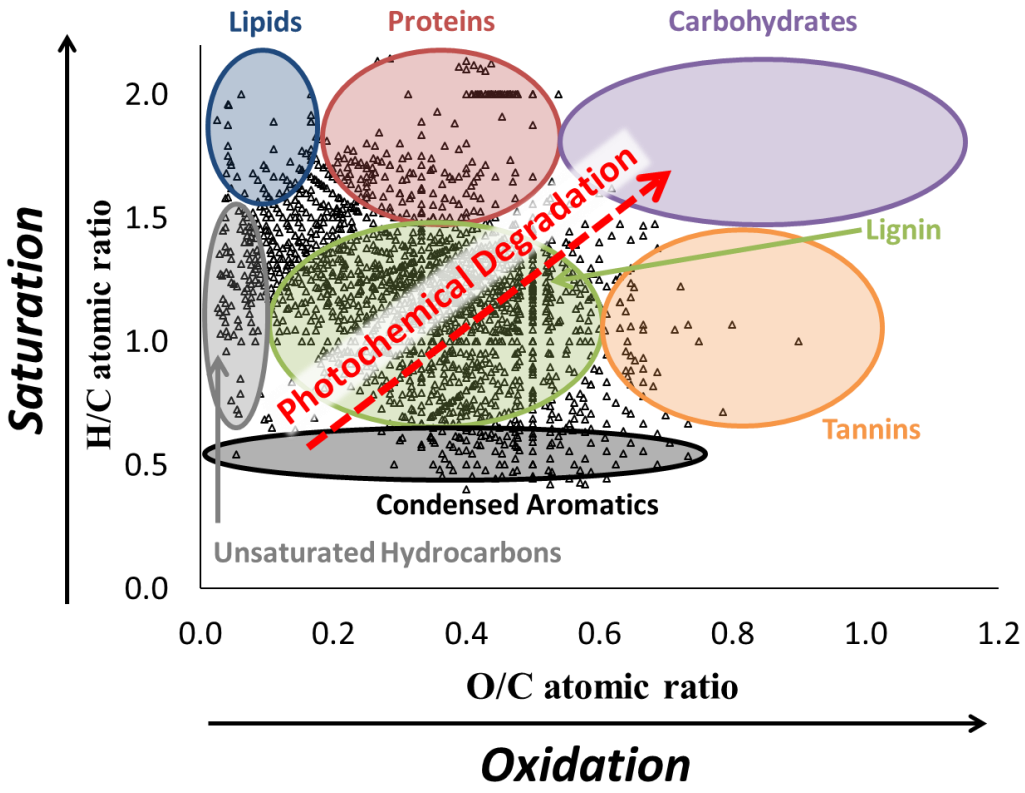

Figure 1.2 van Krevelen diagram showing compound classes defined by the atomic ratios of major biomolecules (colored circles). Oxidation increases along the x-axis, while saturation increases along the y-axis. The current understanding is that photochemical degradation produces less saturated, more oxidized compounds.

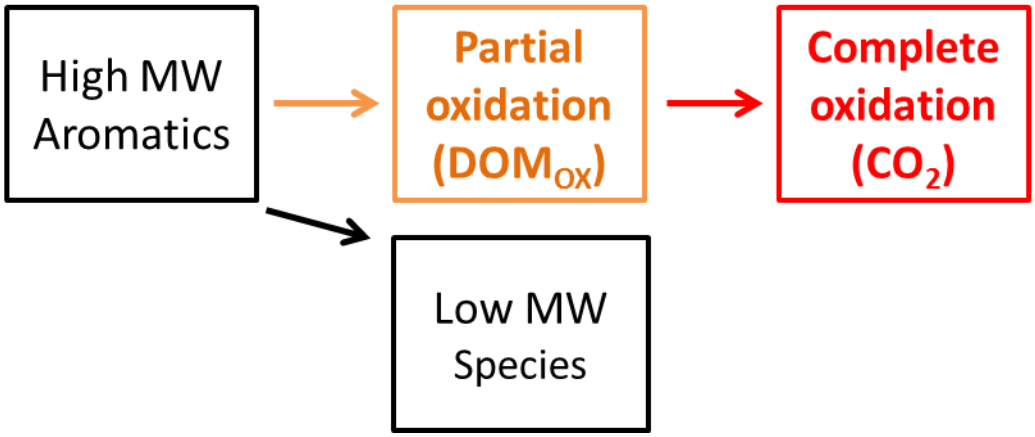

Figure 1.3 Conceptual framework for the oxidation of DOM by sunlight.

References

1. A. K. Aufdenkampe, E. Mayorga, P. A. Raymond, J. M. Melack, S. C. Doney, S. R. Alin, R. Aalto, and K. Yoo, *Front. Ecol. Environ.*, 2011, **9**, 53–60.

2. T. J. Battin, L. A. Kaplan, S. Findlay, C. S. Hopkinson, E. Marti, A. I. Packman, J. D. Newbold, and F. Sabater, *Nat. Geosci.*, 2008, **1**, 95–100.

3. J. J. Cole, Y. T. Prairie, N. F. Caraco, W. H. McDowell, L. J. Tranvik, R. G. Striegl, C. M. Duarte, P. Kortelainen, J. A. Downing, J. J. Middelburg, and J. Melack, *Ecosystems*, 2007, **10**, 171–184.

4. P. A. Raymond, J. Hartmann, R. Lauerwald, S. Sobek, C. McDonald, M. Hoover, D. Butman, R. Striegl, E. Mayorga, C. Humborg, P. Kortelainen, H. Dürr, M. Meybeck, P. Ciais, and P. Guth, *Nature*, 2013, **503**, 355–9.

5. A. D. McGuire, L. G. Anderson, T. R. Christensen, S. Dallimore, L. Guo, D. J. Hayes, M. Heimann, T. Lorenson, R. W. Macdonald, and N. Roulet, *Ecol. Monogr.*, 2009, **79**, 523–555.

6. G. W. Kling, G. W. Kipphut, and M. C. Miller, *Science*, 1991, **251**, 298–301.

7. R. M. Cory, C. P. Ward, B. C. Crump, and G. W. Kling, *Science*, 2014, **345**, 925–928.

8. C. Tarnocai, J. G. Canadell, E. A. G. Schuur, P. Kuhry, G. Mazhitova, and S. Zimov, *Global Biogeochem. Cycles*, 2009, **23**, GB2023.

9. C.-L. Ping, G. J. Michaelson, M. T. Jorgenson, J. M. Kimble, H. Epstein, V. E. Romanovsky, and D. A. Walker, *Nat. Geosci.*, 2008, **1**, 615–619.

10. E. A. G. Schuur, J. G. Vogel, K. G. Crummer, H. Lee, J. O. Sickman, and T. E. Osterkamp, *Nature*, 2009, **459**, 556–9.

11. A. H. MacDougall, C. A. Avis, and A. J. Weaver, *Nat. Geosci.*, 2012, **5**, 719–721.

12. T. Dittmar and A. Stubbins, *Treatise on Geochemistry: Dissolved Organic Matter in Aquatic Systems*, Elsevier Ltd., Oxford, UK, 2nd edn., 2014, vol. 12.

13. R. L. Sleighter and P. G. Hatcher, *Mar. Chem.*, 2008, **110**, 140–152.

14. A. C. Stenson, A. G. Marshall, and W. T. Cooper, *Anal. Chem.*, 2003, **75**, 1275–1284.

15. S. Kim, R. W. Kramer, and P. G. Hatcher, *Anal. Chem.*, 2003, **75**, 5336–44.

16. R. L. Sleighter, R. M. Cory, L. A. Kaplan, H. A. N. Abdulla, and P. G. Hatcher, *J. Geophys. Res. Biogeosciences*, 2014, **119**, 1520–1537.

17. R. M. Cory and L. A. Kaplan, *Limnol. Oceanogr.*, 2012, **57**, 1347–1360.

18. A. Stubbins, R. G. M. Spencer, H. Chen, P. G. Hatcher, K. Mopper, P. J. Hernes, V. L. Mwamba, A. M. Mangangu, J. N. Wabakanghanzi, and J. Six, *Limnol. Oceanogr.*, 2010, **55**, 1467–1477.

19. M. Gonsior, B. M. Peake, W. T. Cooper, D. Podgorski, J. D'Andrilli, and W. J. Cooper, *Environ. Sci. Technol.*, 2009, **43**, 698–703.

20. O. C. Zafiriou, J. Joussot-Dubien, R. G. Zepp, and R. G. Zika, *Environ. Sci. Technol.*, 1984, **18**, 358 – 371.

21. W. L. Miller and R. G. Zepp, *Geophys. Res. Lett.*, 1995, **22**, 417–420.

22. E. M. White, D. J. Kieber, J. Sherrard, W. L. Miller, and K. Mopper, *Mar. Chem.*, 2010, **118**, 11–21.

23. M. A. Moran and R. G. Zepp, *Limnol. Oceanogr.*, 1997, **42**.

24. R. M. Cory, K. McNeill, J. P. Cotner, A. Amado, J. M. Purcell, and A. G. Marshall, *Environ. Sci. Technol.*, 2010, **44**, 3683–9.

25. N. V. Blough and R. G. Zepp, in *Active Oxygen in Chemistry*, Springer, Netherlands, 1995, pp. 280 – 333.

26. J. V. Goldstone, M. J. Pullin, S. Bertilsson, and B. M. Voelker, *Environ. Sci. Technol.*, 2002, **36**, 364–372.

27. P. J. Mann, A. Davydova, N. Zimov, R. G. M. Spencer, S. Davydov, E. Bulygina, S. Zimov, and R. M. Holmes, *J. Geophys. Res.*, 2012, **117**, G01028.

28. R. G. M. Spencer, A. Stubbins, P. J. Hernes, A. Baker, K. Mopper, A. K. Aufdenkampe, R. Y. Dyda, V. L. Mwamba, A. M. Mangangu, J. N. Wabakanghanzi, and J. Six, *J. Geophys. Res.*, 2009, **114**.

29. M. Gonsior, N. Hertkorn, M. H. Conte, W. J. Cooper, D. Bastviken, E. Druffel, and P. Schmitt-Kopplin, *Mar. Chem.*, 2014, **163**, 10–18.

30. A. Stubbins, J. Niggemann, and T. Dittmar, *Biogeosciences*, 2012, **9**, 1661–1670.

31. C. Hu, F. E. Muller-Karger, and R. G. Zepp, *Limnol. Oceanogr.*, 2002, **47**, 1261–1267.

32. L. C. Powers and W. L. Miller, *Mar. Chem.*, 2015, **171**, 21–35.

33. S. C. Johannessen and W. L. Miller, *Mar. Chem.*, 2001, **76**, 271–283.

34. M. Aeschbacher, C. Graf, R. P. Scwarzenbach, and M. Sander, *Environ. Sci. Technol.*, 2012, **46**, 4916–4925.

35. R. Jaffé, Y. Yamashita, N. Maie, W. T. Cooper, T. Dittmar, W. K. Dodds, J. B. Jones, T. Myoshi, J. R. Ortiz-Zayas, D. C. Podgorski, and A. Watanabe, *Geochim. Cosmochim. Acta*, 2012, **94**, 95–108.

36. C. Miles and P. Brezonik, *Environ. Sci. Technol.*, 1981, **15**, 1089–1095.

37. P. Schmitt-Kopplin, N. Hertkorn, H.-R. Schulten, and A. Kettrup, *Environ. Sci. Technol.*, 1998, **32**, 2531–2541.

38. H. Xie, O. C. Zafiriou, W.-J. Cai, R. G. Zepp, and Y. Wang, *Environ. Sci. Technol.*, 2004, **38**, 4113–9.

39. D. Budac and P. Wan, *J. Photochem. Photobiol. A Chem.*, 1992, **67**, 135–166.

40. M. Xu and P. Wan, *Chem. Commun.*, 2000, 2147–2148.

41. J. R. Helms, A. Stubbins, J. D. Ritchie, E. C. Minor, D. J. Kieber, and K. Mopper, *Limnol. Oceanogr.*, 2008, **53**, 955–969.

42. J. R. Helms, A. Stubbins, E. M. Perdue, N. W. Green, H. Chen, and K. Mopper, *Mar. Chem.*, 2013, **155**, 81–91.

43. R. Cory, M. Miller, and D. McKnight, *Limnol. Oceanogr. Methods*, 2010, **8**, 67–78.

44. AMAP, *Arctic Climate Issues 2011: Changes in Arctic Snow, Water, Ice and Permafrost.*, 2011.

45. L. Hinzman, C. Deal, A. D. McGuire, S. H. Mernild, I. V. Polyakov, and J. E. Walsh, *Ecol. Appl.*, 2013, **23**, 1837–1868.

46. M. Moritz, M. Parisien, and E. Batllori, *Ecosphere*, 2012, **3**, 1–22.

47. K. Keller, J. D. Blum, and G. W. Kling, *Chem. Geol.*, 2010, **273**, 76–81.

48. G. W. Kling, H. E. Adams, N. D. Bettez, W. B. Bowden, B. C. Crump, A. E. Giblin, K. E. Judd, K. Keller, G. W. Kipphut, E. R. Rastetter, G. R. Shaver, and M. Stieglitz, in *A Changing Arctic: Ecological Consequences for Tundra, Streams, and Lakes.*, eds. J. E. Hobbie and G. W. Kling, Oxford University Press, New York, 2014, pp. 143 – 172.

49. K. M. Schreiner, T. S. Bianchi, and B. E. Rosenheim, *Geophys. Res. Lett.*, 2014, **41**, 3117–3126.

50. M. R. Turetsky, B. Benscoter, S. Page, G. Rein, G. R. van der Werf, and A. Watts, *Nat. Geosci.*, 2015, **8**, 11–14.

51. A. L. Westerling, H. G. Hidalgo, D. R. Cayan, and T. W. Swetnam, *Science*, 2006, **313**, 940–944.

52. N. P. Gillett, A. J. Weaver, F. W. Zwiers, and M. D. Flannigan, *Geophys. Res. Lett.*, 2004, **31**, L18211.

53. R. Jaffé, Y. Ding, J. Niggemann, A. Vähätalo, A. Stubbins, R. G. M. Spencer, J. Campbell, and T. Dittmar, *Science*, 2013, **340**, 345–347.

54. C. D. Koven, B. Ringeval, P. Friedlingstein, P. Ciais, P. Cadule, D. Khvorostyanov, G. Krinner, and C. Tarnocai, *Proc. Natl. Acad. Sci. U. S. A.*, 2011, **108**, 14769–74.

55. E. A. G. Schuur, J. Bockheim, J. . Canadell, E. Euskirchen, C. B. Field, and S. V. Goryachkin, *Bioscience*, 2008, **58**, 701–714.

56. S. A. Zimov, E. A. G. Schuur, and F. S. Chapin, *Science*, 2006, **312**, 1612–1613.

57. M. Heimann and M. Reichstein, *Nature*, 2008, **451**, 289–92.

58. J. E. Vonk and Ö. Gustafsson, *Nat. Geosci.*, 2013, **6**, 675–676.

59. P. J. Mann, W. V Sobczak, M. M. Larue, E. Bulygina, A. Davydova, J. E. Vonk, J. Schade, S. Davydov, N. Zimov, R. M. Holmes, and R. G. M. Spencer, *Glob. Chang. Biol.*, 2014, **20**, 1089–100.

60. R. M. Cory, B. C. Crump, J. A. Dobkowski, and G. W. Kling, *Proc. Natl. Acad. Sci. U. S. A.*, 2013, **110**, 3429–3434.

61. A. V. Vähätalo, M. Salkinoja-Salonen, P. Taalas, and K. Salonen, *Limnol. Oceanogr.*, 2000, **45**, 664–676.

62. B. Koehler, T. Landelius, G. A. Weyhenmeyer, N. Machida, and L. J. Tranvik, *Global Biogeochem. Cycles*, 2014, **28**, 696–711.

Chapter 2

Insights into the complete and partial photo-oxidation of black carbon in surface waters[4]

2.1 Abstract

Increasing wildfire activity in the Alaskan Arctic may result in new sources of black carbon (BC) to arctic watersheds. Black carbon, primarily comprised of condensed aromatics, is one of the most chemically recalcitrant fractions of organic carbon. However, lateral transfer of particulate and dissolved BC from soils to sunlit surface waters is increasingly suggested to result in the photochemical mineralization of BC to CO_2. While sunlight can also partially photooxidize aromatic compounds in surface waters, producing compounds with a higher O/C than the parent compound, this degradation pathway has not yet been identified for either particulate or dissolved BC. To address knowledge gaps on the photochemical degradation of particulate and dissolved BC, we quantified the complete and partial photo-oxidation of particulate and dissolved BC derived from arctic biomass as photochemical CO_2 production and O_2 consumption relative to dark controls. Concurrently, we investigated shifts in the chemical composition of dissolved BC following exposure to sunlight using UV-visible absorbance, fluorescence spectroscopy, and Fourier transform ion cyclotron resonance mass spectrometry (FT-ICR MS). The chemical and physical properties of BC produced from charring arctic biomass were similar to BC produced by wildfires in terrestrial ecosystems based on elemental analysis and FT-ICR MS. Based on the concentration of light-absorbing carbon in each fraction, dissolved BC was disproportionately more susceptible to complete and partial photo-oxidation

[4]C. P. Ward, R. L. Sleighter, P. G. Hatcher, and R. M. Cory, *Environ. Sci. Process. Impacts*, 2014, 721–731.

compared to particulate BC. Upon exposure to sunlight, the predominant fate of dissolved BC was partial photo-oxidation, while a smaller fraction of dissolved BC was photo-mineralized to CO_2. Shifts in both the optical and mass spectrometry spectra suggested that condensed aromatics likely comprised the fraction of dissolved BC that was completely and partially photo-oxidized. To further refine the meaning of sunlight as a sink for aquatic BC, the reactivity of partially oxidized photoproducts of BC in the aquatic organic carbon pool must be determined.

2.2 Introduction

Wildfire regime models predict that by the end of the 21st century, 62% of mid- to high-latitude regions will experience increases in wildfire activity.[1] These estimates include the Alaskan Arctic, a biome that has historically lacked wildfire activity over the last 10,000 years,[2] and is shifting to a fire regime of increased frequency and magnitude.[3,4] Increased fire activity likely results in increased production of black carbon (BC), a molecularly diverse organic residue of wildfires formed from the incomplete combustion of organic matter. Black carbon has a longer residence time in soils compared to uncharred (parent) biomass[5-7] and thus is one of the most recalcitrant components of the natural organic matter (NOM) pool, resulting in a long-term sink of atmospheric CO_2.[6,7] While wildfires and associated sources of BC are widespread in the pan-arctic region,[8] new sources of BC due to increased wildfire activity in the Alaskan Arctic may stabilize a fraction of the NOM pool in this critical region that stores vast amounts of C and is sensitive to climate change impacts on C storage.[9-11]

The recalcitrant nature of BC is due to its chemical and physical properties, which vary along a continuum of carbon rich combustion residues from slightly charred biomass to soot.[12,13] As charring temperature increases, atomic H/C and O/C ratios of the biomass decrease and the

fraction of condensed aromatics in BC increases due to dehydration and condensation reactions.[14,15] In contrast, the fraction of aliphatic compounds decreases with increasing charring temperatures. Thus, while BC is a mixture of compounds, its defining feature is hydrogen deficient condensed aromatic ring structures that are formed at high temperatures.[16]

For instance, approximately 65% of formulas detected in the Fourier transform ion cyclotron resonance mass spectrum (FT-ICR MS) of the water soluble fraction of 100-year-old fire-derived soil BC particles were classified as condensed aromatics formed from the incomplete combustion of terrestrial biomass, while the remaining 35% were primarily thermally resistant aliphatics, e.g., compounds not derived from charred biomass.[17,18] A similar distribution of compound classes was observed in a laboratory study comparing uncharred to charred oak.[15] Of the condensed aromatic formulas detected in soil BC by FT-ICR MS, many are extensively substituted with oxygen-containing functional groups, which has been inferred to mean that oxidation and dissolution of BC occurs on centennial timescales.[17–19]

Abiotic and microbial oxidation and subsequent dissolution of condensed aromatics within soils results in the export of "water-soluble" BC from soils to sunlit surface waters,[20] where BC comprises a significant fraction (2 - 10%) of the riverine or marine dissolved organic matter (DOM) pool.[21,22] Particulate BC may also be flushed from soils to surface waters, and thus mobilization and lateral transfer of particulate and dissolved BC from terrestrial ecosystems to rivers or oceans is an important loss process for wildfire produced BC in soils.[8,17,18,21,23–26] Once in sunlit surface waters, sunlight may degrade the light-absorbing condensed aromatics found in both the particulate and dissolved BC given that photochemical reactions are a well-characterized sink for aromatics within the aquatic particulate organic matter and DOM pools.[27,28] While no study has determined the susceptibility of particulate BC to degradation by

sunlight, several studies have demonstrated that condensed aromatics associated with BC and detected in the riverine or marine DOM pools are susceptible to photochemical degradation.[28–30] All condensed aromatics detected in Congo River DOM were absent from the mass spectrum after the sample was exposed to 57 days of simulated sunlight, suggesting that condensed aromatics were more susceptible to photo-degradation than other types of compounds within the DOM pool.[28] In a subsequent study of BC in the marine DOM pool, Stubbins et al. (2012) reported that sunlight was the primary sink for dissolved BC resulting in the production of CO_2, and estimated a half-life of < 800 years for photo-labile BC in the marine DOM pool, more than an order of magnitude shorter than the average apparent age of dissolved BC in the ocean.[30]

These previous investigations of photochemical degradation of dissolved BC have demonstrated the loss of condensed aromatics in surface waters using FT-ICR MS[28] or detection as benzene polycarboxylic acids (BPCAs),[29,30] which are molecular markers for condensed aromatics.[31] Loss of condensed aromatics or BPCA markers upon exposure to sunlight has been interpreted as the complete photochemical oxidation of these compounds to CO_2. However, in addition to complete oxidation to CO_2, sunlight can partially oxidize dissolved aromatics,[32–37] producing lower molecular weight products with higher O/C ratios than the parent compound. Thus, while studies have demonstrated the partial oxidation of aromatic compounds within bulk DOM[32] or the decrease in condensation of BPCAs following exposure to sunlight,[29] no study has determined the degree to which photo-degradation of condensed aromatics associated with aquatic BC results in complete oxidation to CO_2 vs. partial oxidation to compounds no longer detected as "BC." Determining the degree of complete vs. partial oxidation of BC is important because CO_2 may once again participate in the carbon cycle, while the residence time and reactivity of partially oxidized photoproducts of BC that remain sequestered in the aquatic

organic C pool is unknown. The disadvantage of using FT-ICR MS and BPCA markers to investigate the photochemical degradation of BC in riverine or marine waters is that there is no way to untangle the relative importance of complete or partial photo-oxidation of BC, given the presence of thousands of other dissolved organic compounds also undergoing photochemical degradation.

To address these knowledge gaps in the photochemical degradation of particulate and dissolved BC in surface waters, we investigated their susceptibility to complete and partial photo-oxidation under conditions that allowed for the relative importance of each pathway to be estimated. Aqueous suspensions of particulate BC and aqueous solutions of dissolved BC derived from arctic biomass were exposed to sunlight, and the complete and partial oxidation was quantified as photochemical CO_2 production and photochemical O_2 consumption relative to dark controls. In order to connect degradation pathways of condensed aromatics associated with dissolved BC to complete or partial photo-oxidation, concurrent changes in the chemical composition of dissolved BC following exposure to sunlight were measured by UV-visible absorbance, fluorescence spectroscopy, and FT-ICR MS.

2.3 Methods

2.3.1 Production and elemental composition of precursor and charred biomass

Charred biomass was generated from a mixture of two precursor plant species following the guidelines of Hammes et al. (2006). Tealeaf willow (*Salix pulchra*) and feather moss (*Pleurozium schreberi*) were collected near Toolik Lake Field Station (68.63 N, 149.60 W), separated into subsamples, and placed into a Barnstead Thermolyne 6000 muffle furnace. The parent biomass was not dried before charring. The plant species were chosen because they are

common in the Alaskan Arctic and were the major species charred in a recent tundra fire.[4] To mimic the oxygen-free conditions that exist inside of charring biomass,[38] a stream of nitrogen gas was delivered to the furnace for 30 minutes prior to and throughout the duration of the charring. The average temperature throughout the five hour charring process, measured with a high-temperature ceramic thermocouple (Omega Engineering, Inc.), was 452 ± 2 °C (n = 11). Following charring, the samples were cooled overnight, ground with a mortar and pestle, and passed through a 425 μm sieve.

Elemental composition (C, H, and N) of pre-dried (65 °C for 24 hours) precursor and charred biomass was measured by Huffman Laboratories (Golden, CO). Ash content of the precursor and charred biomass was measured using loss-on-ignition following Hammes et al. (2006); however, a combustion temperature of 550 ºC and a combustion time of 24 hours was used. Oxygen content of the precursor and charred biomass was estimated as the difference between the ash-free mass and the summed mass of the C, H, and N contents of the biomass. Sulfur content of the precursor and charred biomass was not measured. Thus, estimates of the mass of O may include mass due to small amounts of S (< 1%).[39] The charred biomass was used as the source of black carbon (BC) in this study.

2.3.2 Particulate and dissolved BC treatments

Two treatments were considered in this study: 1) unfiltered aqueous suspensions containing particulate and dissolved BC (pBC) and 2) filtered aqueous solutions containing dissolved BC (dBC). The pBC treatment was prepared by adding a known mass of BC to a known volume of laboratory-grade DI water, followed by equilibration with the atmosphere by stirring the suspension for 48 hours at room temperature in the dark. The C concentration of the

pBC treatment was determined by multiplying the added mass of BC by the percent C of BC (determined by elemental analysis), dividing by the volume of DI water in suspension, and then converting to a molar basis. The dBC treatment was prepared by filtering the room temperature equilibrated pBC treatment (pre-combusted GF/F, ~ 0.7 μm, Whatman). The C concentration of the dBC treatment was quantified as CO_2 after high-temperature catalytic combustion using potassium hydrogen phthalate as the calibration standard, and likely was a minimum value due to the presence of aromatic compounds less efficiently combusted to CO_2 when compared to the standard potassium hydrogen phthalate.[40]

2.3.3 Light absorption of the pBC and dBC treatments

Absorption spectra of pBC were determined by subtracting the reflectance from the transmittance of the suspension using a 150 mm integrating sphere attached to a Cary 5000 UV-visible spectrophotometer (Varian, Inc.). This method corrects for the influence of light scattering on the absorption properties of suspended particles.[41] The suspensions were stirred continuously during measurements to avoid settling and aggregation. Absorption spectra of a pBC dilution series made over the range of 3 to 30 mM-C resulted in a linear relationship (r^2 = 0.99, Fig. S1), suggesting similar contributions from scattering at all concentrations and multiple scattering effects were likely minimized at high concentrations. Absorption spectra of dBC were measured using a UV-visible spectrophotometer (Horiba Scientific). Decadic absorption coefficients of pBC and dBC were converted to Napierian absorption coefficients by multiplying by 2.303 and dividing by the pathlength of the 0.01 m quartz cuvette.

2.3.4 Photo-oxidation Experiments

2.3.4.1 Photochemical O_2 consumption and CO_2 production

The pBC and dBC treatments were pre-equilibrated with air in the dark at room temperature, transferred to acid and DI rinsed, pre-combusted, air-tight borosilicate vials (Labco Limited), and exposed to natural sunlight for 17 hours at Toolik Lake Field Station in June 2013. Dark controls were wrapped in aluminum foil. Average air temperature, measured every 5 minutes throughout the experiment, was 17 ± 2 °C (n = 209). Following the experiment, the light exposed and dark control treatments were equilibrated to room temperature in the dark and analyzed for their dissolved oxygen concentration (O_2) using a membrane inlet mass spectrometer (MIMS; Bay Instruments) and dissolved inorganic carbon (DIC) concentration using a DIC analyzer (Apollo SciTech). In order to avoid clogging the inlets of the MIMS and DIC analyzer, particles in the pBC treatment were allowed to settle out of solution and the inlets were held directly above the settled particles during analysis. Photochemical O_2 consumption (µM) was quantified as the dark – light difference in O_2 concentration, while photochemical CO_2 production (µM) was quantified as the light – dark difference in DIC concentration.

Because several studies have reported the abiotic sorption of O_2 to pBC and desorption of CO_2 from pBC (e.g., Spokas and Reicosky 2009), rates of O_2 sorption and CO_2 desorption from the pBC produced in this study were measured to determine the influence of sorption or desorption on the photochemical O_2 consumption or CO_2 production. The same equilibrated pBC treatment as used in the photochemical experiments was transferred to acid and DI rinsed, pre-combusted, air-tight borosilicate vials. Dissolved oxygen and DIC concentrations were measured at the start and at the end of a two-week long incubation at room temperature in the dark. The measured rates of O_2 consumption and CO_2 production were 2.2 ± 0.1 and 0.8 ± 0.2 µM day^{-1} (n = 3), respectively. The rates were calculated as the amount of O_2 consumption or CO_2 production

(μM) divided by the incubation time (days), assuming a constant rate throughout the incubation.[42] Even though steps were taken to limit microbial activity (i.e., acid and DI rinsing, and pre-combustion of experimental vials), and no bacteria was added to the pBC treatment, the possibility of microbial activity cannot be ruled out. However, the rates of O_2 consumption or CO_2 production due to any combination of sorption, desorption, or microbial activity were approximately 10-fold lower than the rates of photochemical O_2 consumption and CO_2 production of 57.1 ± 4.5 and 8.6 ± 1.6 μM day^{-1} (n = 3), respectively. Thus, at a minimum, photochemical processes accounted for 96% and 91% of O_2 consumption and CO_2 production in the pBC treatment, respectively. The contribution of sorption and desorption to photochemical O_2 consumption and CO_2 production was likely less important for the dBC treatment, which contained approximately 200-fold less C than the pBC treatment.

2.3.4.2 Effect of sunlight on dBC chemical characterization

A 4L dBC solution containing < 40 μM-C was equally divided and transferred to two DI-rinsed UV-transparent whirlpak bags (Nasco). The light exposed dBC sample bag was placed in a Suntest XLS+ solar simulator for 48 hours (Atlas Material Testing, Inc.), while the dBC dark control bag was wrapped in aluminum foil and placed outside of the solar simulator. The Suntest XLS+ emits 3-fold more UV light (integrated from 305 to 395 nm) than June sunlight at Toolik Lake Field Station (Fig. S2). Thus, 48 hours of exposure in the solar simulator was equivalent to 6 days of exposure to natural sunlight at Toolik Lake Field Station. Within the experimental chamber of the solar simulator, the sample was placed in a temperature regulated pooling tray. The average temperature of the circulating water in the pooling tray, measured every ~ 5 hours using a Fisher Scientific Traceable thermocouple, was 16 ± 1 °C (*n* = 9). Shifts in optical

properties of dBC were similar when exposed to natural and simulated light sources, likely because there were little differences between the spectral shape and photon flux of natural and simulated light sources, and between the temperature throughout the field and lab experiments. Following the exposure to simulated sunlight, the light exposed and dark control dBC treatments were subjected to analysis by UV-visible absorbance spectroscopy, fluorescence spectroscopy, and mass spectrometry.

Collection of UV-visible absorption spectra was previously described (see section 2.3). Spectral slope ratio (S_R) was calculated from the absorption spectrum of each sample as the ratio of the slope from 275 to 295 nm to the slope from 350 to 400 nm following Helms et al. (2008). Fluorescence excitation-emission matrices (EEMs) of the samples were measured with an Aqualog fluorometer (Horiba Scientific). EEMs were collected over an excitation and emission range of 240 to 600 nm by excitation/emission increment pairs of 5/1.64 nm/nm, using an integration time of 4 s. EEMs were corrected for inner-filter and instrument specific excitation and emission effects in Matlab (version 7.12) using manufacturer provided excitation and emission correction spectra.[44] Blank EEMs were collected using fluorescent free, laboratory-grade DI water, and were subtracted from sample EEMs to minimize the influence of water Raman peaks. Finally, intensities of corrected sample EEMs were converted to Raman units.

The remaining ~ 1.6 L of the light exposed and dark control dBC treatments were reserved for Fourier transform ion cyclotron resonance mass spectrometry (FT-ICR MS). A maximum of 1.6 mmol-C of each dBC treatment was loaded onto the 1-g PPL solid-phase cartridges (Agilent Technologies) following Dittmar et al. (2008). Due to the qualitative nature of FT-ICR MS, C recovery from the PPL extraction was not quantified, although previous studies have reported up to 70% C recovery.[45] The PPL column was eluted with 100% LC-MS

grade methanol, and diluted with LC-MS grade water to give a final sample composition of 50:50 (v/v) methanol:water. Samples were continuously injected into an Apollo II ESI ion source of a Bruker Daltonics 12 Tesla Apex Qe FT-ICR MS. Samples were injected at a rate of 120 µL h^{-1} and were analyzed in negative ion mode. Ions were accumulated in a hexapole for 1.5 s before being transferred to the ICR cell, where 300 scans, collected with a 4 MWord time domain, were co-added for each sample. The summed free induction decay signal was zero-filled once and Sine-Bell apodized prior to fast Fourier transformation and magnitude calculation using the Bruker Daltonics Data Analysis software. Similarly, a 50:50 (v/v) methanol:water blank spectrum was collected to test for contamination.

Mass spectra were externally calibrated using a polyethylene glycol standard and internally calibrated using fatty acids and other CH_2 homologous series naturally present in the sample.[46] Only peaks with a signal to noise ratio ≥ 4 were assigned molecular formulas. A molecular formula calculator (Molecular Formula Calc v.1.0 ©NHMFL, 1998) generated formulas using carbon, hydrogen, oxygen, nitrogen, and sulfur. Mass lists were screened to remove peaks also detected in the blank spectrum.[28] Only formulas that agreed within an error of $\leq \pm 0.5$ ppm to the calculated exact mass of the formula were considered, and all formulas were screened to meet the following criteria:[28]

1) Double bond equivalents (DBE) ≥ 0, and must be a whole number, where:

$$DBE = 1 + 0.5(2C - H + N) \quad (1)$$

2) $C \leq 50$

3) $2 \leq H \leq (2C + 2)$

4) $0 \leq O \leq (C+2)$

5) $O/C < 1.2$

6) $0.3 \leq H/C \leq 2.25$

7) $N/C < 0.5$

8) $S/C < 0.2$

The modified aromaticity index (AI_{mod}), which reflects the C-C double-bond density of each formula, was calculated following equation 2:[48]

$$AI_{mod} = (1 + C - 0.5O - S - 0.5H) / (C - 0.5O - S - N) \quad (2)$$

The formulas were categorized into three compound classes according to their AI_{mod}: aliphatic ($AI_{mod} < 0.5$), aromatic (non-condensed; $0.67 < AI_{mod} \geq 0.5$), and condensed aromatic ($AI_{mod} \geq 0.67$). Although the trends were similar for number and abundance-weighted data, number-weighted averages of molecular weight, atomic ratios, and indices were used to characterize dBC because the dark control and light exposed dBC treatments exhibited substantial differences in molecular composition (i.e., compound class distribution). Using differences in number-weighted averages, rather than abundance-weighted averages, has been recommended for aquatic DOM that exhibits large differences in molecular composition.[49]

2.4 Results

2.4.1 Elemental composition of precursor and charred biomass

Charring altered the elemental composition of the arctic biomass. The charred biomass had significantly higher %C and lower %O and %H compared to the precursor biomass (Table 1). It follows that charring decreased the atomic H/C ratio from 1.45 to 0.40 and the atomic O/C ratio from 0.53 to 0.09 (Table 1). The elemental composition of the charred biomass was similar to the charcoal and soot classes of residues comprising the black carbon (BC) combustion

continuum.[38] Thus, aqueous suspensions and solutions of the charred biomass were used to determine the light absorption and photo-oxidation of BC.

2.4.2 Filter separation of pBC and dBC treatments

Equilibration of BC in laboratory-grade DI water for 48 hours resulted in less than 1% of the initial C partitioning to the operationally defined dissolved phase, based on GF/F filtration. For example, BC suspensions prepared at C concentrations ranging from 15 to 118 mM-C resulted in dissolved C concentrations ranging from 63 to 279 μM-C after filtration (Fig. S3). Because > 99% of the C in the unfiltered treatment was retained by a GF/F filter, independent of the initial C concentration, the unfiltered treatment was operationally defined as particulate BC (pBC). Similarly, the filtered BC treatment was operationally defined as dissolved BC (dBC).

2.4.3 Light absorption and photo-oxidation of pBC vs. dBC

The absorption spectrum of pBC, containing 15 mM-C, decreased with increasing wavelength in the UV, with absorption coefficients ranging from 25.5 ± 2.7 m^{-1} at 280 nm to 22.6 ± 2.1 m^{-1} at 400 nm (n = 2; Fig. 1). The absorption coefficient remained relatively stable across the visible portion of the spectrum, e.g., the absorption coefficient at 600 nm was 94% of the absorption coefficient at 400 nm. The pBC treatment consumed 40 ± 3 μM-O_2 upon exposure to sunlight relative to the dark control (n = 3; Fig. 2). For the same suspension, photochemical CO_2 production was 6 ± 1 μM (n = 3), seven-fold less than photochemical O_2 consumption (Fig. 2).

The absorption spectrum of dBC, containing 63 ± 2 μM-C, decayed exponentially across the UV and the visible, with absorption coefficients ranging from 4.9 ± 0.4 m^{-1} at 280 nm to

0.73 ± 0.1 m^{-1} at 600 (*n* = 3; Fig. 1). The dBC treatment consumed 42 ± 6 µM-O_2 and produced 7 ± 1 µM-CO_2 upon exposure to sunlight relative to the dark control (*n* = 3; Fig. 2). Photochemical CO_2 production was six-fold less than photochemical O_2 consumption (Fig. 2).

Despite 200 times greater C concentration and a six-fold higher absorption coefficient (at 305 nm) between the pBC and dBC treatments, there was no detectable difference in the photochemical O_2 consumption or the photochemical CO_2 production between these treatments (not significantly different by unpaired Student's t-test, p = 0.3; Fig. 2). This result suggested that the majority of the O_2 consumed and CO_2 produced upon exposure to sunlight was associated with the photo-oxidation of dBC instead of pBC. Thus, only dBC was subjected to mass balance analysis and chemical characterization following exposure to sunlight.

The concentration of C in the dBC treatment ranged from a measured minimum of 61 µM-C to an estimated maximum of 77 µM-C (Fig. 3, Table S1), 20% higher than the maximum measured concentration because aromatic compounds have been shown to be on average 20% less efficiently oxidized to CO_2 by high-temperature catalytic combustion compared to aliphatic compounds used as standards for quantifying C.[40] Based on the range of C estimated in the dBC treatment and given that the photochemical production from the dBC treatment was 6 - 8 µM CO_2, 8 - 13% of the C in the dBC was mineralized to CO_2 by sunlight (Fig. 2, Table S1). Assuming that 1 mol of O_2 was consumed for 1 mol of CO_2 produced, the difference between photochemical O_2 consumption and CO_2 production (29 - 39 µM-O_2; Fig. 2, Table S1) was the range of O_2 incorporated into organic compounds within the dBC treatment. We converted this O_2 uptake concentration to carbon units representing the concentration of partially oxidized C formed by oxygen incorporation to dBC compounds using the following two assumptions. First, we assumed that the partially oxidized photoproducts would have O/C stoichiometry within the

range observed from the mass spectrum of the dark dBC treatment (0.05 - 1.1; consistent with the average value reported for bulk DOM).[50] Second, we took a mass balance approach to constrain the upper limit of partially oxidized C that could be produced. The maximum amount of C that could be partially oxidized was the maximum estimate of C initially present in the dBC treatment (77 µM-C) minus the amount of C in dBC that was mineralized to CO_2 (6 - 8 µM-C, Fig. 2). Using these assumptions, we estimated that at the highest O/C ratio detected in the dBC dark control (1.1 mol O per mol C) 29 - 39 µM-O_2 incorporation yields 52 - 72 µM partially oxidized C, meaning 70 - 117% of the maximum amount of C in the dBC treatment was partially oxidized by sunlight (Fig. 3, Table S1). The lowest O/C ratio detected in the dBC dark control that did not produce more oxidized C than was available for oxidation in the dBC treatment was 0.82 mol O per mol C; using this ratio with the minimum measured O_2 incorporation of 29 µM-O_2 yielded 70 µM of partially oxidized C. Thus, the best estimate was that 52 - 70 µM-C or 68 - 91% of the C in the dBC treatment was partially oxidized by sunlight (Fig. 3, Table S1).

2.4.4 Effects of sunlight on the chemical characterization of dBC

The fluorescence spectrum of dBC was comprised of two peaks characterized by excitation/emission wavelength maxima at 245/415 nm/nm (peak 1) and 305/415 nm/nm (peak 2) (Fig. 4, Table S2). Compared to the dBC dark control, fluorescence intensities of peak 1 and peak 2 decreased by 81 ± 3% and 88 ± 1%, respectively (Fig. 4, Table S2). In addition to a loss in fluorescence intensity, there was a decrease in absorption coefficients and a shift in the spectral slope ratio (S_R) compared to the dark control. Absorption coefficients of dBC decreased by 24 ± 1% (at 305 nm) compared to the dark control (Table S2). Because the loss of absorption following exposure to sunlight was greater at longer wavelengths compared to shorter

wavelengths, there was an 18 ± 9 % increase in the spectral slope ratio, a proxy that has been used to evaluate shifts in average molecular weight of aquatic dissolved organic carbon upon exposure to sunlight (Table S2).[43]

Over 2000 molecular formulas were assigned to the peaks detected in the mass spectrum of the dBC dark control (excluding contributions from ^{13}C isotopes, Table 2). The mass spectral peaks spanned a mass range of 250-700 Da, with an average molecular weight of 434 Da (Table 2). The average H/C and O/C of all assigned formulas was 0.88 and 0.37, respectively (Table 2). The average number of double bound equivalents (DBE) per formula, an indicator of the degree of condensation, was 14 (Table 2). The average modified aromaticity index (AI_{mod}) of each formula, a proxy for aromatic C content, was 0.54 (Table 2). On a number basis, the majority of formulas were classified as condensed aromatics (53%) or aliphatics (36%), while aromatics (non-condensed) comprised a minority fraction (11%; Table 2, Fig. 5). Analysis of the condensed aromatic, aromatic, and aliphatic formulas in van Krevelen space showed that within each compound class, there was a range of elemental composition (Fig. 5). Condensed aromatics were centered on an H/C of 0.50, spanning a range from 0.31 to 0.73. By definition, aromatic and aliphatic formulas had higher H/C ratios than condensed aromatics, but the aliphatics spanned a larger range of H/C than the aromatics and condensed aromatics (Fig. 5). While all three compound classes spanned a similar O/C range, the mean O/C of aliphatics and aromatics was lower when compared to condensed aromatics (Fig. 5).

Compared to the dBC dark control, the mass spectrum of the light exposed dBC treatment contained 42% fewer assigned formulas, and there was a shift in the average elemental composition and compound class distribution (Fig. 5). After sunlight exposure, there was a decrease in the average molecular weight, DBE, and O/C, while there was an increase in the

average H/C (Table 2). Compared to the dark control, the number and abundance of condensed aromatics decreased by 43 and 51%, respectively, while the number and abundance of aliphatics increased by 49 and 55%, respectively (Table 2). Of the 100 most abundant formulas that were identified only in the dBC dark control (not in the light-exposed dBC treatment), 92 were condensed aromatics (Fig. 6), suggesting the compounds corresponding to these formulas were preferentially removed by photo-oxidation. In contrast, of the 100 most abundant formulas that were found only in the light exposed dBC treatment (e.g., not detected in the dBC dark control), 93 were aliphatics (Fig. 6), suggesting that the compounds corresponding to these formulas were preferentially produced upon exposure to sunlight. Thus, following exposure of dBC to sunlight, the majority of molecular formulas on a number basis was aliphatics (85%), with condensed aromatics (10%) and aromatics (5%) comprising smaller fractions (Fig. 5, Table 2).

In addition to a shift in the distribution of major compound classes within dBC, there was a shift in the elemental composition of the formulas in each compound class following sunlight exposure. Compared to the dBC dark control, the average H/C of aliphatics, aromatics, and condensed aromatics increased following light exposure (Table 2). Compared to the dBC dark control, sunlight exposure increased the average O/C of condensed aromatics, but decreased the average O/C of aromatics and aliphatics (Table 2). Additionally, following sunlight exposure, the range of O/C exhibited by aliphatic formulas in the dBC treatment increased, while the range of O/C exhibited by condensed aromatics and aromatics decreased (Fig. 5).

2.5 Discussion

2.5.1 Characterization of BC

The chemical and physical properties of the black carbon (BC) produced in this study were similar to BC produced by wildfires in terrestrial ecosystems. The atomic H/C and O/C ratios of the BC produced in this study were within the range reported for BC-rich residues that comprise the BC combustion continuum.[38] The weak exponential decay throughout the visible region of the absorption spectrum of particulate BC (pBC) was consistent with absorption spectra of particulate BC aerosols in the atmosphere also lacking strong wavelength dependence throughout the visible region.[51] That only a trace fraction of pBC (< 1% of C in the pBC treatment) was operationally defined as water soluble by GF/F filtration was consistent with the similarly low aqueous solubility of wildfire produced soil BC[17] and laboratory produced BC.[24,52,53] The lower H/C and O/C of the pBC treatment (determined using elemental analysis) compared to the H/C and O/C of the dissolved BC (dBC) treatment (determined using FT-ICR MS), suggested that less condensed, more oxidized compounds partitioned to the dissolved phase (Tables 1 and 2). Given that the elemental composition of dissolved organic matter (DOM) determined using elemental analysis and FT-ICR MS are in close agreement (± 15%),[54] and the differences in elemental composition observed between the pBC and dBC treatments were > 15% (Tables 1 and 2), we interpreted these differences in elemental composition as significant. The observation of less condensed and more oxidized compounds in the dissolved phase was consistent with previous reports of the Fourier transform infrared absorption spectra of pBC and dBC, where dBC had more oxygen containing functional groups than pBC, suggesting that dBC had higher polarity and H-bonding with water than pBC.[55]

The elemental composition of formulas assigned to peaks detected in the dBC dark control FT-ICR mass spectrum was similar to the elemental composition of formulas from the soluble fraction of wildfire-derived 100-year-old soil BC particles, suggesting that the chemical

composition of dBC used to investigate photochemical reactivity in this study was similar to dBC exported from terrestrial to aquatic ecosystems.[17,18] For example, the range of H/C and O/C exhibited by the formulas in the dBC dark control overlapped with the H/C and O/C range reported for compounds in the wildfire-derived dBC[18] (0.1 - 2.0 and 0.0 - 0.7, respectively). Likewise, assignment of compound classes based on the modified aromaticity index (Eqn. 2) showed that condensed aromatics accounted for the majority (53%) of formulas assigned to the peaks in the mass spectrum of the dBC dark control, similar to the fraction of peaks assigned to condensed aromatics in wildfire-derived dBC (65%).[17]

Condensed aromatics, such as those detected in the mass spectrum of wildfire-derived dBC,[17] have been attributed to the incomplete combustion of organic matter and thus are included in the operationally defined pool of BC. However, the thermal origin of the aliphatics increasingly detected alongside condensed aromatics in environmental and laboratory produced BC is less clear.[15,17,38] Based on their elemental composition, Hockaday et al. (2006) classified the aliphatics detected in wildfire-derived dBC as "lignin-like" compounds and suggested that these aliphatics were derived from the thermally resistant, uncharred woody domains of BC. The majority of the aliphatics in the dBC dark control (~81%) overlapped in elemental composition with those detected by Hockaday et al. (2006) and thus could also be classified as thermally resistant "lignin-like" compounds. However, biomass can undergo partial combustion to yield thermally altered, "lignin-like" aliphatic compounds.[15,55] Consequently, the aliphatics in the dBC dark control were likely a mixture of thermally resistant and partially combusted compounds.

2.5.2 Photochemical reactivity of dBC

Dissolved BC was disproportionately more photoreactive compared to the C in the pBC treatment (Fig. 2). The photochemical O_2 consumption and CO_2 production attributed to dBC, constrained by the mass balance estimates of C in the dBC treatment, indicated that 8-13% of the C in the dBC treatment was photo-mineralized to CO_2, while 68-91% of the C was partially photo-oxidized to compounds remaining in the dBC treatment (Fig. 3, Table S1). Beginning with photo-mineralization, we evaluated three possibilities for the class of compounds meeting this fate: (1) condensed aromatics and aromatics were photo-mineralized to CO_2, (2) aliphatics were photo-mineralized to CO_2, or (3) a mixture of compounds (condensed aromatics, aromatics, and aliphatics) was mineralized to CO_2. Evidence in support of preferential photo-mineralization of condensed aromatics and aromatics was that 89% of condensed aromatics and 73% of aromatics were absent from the mass spectrum following sunlight exposure (Table 2). Furthermore, most of the formulas unique to the dBC dark control were condensed aromatics (Figs. 5 and 6), suggesting that these compounds were degraded upon exposure to sunlight and thus absent from the mass spectrum of light-exposed dBC. These results were consistent with a previous study showing loss of proxy compounds for condensed aromatics in the marine dBC pool following exposure to sunlight.[29] Consistent with the loss of condensed aromatics and aromatics following exposure to sunlight was the decrease in absorption coefficients by 24% and the decrease in fluorescence intensities by > 80% (Fig. 4, Table S2). Condensed aromatics and aromatics are chromophoric (i.e., light absorbing) and were thus much more likely to account for the light absorbing and emitting spectra of dBC compared to the non-light absorbing aliphatics.

Evidence against the preferential photo-mineralization of aliphatics was that aliphatics were the most abundant formulas unique to the light exposed dBC treatment (Figs. 5 and 6), suggesting that aliphatics were likely produced by the photochemical degradation of condensed

aromatics and aromatics. While the simultaneous loss of condensed aromatics and aromatics and production of aliphatics is consistent with photochemical degradation studies of DOM,[28] the production of aliphatics upon exposure to sunlight was inconsistent with an expected loss if aliphatics were preferentially photo-mineralized to CO_2. Although it was possible that differences in extraction and ionization efficiency of compounds in the dBC treatment before and after exposure to sunlight masked some changes in compound distributions, shifts in the mass and optical spectra together following exposure to sunlight suggested that condensed aromatics (and non-condensed aromatics to a smaller degree) most likely comprised the fraction of dBC that was photo-mineralized to CO_2.

Evaluating the same three possibilities for the class of compounds that was partially photo-oxidized, we suggest that the most likely explanation was that condensed aromatics were preferentially partially oxidized by sunlight. There was a decrease in the average O/C of aromatics and aliphatics, while in contrast there was an increase in the average O/C of condensed aromatics remaining after photo-oxidation compared to the dark control, suggesting that condensed aromatics were more susceptible to partial photo-oxidation than aromatics and aliphatics (Table 2). The decrease in O/C for aromatics and aliphatics was likely due to the breakdown of higher molecular weight compounds leading to the production of less oxidized (lower O/C) and more oxidized (higher O/C) compounds compared to the parent compound. We hypothesize that the more oxidized photoproducts were of lower molecular weight[34,37] and thus were likely outside the analytical window of detection using FT-ICR MS (250 - 700 m/z), consistent with the decrease in average molecular weight for the remaining aromatics and aliphatics (Table 2). The increase in O/C of the condensed aromatics after exposure to sunlight was consistent with the partial photo-oxidation of aromatics yielding photoproducts with higher

O/C ratios than the parent compound.[32–37] To account for the observed increase in O/C of 0.02 (for condensed aromatics, Table 2), approximately 504 condensed aromatics would have had to incorporate one oxygen (O) upon exposure to sunlight. The partial photoxidation of 504 condensed aromatics was equivalent to 24% of the 2058 formulas in the dBC dark control and thus less than the estimated 68-91% of C that was partially photo-oxidized based on mass balance calculations (Table 2, Fig. 3).

Possibilities for the "missing" partially oxidized C include: more than one O was incorporated into condensed aromatics, and partial photo-oxidation of condensed aromatics may have produced oxidized low molecular weight products that fell outside the analytical window of detection using FT-ICR MS (250 - 700 *m/z*). Partial photo-oxidation of aquatic DOM produces oxidized, low molecular weight compounds[34,37] outside the analytical window of detection using FT-ICR MS. Consistent with the production of low molecular weight photoproducts, condensed aromatics exhibited an 11% decrease in average molecular weight upon exposure to sunlight (Table 2). In addition, there was a shift in the spectral slope ratio (S_R) of the dBC absorption spectrum, indicating decreased average molecular weight of the light-absorbing fraction of dBC (i.e., condensed aromatics and aromatics) following sunlight exposure (Table S2). In contrast, aromatics and aliphatics exhibited a smaller decrease in average molecular weight upon exposure to sunlight compared to condensed aromatics (6% and 7%, respectively; Table 2). Thus, the production of low molecular weight photoproducts most likely resulted from the partial photo-oxidation of condensed aromatics compared to aromatics and aliphatics.

2.5.3 Environmental implications: photochemical fate of BC

The finding that the smaller operationally defined dBC treatment was disproportionately more susceptible to photo-oxidation than the larger pBC treatment strongly suggests that the size of BC compounds transferred from terrestrial to aquatic ecosystems may influence the susceptibility of BC to photo-oxidation. However, considering a larger size fraction of BC particles was used in the pBC treatment (< ~ 425 μm) than is expected to be transferred from terrestrial to aquatic ecosystems (< 200 μm),[24] and no study has quantified the size distribution of BC in arctic surface waters, the apparent resistance of pBC to complete and partial photo-oxidation under the experimental conditions tested here may not apply across the size fraction of BC particles in arctic surface waters.

The balance of evidence suggested that of the formulas present in the dBC treatment, condensed aromatics likely accounted for the majority of complete and partial photo-oxidation. Considering that most studies define, quantify, and study dBC based on a measurement of condensed aromatics in the bulk DOM pool,[22,23,28,29] our findings on the photochemical fate of soluble condensed aromatics from charred biomass are relevant for the fate of water-soluble BC produced by fires and transferred from terrestrial to aquatic ecosystems. Furthermore, complete and partial photo-oxidation of dBC in this study occurred on timescales similar to residence times in sunlit surface waters and transit time in rivers (e.g., days to weeks).[56] Given that the minimum estimate of partially photo-oxidized C (68% of C in the dBC treatment) was five-fold higher than the maximum estimate of complete photo-oxidation to CO_2 (13%, Fig. 3), the predominant fate of dBC exposed to sunlight was partial photo-oxidation to less aromatic photoproducts with unknown susceptibility to further degradation.

Sunlight has previously been reported as the primary sink for marine dBC, with CO_2 reported as the main photoproduct.[29] For example, exposing DOM collected from the deep North

Atlantic to six days of simulated sunlight resulted in a 29% decrease in the dBC fraction of the DOM. The dBC fraction of the DOM pool was quantified as benzene polycarboxylic acids (BPCAs), molecular markers for the combustion derived condensed aromatic fraction of DOM.[31] However, presence, absence, or decreasing concentrations of the proxy BPCA markers does not distinguish between complete or partial photo-oxidation. While there are likely differences in the photoreactivity between freshly charred biomass and "aged" black carbon in the marine DOM pool, our findings suggest that the majority of the photo-degraded dBC in the North Atlantic was not completely oxidized to CO_2 but was instead converted to partially oxidized C no longer recognizable as "black carbon" (e.g. not detectable as BPCAs). Because the susceptibility of these partially oxidized photoproducts to further degradation is unknown, so is the long-term stability of these compounds in the DOM pool. Thus, to better refine the interpretation of sunlight as a sink for dBC, our results suggest that further work is required to relate the loss of condensed aromatics to their complete or partial photo-oxidation and to test the susceptibility of the partially oxidized photoproducts to further degradation.

The changing fire regime in the Alaskan Arctic will likely provide new sources of BC to arctic soils. Given that microbial degradation of BC is temperature sensitive,[57] the lower temperatures in arctic soils compared to temperate or tropical regions may limit microbial degradation, and in turn increase the relative importance of other BC degradation processes such as photo-oxidation. Thus, the persistence of BC in arctic soils may be controlled by the lateral transfer of BC from arctic soils to sunlit surface waters and the subsequent photo-oxidation of BC. Accordingly, the strong terrestrial-aquatic linkage in the Arctic associated with the annual flush of soil C to sunlit surface waters[58] may facilitate opportunities for the photochemical oxidation of BC during riverine transport to the Arctic Ocean.

2.6 Acknowledgements

We thank M. Brennaman, J. Dobkowski, S. Fortin, K. Harrold, S. Michael, Y. Nyguyen, and researchers, technicians, and support staff of the Toolik Lake Arctic LTER for assistance. Special thanks to G. W. Kling for his invaluable advice during the research planning stages. Thanks to the staff at College of Sciences Major Instrument Cluster (COSMIC) at Old Dominion University for assistance with FT-ICR MS analysis. We also thank the anonymous reviewers, whose comments significantly improved the quality of this manuscript. Research was supported by NSF OPP–1023270.

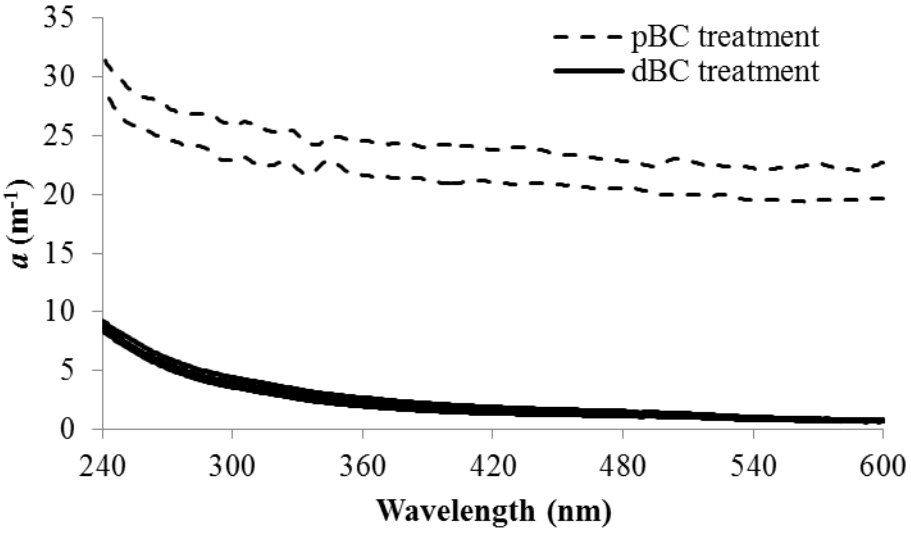

Figure 2.1 Duplicate and triplicate absorption spectra of the pBC and dBC treatment containing 15 mM-C and 63 µM-C, respectively. Values show Napierian absorption coefficients (m^{-1}).

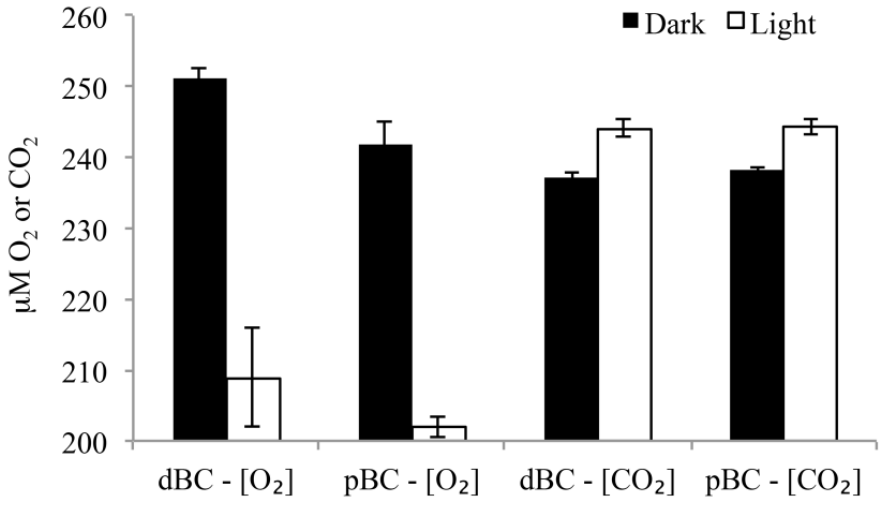

Figure 2.2 Effect of sunlight on the dissolved O_2 and CO_2 concentrations (µM) of the dark control and light exposed dBC and pBC treatments containing 63 µM-C and 15 mM-C, respectively. The series on the left is dark and light dissolved O_2 concentration, while the series on the right is dark and light dissolved CO_2 concentration. Dark controls were wrapped in aluminum foil. Error bars show ± standard deviation from the mean (n = 3).

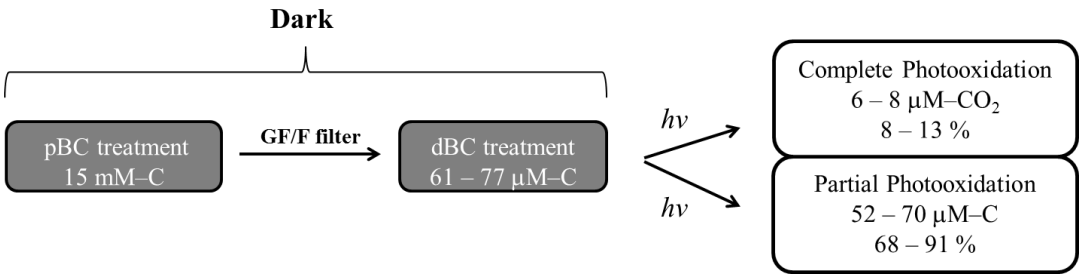

Figure 2.3 Mass balance analysis of the complete and partial photo-oxidation of C in the dBC treatment. The minimum estimate of partially photo-oxidized C (68%) was five-fold higher than the maximum estimate of complete photo-oxidation to CO_2 (13%), suggesting that the predominant fate of dBC exposed to sunlight was partial photo-oxidation.

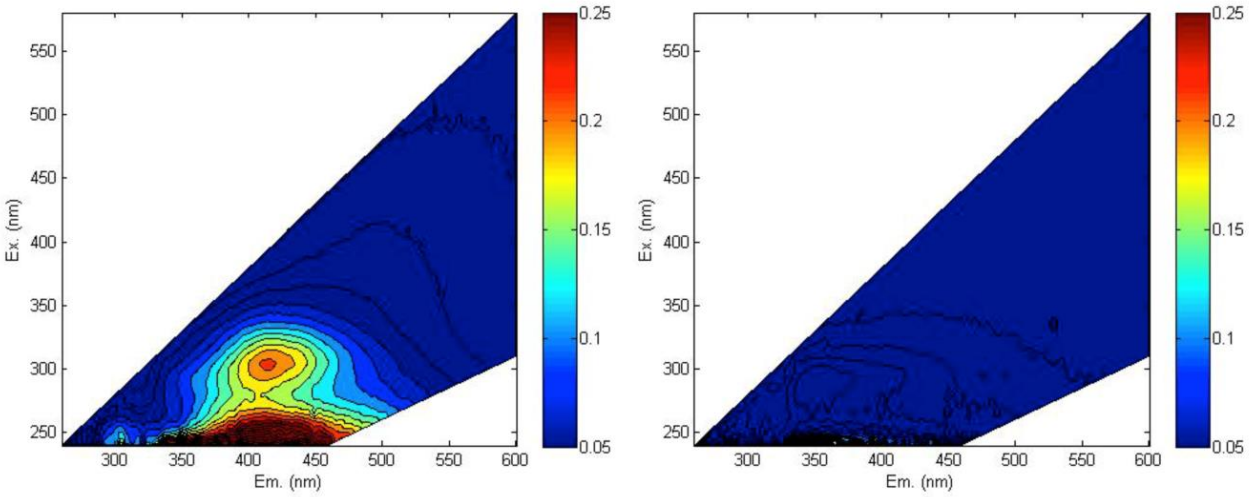

Figure 2.4 Effect of sunlight on EEMs of the dark control (left spectrum) and light exposed (right spectrum) dBC treatments. The spectra are characterized by excitation/emission wavelength maxima at 245/415 nm/nm (peak 1) and 305/415 nm/nm (peak 2). Compared to the dBC dark control, the fluorescence intensities of peak 1 and peak 2 in the light exposed dBC treatment decreased by 81% and 88%, respectively.

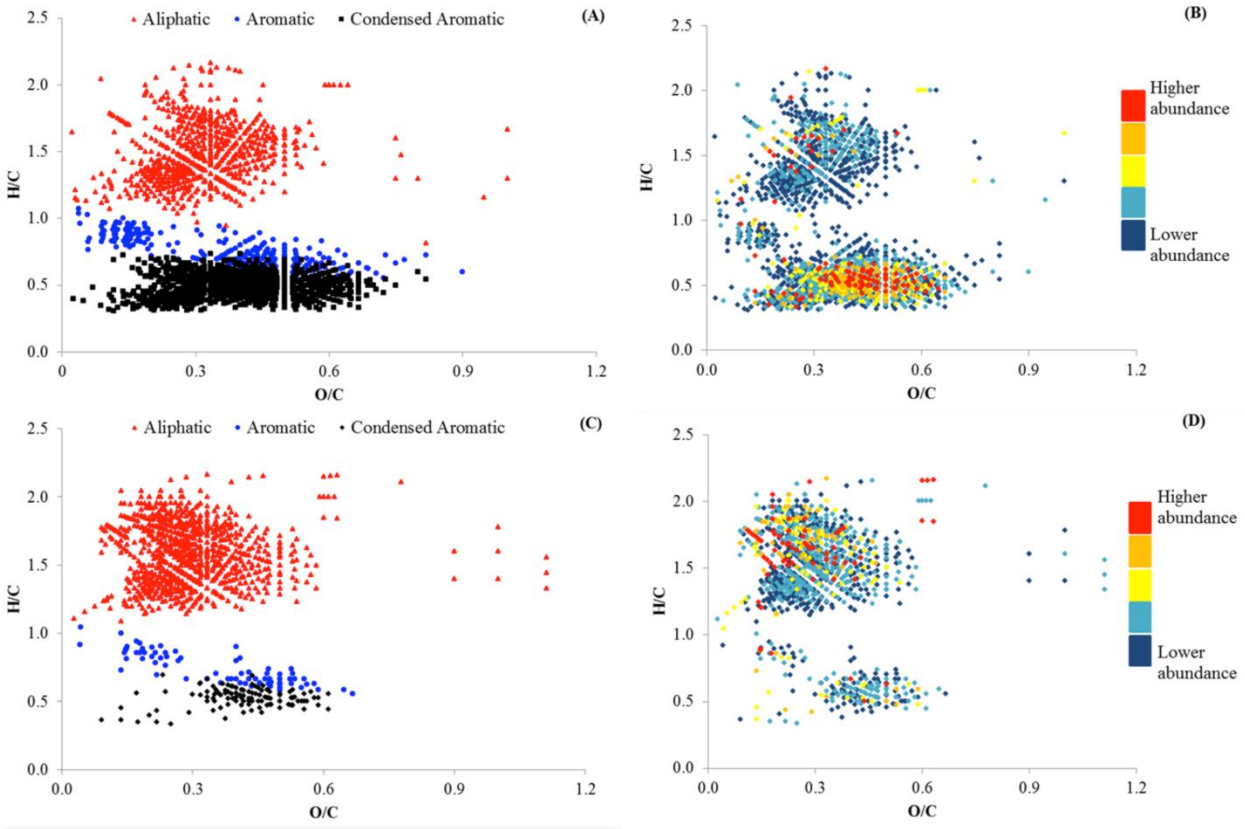

Figure 2.5 Van Krevelen diagrams for formulas assigned via FT-ICR MS analysis of the dark control (A and B) and light exposed dBC treatment (C and D).The color scheme in (A) and (C) corresponds to the class of each formula based on AI_{mod}, while the color scheme in (B) and (D) corresponds to the relative abundance of each formula.

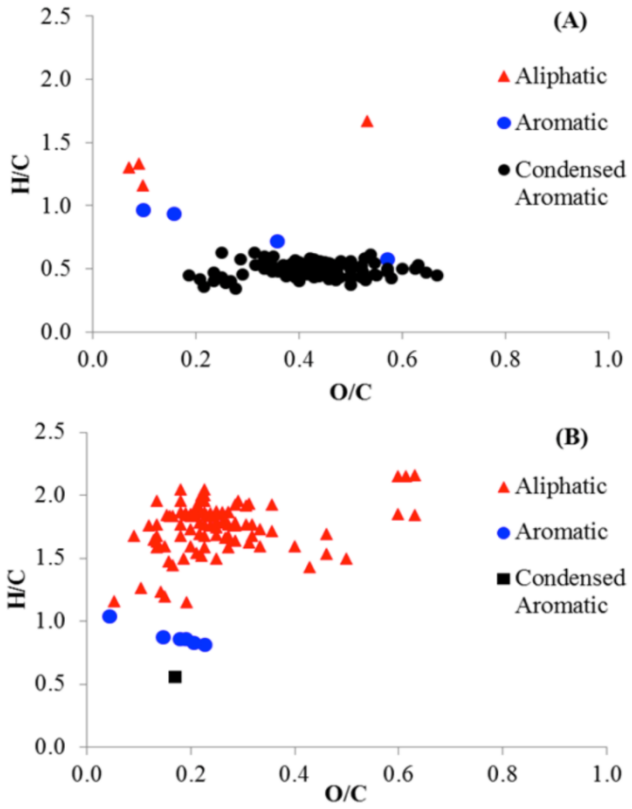

Figure 2.6 Van Krevelen diagram (A) shows the 100 most abundant formulas found only in the dBC dark control treatment. Van Krevelen diagram (B) shows the 100 most abundant formulas found only in the light exposed dBC treatment. Each diagram is colored according to the compound class of each formula, based on AI_{mod}.

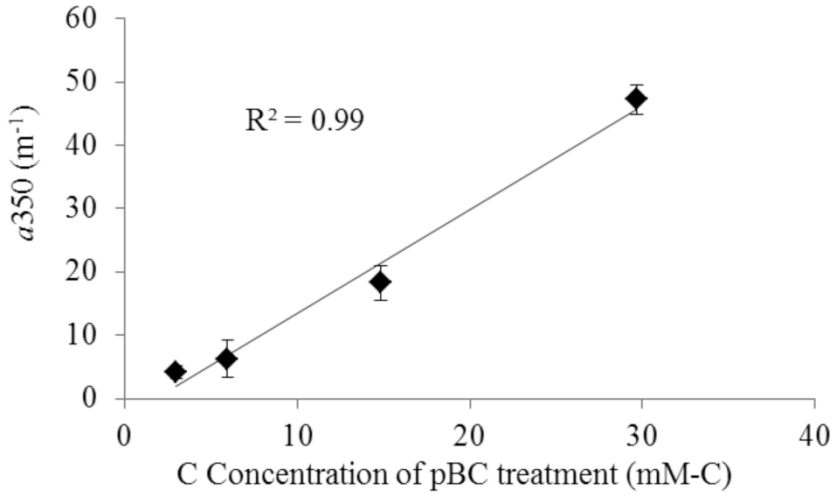

Figure 2.S1. Absorption coefficients at 350 nm (*a*350; m^{-1}, Napierian) of the particulate BC (pBC) treatment derived from a dilution series ranging in C concentration from 3 to 30 mM-C. The linear increase in absorption with increasing C concentration suggested similar contributions from scattering at all C concentrations, and multiple scattering effects were likely minimized at high concentrations. Error bars show ± standard error from the mean (n = 2).

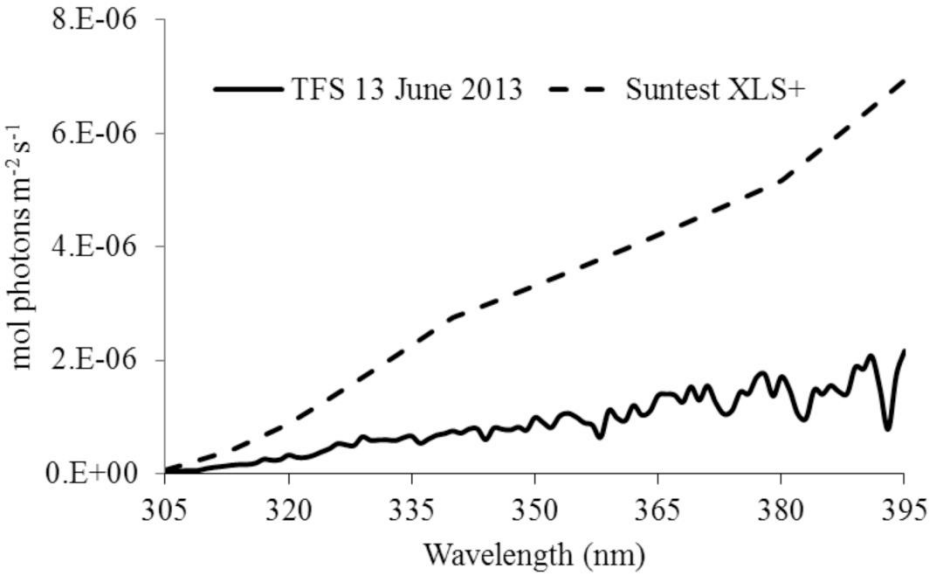

Figure 2.S2. Comparison of the sunlight spectrum collected at Toolik Lake Field Station on 13 June 2013 to the simulated sunlight spectrum emitted from a Suntest XLS+ (Atlas Materials Testing, Inc.). Integration of both spectra from 305 to 395 nm revealed that the simulated sunlight spectrum was approximately three times more intense than the natural sunlight spectrum. UVA and UVB measurements were collected every 5 minutes throughout the 17 hour experiment, averaged, and then normalized to a modeled sunlight spectrum using the National Center for Atmospheric Radiation (NCAR) tropospheric ultraviolet and visible (TUV) radiation model. Irradiance measurements (W m^{-2} nm^{-1}) of the simulated sunlight spectrum were collected at six discrete wavelengths (Biospherical Instruments, Inc.; 305, 313, 320, 340, 380, 395 nm), interpolated to 1-nm increments, and converted to a photon flux density spectrum (mol photons m^{-2} s^{-1}).

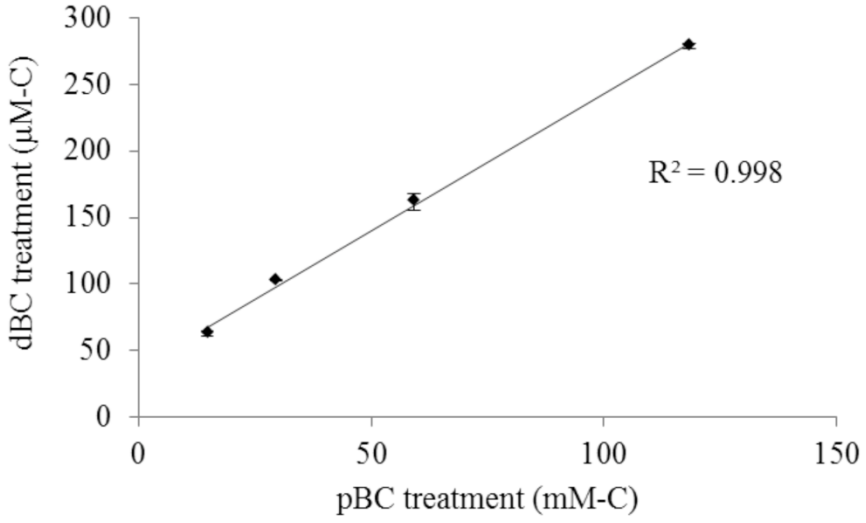

Figure 2.S3. Particulate BC (pBC) treatments ranging in C concentration from 15 to 118 mM-C resulted in dissolved BC (dBC) treatments ranging in C concentration from 63 to 279 μM-C after GF/F filtration. Because > 99% of the C in the unfiltered treatment was retained by a GF/F filter, independent of the initial C concentration, the unfiltered treatment was operationally defined as particulate BC (pBC). Similarly, the filtered BC treatment was operationally defined as dissolved BC (dBC). Error bars show ± standard deviation of the mean (n = 3).

Table 2.1 Elemental analysis of the precursor and charred biomass.

	% by mass					atomic ratios	
Biomass	**C**	**H**	**N**	**O**	**ash**	**H/C**	**O/C**
Precursor	49.81 (0.18)	6.02 (0.04)	0.78 (0.02)	34.91 (0.19)	8.54 (2.15)	1.45 (<0.01)	0.53 (<0.01)
Charred	71.24 (0.17)	2.40 (0.02)	1.49 (0.01)	8.98 (0.18)	15.93 (0.43)	0.40 (<0.01)	0.09 (<0.01)

Parenthetical values are the standard deviation from the mean (n = 2 for all measurements, except for ash where n = 6).

Table 2.2 Summary of FT-ICR MS data for the dark control and light exposed dBC treatments.

dBC Treatment	# of Formulas	% of Formulas	% Spectral Magnitude	MW	H/C	O/C	DBE	AI_{mod}
Dark Control	2058	100%	100%	434 ± 86	0.88 ± 0.49	0.37 ± 0.14	14 ± 6	0.54 ± 0.30
Aliphatic	735	36%	33%	432 ± 82	1.49 ± 0.22	0.32 ± 0.11	7 ± 3	0.16 ± 0.15
Aromatic	235	11%	8%	430 ± 80	0.76 ± 0.11	0.37 ± 0.19	16 ± 3	0.59 ± 0.04
Condensed Aromatic	1088	53%	59%	435 ± 90	0.49 ± 0.09	0.40 ± 0.13	18 ± 4	0.77 ± 0.06
Light Exposed	1200	100%	100%	404 ± 75	1.42 ± 0.40	0.32 ± 0.13	7 ± 4	0.22 ± 0.23
Aliphatic	1016	85%	88%	406 ± 76	1.57 ± 0.21	0.31 ± 0.12	6 ± 3	0.14 ± 0.13
Aromatic	63	5%	5%	400 ± 67	0.77 ± 0.12	0.34 ± 0.16	15 ± 3	0.60 ± 0.05
Condensed Aromatic	121	10%	8%	388 ± 66	0.53 ± 0.07	0.42 ± 0.11	16 ± 3	0.73 ± 0.05

MW = molecular weight, DBE = double bond equivalents, and AI_{mod} = modified aromaticity index.
Values show ± standard deviation from the number averaged mean.

Table 2.S1: Mass balance calculations for the complete and partial photo-oxidation of dBC.

	Measured	Calculated	Measured	Calculated: dBC Remaining after Complete Photooxidation		Calculated: Complete Photooxidation as % of Initial dBC		Measured	Calculated: Partial Photooxidation	Measured	Calculated	Calculated: Partial Photooxidation as % of initial dBC	
Sample	Min dBC	Max dBC[1]	Complete Photooxidation	Min	Max	Min[2]	Max[2]	Photooxidation	O_2 incorporated into dBC[3]	Min Initial O/C[4]	Partially Photooxidized-C[5]	Min[6]	Max[6]
	(μM-C)		(μM-CO_2)	(μM-C)		(%)		(μM-O_2)		Max	(μM-C)	(%)	
dBC Rep 1	61	73	8	69	53	10	13	45	38	1.1	68	89	112
dBC Rep 2	63	75	7	70	54	9	11	36	29	1.1	52	68	85
dBC Rep 3	64	77	6	71	55	8	10	45	39	1.1	72	93	117
										Min	(μM-C)	(%)	
										0.82	91	119	150
										0.82	70	91	115
										0.82	96	125	157

Shaded values are the results shown in Figure 3.

[1]Assuming the calculated dBC concentration may be up to 20% higher than the measured concentration. Aromatic compounds have been shown to be on average 20% less efficiently oxidized to CO_2 by high-temperature catalytic combustion compared to aliphatic compounds used as standards for quantifying C.[40]

[2]Min = ([CO_2]/ [max dBC]) * 100; Max = ([CO_2] / [min dBC]) * 100

[3]Assuming that 1 mol of O_2 was consumed for 1 mol of CO_2 produced.[50]

[4]Max stoichiometry is highest detected O/C in FT-ICR MS spectrum of dBC dark control; Min stoichiometry is lowest O/C ratio detected in the dBC dark control that did not produce more oxidized C than was available for oxidation (e.g. initial dBC concentration minus CO_2 produced).

[5]Partially photo-oxidized-C calculated as (2*[O_2 incorporated into dBC]) / (O/C stoichiometry)

[6]Min = ([partially photo-oxidized-C] / [max dBC]) * 100; Max = ([partially photo-oxidized-C] / [min dBC]) * 100

Table 2.S2. Optical characterization of the dark control and light exposed dBC treatments. This table shows that both absorbance and fluorescence intensity of the dBC treatment decreased after exposure to sunlight. The observed increase in slope ratio (S_R) indicated that the average molecular weight of the compounds in the dBC treatment decreased upon exposure to sunlight.

dBC Treatment	$a305$ (m^{-1})	S_R	Peak 1 (RU)	Peak 2 (RU)
Dark Control	1.81 ± 0.04	1.60 ± 0.10	0.38 ± 0.01	0.22 ± 0.01
Light Exposed	1.37 ± 0.03	1.88 ± 0.05	0.07 ± 0.01	0.03 ± 0.01

$a305$ = absorption coefficient at 305 nm (Napierian), S_R = spectral slope ratio, Peak 1 = excitation/emission wavelength maxima at 245/415 nm/nm in Raman units (RU), Peak 2 = excitation/emission wavelength maxima at 305/415 nm/nm in RU. Values show ± standard deviation from the mean (n = 3).

References

1. M. Moritz, M. Parisien, and E. Batllori, *Ecosphere*, 2012, **3**, 1–22.

2. P. E. Higuera, L. B. Brubaker, P. M. Anderson, T. A. Brown, A. T. Kennedy, and F. S. Hu, *PLoS One*, 2008, **3**, e0001744.

3. B. M. Jones, C. A. Kolden, R. Jandt, J. T. Abatzoglou, F. Urban, and C. D. Arp, *Arctic, Antarct. Alp. Res.*, 2009, **41**, 309–316.

4. M. C. Mack, M. S. Bret-Harte, T. N. Hollingsworth, R. R. Jandt, E. A. G. Schuur, G. R. Shaver, and D. L. Verbyla, *Nature*, 2011, **475**, 489–92.

5. L. Pessenda, S. Gouveia, and R. Aravena, *Radiocarbon*, 2001, **43**, 595–601.

6. J. Lehmann, J. Skjemstad, S. Sohi, J. Carter, M. Barson, P. Falloon, K. Coleman, P. Woodbury, and E. Krull, *Nat. Geosci.*, 2008, **1**, 832–835.

7. M. W. I. Schmidt, M. S. Torn, S. Abiven, T. Dittmar, G. Guggenberger, I. A. Janssens, M. Kleber, I. Kögel-Knabner, J. Lehmann, D. A. C. Manning, P. Nannipieri, D. P. Rasse, S. Weiner, and S. E. Trumbore, *Nature*, 2011, **478**, 49–56.

8. M. Elmquist, I. Semiletov, L. Guo, and Ö. Gustafsson, *Global Biogeochem. Cycles*, 2008, **22**.

9. E. A. Davidson and I. A. Janssens, *Nature*, 2006, **440**, 165–73.

10. M. C. Mack, E. A. G. Schuur, M. S. Bret-Harte, G. R. Shaver, and F. S. Chapin, *Nature*, 2004, **431**, 440–3.

11. E. A. G. Schuur, J. G. Vogel, K. G. Crummer, H. Lee, J. O. Sickman, and T. E. Osterkamp, *Nature*, 2009, **459**, 556–9.

12. C. A. Masiello, *Mar. Chem.*, 2004, **92**, 201–213.

13. M. Elmquist and G. Cornelissen, *Glob. Chang. Biol.*, 2006, **20**, 1–11.

14. X. Cao, J. Pignatello, Y. Li, C. Lattao, M. A. Campbell, N. Chen, M. F. Lesley, and J. Mao, *Energy & Fuels*, 2012, **26**, 5983–5991.

15. D. C. Podgorski, R. Hamdan, A. M. McKenna, L. Nyadong, R. P. Rodgers, A. G. Marshall, and W. T. Cooper, *Anal. Chem.*, 2012, **84**, 1281–1287.

16. S. Kim, L. A. Kaplan, R. Benner, and P. G. Hatcher, *Mar. Chem.*, 2004, **92**, 225–234.

17. W. C. Hockaday, A. M. Grannas, S. Kim, and P. G. Hatcher, *Org. Geochem.*, 2006, **37**, 501–510.

18. W. C. Hockaday, A. M. Grannas, S. Kim, and P. G. Hatcher, *Geochim. Cosmochim. Acta*, 2007, **71**, 3432–3445.

19. N. Singh, S. Abiven, M. S. Torn, and M. W. I. Schmidt, *Biogeosciences*, 2012, **9**, 2847–2857.

20. C. I. Czimczik and C. a. Masiello, *Global Biogeochem. Cycles*, 2007, **21**, 1–8.

21. R. Jaffé, Y. Ding, J. Niggemann, A. Vähätalo, A. Stubbins, R. G. M. Spencer, J. Campbell, and T. Dittmar, *Science*, 2013, **340**, 345–347.

22. T. Dittmar and B. P. Koch, *Mar. Chem.*, 2006, **102**, 208–217.

23. T. Dittmar, J. Paeng, T. M. Gihring, I. G. N. A. Suryaputra, and M. Huettel, *Limnol. Oceanogr.*, 2012, **57**, 1171–1181.

24. J. Major, J. Lehmann, M. Rondon, and C. Goodale, *Glob. Chang. Biol.*, 2010, **16**, 1366–1379.

25. S. Mitra, T. S. Bianchi, B. A. McKee, and M. Sutula, *Environ. Sci. Technol.*, 2002, **36**, 2296–302.

26. G. Guggenberger, A. Rodionov, O. Shibistova, M. Grabe, O. A. Kasansky, H. Fuchs, N. Mikheyeva, G. Zrazhevskaya, and H. Flessa, *Glob. Chang. Biol.*, 2008, **14**, 1367–1381.

27. M. L. Estapa and L. M. Mayer, *Mar. Chem.*, 2010, **122**, 138–147.

28. A. Stubbins, R. G. M. Spencer, H. Chen, P. G. Hatcher, K. Mopper, P. J. Hernes, V. L. Mwamba, A. M. Mangangu, J. N. Wabakanghanzi, and J. Six, *Limnol. Oceanogr.*, 2010, **55**, 1467–1477.

29. A. Stubbins, J. Niggemann, and T. Dittmar, *Biogeosciences*, 2012, **9**, 1661–1670.

30. L. A. Ziolkowski and E. R. M. Druffel, *Geophys. Res. Lett.*, 2010, **37**.

31. T. Dittmar, *Org. Geochem.*, 2008, **39**, 396–407.

32. R. M. Cory, K. McNeill, J. P. Cotner, A. Amado, J. M. Purcell, and A. G. Marshall, *Environ. Sci. Technol.*, 2010, **44**, 3683–9.

33. M. Gonsior, B. M. Peake, W. T. Cooper, D. Podgorski, J. D'Andrilli, and W. J. Cooper, *Environ. Sci. Technol.*, 2009, **43**, 698–703.

34. D. Kieber, J. McDaniel, and K. Mopper, *Nature*, 1989.

35. A. Mallakin, D. G. Dixon, and B. Greenberg, *Chemosphere*, 2000, **40**, 1435–1441.

36. B. McConkey and L. Hewitt, *Water. Air. Soil Pollut.*, 2002, **136**, 347–359.

37. K. Mopper and W. Stahovec, *Mar. Chem.*, 1986, **19**, 305–321.

38. K. Hammes, R. J. Smernik, J. O. Skjemstad, A. Herzog, U. F. Vogt, and M. W. I. Schmidt, *Org. Geochem.*, 2006, **37**, 1629–1633.

39. U. Hamer, B. Marschner, S. Brodowski, and W. Amelung, *Org. Geochem.*, 2004, **35**, 823–830.

40. G. Aiken, L. A. Kaplan, and J. Weishaar, *J. Environ. Monit.*, 2002, **4**, 70–74.

41. S. Tassan and G. M. Ferrari, *Appl. Opt.*, 2003, **42**, 4802–4810.

42. K. Spokas and D. Reicosky, *Ann. Environ. Sci.*, 2009, **3**, 179–193.

43. J. R. Helms, A. Stubbins, J. D. Ritchie, E. C. Minor, D. J. Kieber, and K. Mopper, *Limnol. Oceanogr.*, 2008, **53**, 955–969.

44. R. Cory, M. Miller, and D. McKnight, *Limnol. Oceanogr. Methods*, 2010, **8**, 67–78.

45. T. Dittmar, B. Koch, N. Hertkorn, and G. Kattner, *Limnol. Oceanogr. Methods*, 2008, **6**, 230–235.

46. R. L. Sleighter, G. A. McKee, Z. Liu, and P. G. Hatcher, *Limnol. Oceanogr. Methods*, 2008, **6**, 246–253.

47. F. W. McLaffert and F. Turecek, *Interpretation of Mass Spectra*, University Science Books, Sausalito, CA, 1993.

48. B. P. Koch and T. Dittmar, *Rapid Commun. Mass Spectrom.*, 2006, **20**, 926–932.

49. R. L. Sleighter, H. Chen, A. S. Wozniak, A. S. Willoughby, P. Caricasole, and P. G. Hatcher, *Anal. Chem.*, 2012, **84**, 9184–91.

50. S. Andrews, S. Caron, and O. Zafiriou, *Limnol. Oceanogr.*, 2000, **45**, 267–277.

51. Thomas W. Kirchstetter and T. Novakov, *J. Geophys. Res.*, 2004, **109**, D21208.

52. Y. Luo, M. Durenkamp, M. De Nobili, Q. Lin, and P. C. Brookes, *Soil Biol. Biochem.*, 2011, **43**, 2304–2314.

53. S. Abiven, P. Hengartner, M. P. W. Schneider, N. Singh, and M. W. I. Schmidt, *Soil Biol. Biochem.*, 2011, **43**, 1615–1617.

54. W. C. Hockaday, J. M. Purcell, A. G. Marshall, J. a. Baldock, and P. G. Hatcher, *Limnol. Oceanogr. Methods*, 2009, **7**, 81–95.

55. M. J. Norwood, P. Louchouarn, L.-J. Kuo, and O. R. Harvey, *Org. Geochem.*, 2013, **56**, 111–119.

56. T. J. Battin, L. A. Kaplan, S. Findlay, C. S. Hopkinson, E. Marti, A. I. Packman, J. D. Newbold, and F. Sabater, *Nat. Geosci.*, 2008, **1**, 95–100.

57. B. T. Nguyen, J. Lehmann, W. C. Hockaday, S. Joseph, and C. A. Masiello, *Environ. Sci. Technol.*, 2010, **44**, 3324–31.

58. P. A. Raymond, J. W. McClelland, R. M. Holmes, A. V. Zhulidov, K. Mull, B. J. Peterson, R. G. Striegl, G. R. Aiken, and T. Y. Gurtovaya, *Global Biogeochem. Cycles*, 2007, **21**.

Chapter 3

Chemical composition of dissolved organic matter draining permafrost soils[5]

3.1 Abstract

Northern circumpolar permafrost soils contain roughly twice the amount of carbon stored in the atmosphere today, but the majority of this soil organic carbon is perennially frozen. Climate warming in the Arctic is thawing permafrost soils and mobilizing previously frozen dissolved organic matter (DOM) from deeper soil layers to nearby surface waters. Previous studies have reported that ancient DOM draining deeper layers of permafrost soils was more susceptible to degradation by aquatic bacteria compared to modern DOM draining the shallow active layer of permafrost soils, and have suggested that DOM chemical composition may be an important control for the lability of DOM to bacterial degradation. However, the compositional features that distinguish DOM drained from different depths in permafrost soils are poorly characterized. Thus, the objective of this study was to characterize the chemical composition of DOM drained from different depths in permafrost soils, and relate these compositional differences to its susceptibility to biological degradation. DOM was leached from the shallow organic mat and the deeper permafrost layer of soils within the Imnavait Creek watershed on the North Slope of Alaska. DOM draining both soil layers was characterized in triplicate by coupling ultra-high resolution mass spectrometry, ^{13}C solid-state NMR, and optical spectroscopy methods with multi-variate statistical analyses. Reproducibility of replicate mass spectra was high, and compositional differences resulting from interfering species or isolation effects were

[5] C. P. Ward and R. M. Cory, *Geochim. Cosmochim. Acta*, In Review.

significantly smaller than differences between DOM drained from each soil layer. All analyses indicated that DOM leached from the shallower organic mat contained higher molecular weight, more oxidized, and more unsaturated aromatic species compared to DOM leached from the deeper permafrost layer. Bacterial production rates and bacterial efficiencies were significantly higher for permafrost compared to organic mat DOM; however, respiration rates were similar between DOM sources. Increased release of permafrost DOM from arctic soils to surface waters will change the chemical composition of DOM and its lability to bacteria, but this study suggests that these shifts in DOM composition and lability may not increase the carbon dioxide produced by bacterial respiration of permafrost DOM exported to arctic surface waters compared to DOM currently draining the shallow active layer.

3.2 Introduction

Northern circumpolar permafrost soils contain ~1700 Pg of organic carbon (OC),[1,2] roughly twice the 800 Pg-C stored in the atmosphere today. The majority of this soil OC (88% or 1466 Pg-C) is perennially frozen.[2] Because the climate is warming rapidly in the arctic, permafrost soils are thawing and hydrologic flow paths are deepening, leading to the mobilization of ancient dissolved organic matter (DOM) from deeper horizons to nearby surface waters. For instance, the amount of ancient OC drained from deeper permafrost layers of the Eurasian Arctic soils to surface waters has been estimated to have increased by 3 - 6% from 1985 - 2004.[3] Once flushed to surface waters, permafrost DOM can be mineralized by sunlight or bacteria and released back to the atmosphere as carbon dioxide (CO_2) where it can positively reinforce climate warming, or it can be partially degraded, buried in lake sediments, or exported to the ocean.[4] The current estimate is that 25 - 40% of CO_2 released from arctic surface waters to

the atmosphere is produced through the mineralization of DOM by sunlight in the water column.[5] The remaining CO_2 released from surface waters is likely generated through bacterial respiration of DOM in the water column or in aquatic sediments, or is directly transferred from soil waters.[5–8] Thus, understanding the controls on the lability of DOM to degradation to CO_2 by bacteria in arctic soil and surface waters is critical for understanding how much permafrost DOM will be respired to CO_2 versus exported through rivers to the ocean.

The fate of DOM in arctic surface waters may change if permafrost sources comprise a larger fraction of DOM draining arctic soils because permafrost DOM has been found to be more quickly converted to CO_2 by aquatic bacteria compared to DOM currently draining the active layer.[9,10] Given the importance of substrate composition as a control on bacterial respiration in arctic surface waters,[11,12] permafrost DOM has been proposed to be more labile to aquatic bacteria due to differences in chemical composition compared with DOM draining the shallower active soil layer. For example, permafrost DOM has been consistently reported to contain less aromatic C compared with DOM draining the active layer of arctic soils, [9,10,13,14] and proxies for aromatic C content were found to be inversely correlated with the lability of DOM to bacterial respiration in receiving waters.[9,10] However, a previous study found no difference in bacterial respiration between permafrost and modern DOM when degraded by aquatic bacteria in the dark, despite large differences in aromatic C content.[13] Thus, aromatic C may control bacterial respiration in some waters, but the composition of the aromatics present may be as important as the abundance of aromatic C.[15] For example, Mann et al. (2014) proposed that increased phenolic aromatics within modern DOM inhibited aquatic bacterial respiration,[16] compared to ancient permafrost DOM containing less aromatic C. Alternatively, aromatic C content may not be a causal factor in bacterial respiration; that is, other facets of DOM composition may

contribute to variability in bacterial activity, such as molecular weight or oxidation state,[17–20] In one study of Amazon River DOM, the high molecular weight fraction was more labile to bacterial degradation than the low molecular weight fraction.[17] In contrast, lower molecular weight species were more susceptible to biological degradation in a temperate stream than higher molecular weight species.[15] Furthermore, multiple studies have suggested that bacterial growth rates and efficiencies are inversely correlated to the average oxidation state of DOM.[18–20] Given that aromatic C, molecular weight, and oxidation state of DOM have been reported to differ between permafrost and organic mat DOM in arctic soil waters,[21] a more detailed view of DOM chemical composition is needed to identify the organic compounds that govern the susceptibility of DOM to aquatic bacterial degradation.

The most resolved analysis of DOM chemical composition can be achieved using Fourier transform ion cyclotron resonance mass spectrometry (FT-ICR MS). Ultra-high resolution mass spectrometry (i.e., FT-ICR MS) confirms that DOM is a heterogeneous mixture and provides the molecular composition of thousands of individual formulas that comprise the DOM pool.[22] While FT-ICR MS provides the composition (i.e., the amount of CHONSP), molecular weight, oxidation state, and compound class (e.g., aromatic vs. aliphatic) of each formula detected, it does not provide the structural arrangement of the atoms within each formula. Without structural information, it is not possible to identify the distribution of functional groups within each formula, for example, whether any oxygen atom in a formula is present as a phenol or a ketone.[23,24] Thus, FT-ICR MS alone can't identify the phenolic subset of aromatic compounds hypothesized to inhibit bacterial activity in arctic surface waters.[10] To address this limitation, FT-ICR MS analysis of DOM is increasingly coupled with a measure of structural or functional group distribution, such as solid-state ^{13}C nuclear magnetic resonance (^{13}C NMR).[25,26]

FT-ICR MS is also increasingly coupled with optical proxies for average DOM composition[15,27,28] because these optical proxies correlate well with molecular properties of DOM and the lability of DOM to aquatic bacteria.[15,29–31] For example, optical proxies based on the light-absorbing and emitting fractions of the DOM pool (CDOM and FDOM, respectively) have been correlated with aromatic C content and composition,[29,32,33] and average molecular weight.[34] In addition, recent work coupled FT-ICR MS with CDOM and FDOM analyses, finding that aromatic-rich riverine DOM supports bacterial respiration in a watershed where the dominant source of DOM is plant and soil organic matter.[15] Another reason CDOM and FDOM are commonly used as a measure of DOM lability is because this analysis requires little sample manipulation, rendering this approach relatively free of bias introduced during pre-isolation, which is often required for DOM analysis by FT-ICR MS or ^{13}C NMR.

DOM is often isolated using solid-phase extraction (SPE) prior to FT-ICR MS analysis to minimize the influence of interfering species that suppress the ionization of organic compounds (e.g., salts).[35] Pre-isolation of DOM is required for ^{13}C NMR to remove interfering impurities (i.e., paramagnetics). Recoveries of DOM by SPE are < 100% and compounds lost during SPE extraction are likely low molecular weight, less aromatic compounds.[36,37] Thus, SPE may preferentially exclude compounds important for aquatic bacterial degradation. Additionally, due to time, labor, and instrument costs associated with SPE isolation and FT-ICR MS analysis, replicate FT-ICR MS spectra have rarely been reported. Good agreement between FT-ICR MS analysis of filtered, whole water and SPE-isolated DOM have been reported for riverine DOM;[36] however, these comparisons and analyses of reproducibility of FT-ICR MS spectra have not been reported for DOM in soils or surface waters of the Arctic, which exhibit different ratios of DOM vs. interfering constituents compared to the riverine DOM previously studied.

The objective of this study was to resolve the compositional features that distinguish DOM draining different horizons of permafrost soils using complimentary analytical and statistical analyses. To achieve this objective we characterized the chemical composition of DOM draining the shallower organic mat and the deeper permafrost layer of Alaskan Arctic soils by coupling FT-ICR MS, ^{13}C NMR, and optical spectroscopy methods with multi-variate statistical analyses. Because we expected differences in DOM composition to influence bacterial degradation of DOM leached from the organic mat and the deeper permafrost layer, we measured bacterial production, respiration, and growth efficiency for DOM inoculated with native bacterial communities.

3.3 Methods

3.3.1 Study site

Sample collection took place between June and July 2013 in the Imnavait Creek watershed on the North Slope of Alaska (68.62˚ N, 149.28˚ W; elevation ~ 900 m). Imnavait Creek is a 1st order tributary of the Kuparuk River, the 4th largest fluvial source of OC to the Arctic Ocean in the Alaskan Arctic.[38] The Imnavait Creek watershed was glaciated during the Pleistocene (610 - 132 k yr BP), however, paludification of these soils started approximately 11,500 ± 140 years ago.[39,40] Characteristics of the soil column have been previously described in detail.[41] Briefly, the top 20 cm is comprised of live and dead organic matter mixed with glacial till. Beneath the organic horizon, the soil is primarily glacial outwash with occasional evidence of frost-churned organic matter. The entire basin is underlain with permafrost, with average peak thaw depth, measured in August from 2003 to 2012, ranging from 38 to 52 cm (43 ± 11 cm, N

= 2890).[8] The average thaw depth at Imnavait Creek watershed during sampling in July 2013 was 19 ± 2 cm (N = 9).

3.3.2 Experimental Design

The seven-step experimental design to collect dissolved organic matter from the shallower organic mat and deeper permafrost layer of the soil is shown in Figure 3.1. Each of the seven steps was completed in triplicate for both layers of the soil. (1) Three adjacent 1.5 m x 1.5 m soil pits (20 m apart) were constructed ~ 100 m up the west facing hillslope of the Imnavait Creek drainage basin (Pit #1: 68.6139 N, 149.3145 W; Pit #2: 68.6138 N, 149.3145 W; Pit #3: 68.6136 N, 149.3144 W). Soil organic matter (SOM) was collected at two depths, the organic mat (5 - 15 cm) and the permafrost mineral layer (95 - 105 cm), corresponding to the annually thawed and permanently frozen soil layers, respectively. At each depth equal amounts of frozen SOM from each pit were placed into three ziplock bags, transferred to a cooler, and transported to freezers at Toolik Lake Field Research Station (68.63˚ N, 149.60˚ W). Soil from the organic mat was collected on 15-June-2013, while soil from the permafrost mineral layer was collected on 8-July-2013. (2) The frozen soils were thawed prior to leaching. 3600 g of soil from the organic mat layer or 750 g of permafrost soil was added to acid and de-ionized water (DI) rinsed five gallon HDPE buckets and leached overnight in 15 L of laboratory grade DI at room temperature. (3) The dissolved fraction of the leachate was isolated using a series of pre-cleaned nylon filter screens (50, 20, and 10 μm; Cole-Parmer, Inc.) and pre-cleaned 5 and 0.45 μm high-capacity cartridge filters (Geotech Environmental Equipment, Inc.). The dissolved fraction of the soil leachates are from here on referred to as organic mat DOM and permafrost DOM. (4) Splits of DOM were taken for water chemistry (i.e., pH, conductivity), UV-visible and fluorescence

spectroscopy, and high resolution Fourier transform ion cyclotron resonance mass spectrometry (FT-ICR MS). (5) Additional splits of DOM were concentrated and inorganic impurities were removed using solid phase extraction (SPE). (6) SPE eluate from each replicate leachate was reserved for spectroscopic and FT-ICR MS analyses. (7) Functional group distributions of pooled, freeze-dried SPE eluates were measured by solid-state ^{13}C NMR.

3.3.3 Whole water DOM vs. solid phase extraction DOM

In this study, whole water DOM refers to the bulk DOM in a filtered soil leachate, and solid phase extraction (SPE) DOM refers to DOM isolated using Bond Elut PPL cartridges (Agilent Technologies).[37] Briefly, organic mat and permafrost DOM were acidified to pH 2 and loaded onto LC-MS grade methanol rinsed (MeOH; Fisher Scientific) 5-g PPL SPE cartridges. All DOC loadings were less than the 2 mmol-C L^{-1} recommended threshold to avoid breakthrough.[37] The cartridges were flushed with 0.01 M trace metal grade HCl (Fisher Scientific), dried with ultra-high purity N_2 (Airgas), and then eluted with MeOH. Mean recovery of chromophoric DOM by the PPL solid phase, quantified as absorbance at 305 nm of the column effluent divided by the initial DOM absorbance at 305 nm, was 93 ± 3% and 88 ± 8% for organic mat and permafrost DOM, respectively. Carbon recovery by the PPL solid phase was similar between DOM sources (organic mat = 57 ± 1%; permafrost = 67 ± 7%; $p = 0.13$).

3.3.4 DOC concentration and optical characterization

Dissolved organic carbon concentration (DOC) was quantified as CO_2 after high-temperature catalytic combustion using potassium hydrogen phthalate as the calibration standard.[42] UV-visible absorption spectra of whole water DOM were collected using a 1-cm

pathlength UV-visible spectrophotometer (Aqualog; Horiba Scientific). Absorption spectra of SPE isolated DOM were collected by spiking 400 μL of SPE eluate into 40 mL pre-ashed ampules, evaporating the MeOH with ultra-high purity N_2, reconstituting in 25 mL DI, and analyzing using a 5-cm pathlength UV-visible spectrophotometer (Cary 300; Agilent Technologies). Splits of SPE DOM reconstituted in DI were reserved for fluorescence spectroscopy and DOC analyses. Napierian absorption coefficients were calculated by multiplying absorbance (A) by 2.303 and dividing by the pathlength (m) of the quartz cuvette. Spectral slope ratio (S_R) was calculated from the absorption spectra as the ratio of the slope from 275 to 295 nm to the slope from 350 to 400 nm.[34] Specific UV-visible absorbance as 254 nm ($SUVA_{254}$; L mg-C^{-1} m^{-1}) was calculated following Weishaar et al. (2003), where decadic absorbance at 254 nm was divided by the pathlength (m) and by the DOC concentration (mg-C L^{-1}).

Fluorescence excitation-emission matrices (EEMs) of whole water and SPE DOM were collected over excitation and emission ranges of 240 to 600 nm by excitation/emission increments of 5/1.64 nm/nm, respectively, using integration times ranging from 3 to 4 s (Aqualog; Horiba Scientific). When necessary, DOM was diluted to less than 0.6 absorbance units (A) at 254 nm prior to analysis.[43] EEMs were corrected for inner-filter and instrument specific excitation and emission effects in Matlab (version 2013b). Blank EEMs were collected using fluorescence free, laboratory-grade DI water, and were subtracted from sample EEMs to minimize the influence of water Raman peaks. Intensities of corrected sample EEMs were converted to Raman units. Dominant peaks in the corrected EEMs were identified following Coble (1996): Peak A (λ_{ex} = 250 nm; λ_{em} = 380 - 460 nm), Peak C (λ_{ex} = 350; λ_{em} = 420 - 480 nm), and Peak T (λ_{ex} = 275 nm; λ_{em} = 340 nm). The fluorescence index (FI)[32] was calculated as

the ratio of emission intensity at 470 nm to emission intensity at 520 nm at an excitation wavelength of 370 nm.

3.3.5 Fourier transform ion cyclotron resonance mass spectrometry

Whole water and SPE DOM were diluted with LC-MS grade MeOH and water, respectively, to give a final sample composition of 50:50 (v/v) MeOH:H_2O. Additionally, SPE samples were diluted to less than 50 mg-C L^{-1} to minimize charge competition during ionization. DOM was continuously injected into an Apollo II ESI ion source of a Bruker Daltonics 12 Tesla Apex Qe FT-ICR MS housed at the William R. Wiley Environmental Molecular Sciences Laboratory, Pacific Northwest National Laboratory. Samples were injected at a rate of 120 µL h^{-1} and were analyzed in negative ion mode. Accumulation of ions in the hexapole ranged from 0.4 - 3s before being transferred to the ICR cell, where 300 scans, collected with a 4 MWord time domain, were co-added for each sample. The summed free induction decay signal was zero-filled once and Sine-Bell apodized prior to fast Fourier transformation and magnitude calculation using Bruker Daltonics Data Analysis software. Similarly, a 50:50 (v/v) MeOH:H_2O blank spectrum was collected to test for contamination.

Mass spectra were externally calibrated using a polyethylene glycol standard and internally calibrated using fatty acids and other CH_2 homologous series naturally present in the sample.[45] Peaks from 250 to 1000 *m/z* with a signal to noise ratio ≥ 4 were added to mass lists, and those peaks detected in the blank spectrum were discarded prior to formula assignments. The presence or absence of peaks between spectra was quantified, where common peaks were defined as *m/z* values that agree within 0.5 mDa of each other.[46] A molecular formula calculator (Molecular Formula Calc v.1.0 ©NHMFL, 1998) generated formulas using carbon, hydrogen,

oxygen, nitrogen, and sulfur. Only formulas that agreed within an error of ≤ ± 1 ppm to the calculated exact mass of the formula were considered, although the majority of formulas (> 85%) had an error of ≤ ± 0.5 ppm. All formula assignments were screened to meet the criteria described by Stubbins et al. (2010). For whole water DOM replicates, 70 - 78% of all peaks were assigned unique formulas (excluding contributions from ^{13}C isotopes), accounting for 69 - 76% of the spectral intensity. For SPE DOM replicates, 70 - 78% of peaks were assigned formulas (excluding contributions from ^{13}C isotopes), accounting for 75 - 86% of the spectral intensity.

3.3.6 Principal component analysis of whole water and SPE DOM

Principal component analysis (PCA) was performed on the twelve DOM samples (including triplicate analyses) to relate characteristics of organic mat and permafrost DOM determined using optical spectroscopy and FT-ICR MS. PCA was carried out on two data matrices. The first data matrix included averaged bulk characteristics from optical spectroscopy (i.e., S_R, FI, Peak C λ_{em}, and Peak C/A) and from FT-ICR MS (MW, O/C, H/C, AI_{mod}, DBE, and DBE/O). The second data matrix included the relative magnitudes of all formulas in the set of twelve spectra.[15,48] If a formula was not detected in a spectrum, the relative magnitude was set to zero. PCA was conducted using IBM SPSS Statistics V.22.

3.3.7 Solid-state ^{13}C NMR analysis of SPE DOM

The remaining SPE DOM replicate eluates from the two DOM sources were pooled prior to freeze drying to ensure enough powdered DOM for solid-state ^{13}C NMR analysis (Step 7; Fig. 3.1). To avoid thawing throughout freeze-drying, the pooled eluate was evaporated in a drying oven at 50 ˚C and then diluted with DI water to a final concentration of 10:90 (v/v) MeOH:H_2O.

The diluted eluate was then transferred to DI-rinsed, pre-combusted flasks and frozen to -80 ˚C prior to loading on to a FreeZone 4.5 L freeze drier (LabConoco). Solid-state ^{13}C NMR spectra of the powdered SPE DOM were obtained using a Varian Infinity CMX 300 MHz spectrometer at the William R. Wiley Environmental Molecular Sciences Laboratory, Pacific Northwest National Laboratory. Powdered SPE DOM was packed into 4 mm zirconia rotors fitted with Teflon spacers and caps. A ramped (^{13}C pulse) cross polarization magic angle spinning (CPMAS) pulse sequence was used. The contact time was 1 ms, the spinning rate was 14 kHz, and the decoupling field was 71 kHz. The ^{13}C chemical shifts were referenced to tetramethylsilane (0 ppm) using an external reference, hexamethylbenzene (methyl C; 17.36 ppm). Functional group distributions were quantified using Mnova NMR software (Metrelab Research) following Cory et al. (2007).

3.3.8 Bacterial respiration, production, and growth efficiency

Bacterial respiration and production rates were quantified following previously described protocols.[5,13] GF/F filtrate of each replicate leachate was inoculated with its native bacterial community (equivalent to 20% of the filtrate volume), which was prepared by GF/C filtering each replicate leachate. Incubations were carried out for six to seven days in the dark at 6 - 7 ˚C. Respiration incubations were carried out in air-tight, pre-combusted 12 mL exetainer vials (Labco, Inc), while production incubations were carried out in 10-mL plastic vials. Respiration was measured as O_2 consumption and CO_2 production relative to killed controls (1% $HgCl_2$). Membrane inlet mass spectrometry was used to measure bacterial O_2 consumption, while a DIC analyzer (AS-C3; Apollo SciTech, Inc.) was used to measure CO_2 production. There was not a shift from aerobic to anaerobic conditions during the short-term incubations. Final O_2

concentrations in the bacterial incubations were 81 ± 21 μM-O_2 and 337 ± 2 μM-O_2 for organic mat and permafrost DOM, respectively. Bacterial production was determined by measuring ^{14}C-labeled L-leucine incorporation into the cold trichloroacetic acid (TCA)-insoluble fraction of macromolecules in two subsamples and one TCA-killed control incubated for 2 - 4 hours at 6 ˚C in the dark. Bacterial growth efficiency was calculated as bacterial production divided by the sum of bacterial production and respiration. Bacterial respiration and production rates were normalized to initial DOC and initial bacterial concentrations. Bacterial concentrations were quantified from gluteraldehyde-fixed samples following Crump et al. (1998). Mann-Whitney U-tests were used to determine statistical significance in bacterial respiration, production, and growth efficiency between organic mat and permafrost DOM ($\alpha = 0.05$; IBM SPSS Statistics V.22).

3.4 Results

3.4.1 DOC concentration and water chemistry of soil leachates

DOC concentrations were significantly higher for leachates containing soil from the organic mat compared to soil from the permafrost layer (Table 3.1). However, when DOC concentrations were normalized to the amount of soil added to each leachate and to the duration of the leaching process, the rate of DOC leached from both soil layers was similar (organic mat: 12.7 ± 0.8 mmol-DOC g-soil^{-1} day^{-1}; permafrost: 13.3 ± 0.4 mmol-DOC g-soil^{-1} day^{-1}). These leaching rates were not normalized to their dry weight contents, which could have influenced the leaching rates. However, both soil types were saturated prior to leaching, which likely minimized the influence of soil moisture on the leaching rates. Leachates from both organic mat and permafrost layers were mildly acidic (organic mat: pH = 5.7 ± 0.1; permafrost: pH = 5.8 ± 0.1).

Conductivity was low for both leachates but was 4-fold higher for whole water leachate of organic mat compared to permafrost soils (organic mat: 37 ± 3 μS cm^{-1}; permafrost: 9 ± 1 μS cm^{-1}). When normalized to the amount of soil added to each leachate and to the duration of the leaching process, conductivity was similar between the leachates (organic mat: 10 ± 1 nS cm^{-1}; permafrost: 8 ± 1 nS cm^{-1}).

3.4.2 Optical characterization of DOM in whole water leachates

There were significant differences in the characteristics of chromophoric (light-absorbing) and fluorescent (light-emitting) DOM in the whole water organic mat and permafrost leachates (Table 3.1). The mean slope ratio (S_R) of organic mat DOM (0.72 ± 0.03) was lower than the mean S_R of permafrost DOM (0.96 ± 0.06), suggesting that organic mat DOM exhibited a higher average molecular weight than permafrost DOM.[34] DOC normalized specific UV absorbance at 254 nm ($SUVA_{254}$; L mg C^{-1} m^{-1}) was higher for organic mat DOM (mean = 2.7 ± 0.1) compared to permafrost DOM (mean = 1.2 ± 0.2), indicating that organic mat DOM contained more aromatic C than permafrost DOM.[33] EEMs of whole water organic mat and permafrost DOM exhibited similar characteristic humic peaks A and C and protein-like peak T [44]. As expected for terrestrially-derived DOM (e.g., Cory et al., 2007), emission intensities were highest for the humic peaks, i.e., peaks A and C > peak T (Table 3.1). There were no differences in the ratio of peak C to peak A between organic mat and permafrost whole water DOM (Table 3.1). The emission maximum (λ_{em}) of peak C for organic mat DOM was shifted to higher wavelengths by 4 ± 3 nm compared to permafrost DOM, suggesting that organic mat DOM was more condensed than permafrost DOM.[51] Average FI was significantly lower for organic mat

DOM (1.49 ± 0.01) compared to permafrost DOM (1.55 ± 0.02), indicating that organic mat DOM contained more aromatic C than permafrost DOM (Table 3.1; McKnight et al., 2001).

3.4.3 FT-ICR MS characterization of whole water DOM

High resolution mass spectrometry analysis of whole water organic mat and permafrost DOM showed that interfering species such as salts contributed significantly to the peak distribution and intensity. At a maximum, 625 salt ions were detected in organic mat DOM and 367 salt ions were detected in permafrost DOM, accounting for 20 and 18% of organic mat permafrost whole water DOM spectral magnitude, respectively (Fig. 3.2). Salt ions, shown as black peaks in Fig. 3.2, were detected across the mass spectrum from 250 - 785 Da, but the majority of salt ions were detected at m/z < 500 Da. On average, 2794 ± 55 and 2390 ± 190 non-salt ions were detected in organic mat and permafrost whole water DOM, respectively (excluding contributions from ^{13}C isotopes; Table 3.2).

The reproducibility between mass spectra of whole water DOM from triplicate experimental leachates was high for both DOM sources. For instance, 74% of all peaks identified in any replicate leachate of organic mat DOM were common to all three replicates, where common peaks were defined as *m/z* values that agreed within 0.5 mDa. A similar result was obtained for triplicate experimental leachates of permafrost DOM, that is, 76% of observed peaks were common to each of the three experimental replicates. Of the subset of peaks common to all replicate spectra, there was a strong, positive correlation between peak intensities (as shown for triplicate spectra of whole water organic mat DOM in Fig. 3.3). Thus, most of peaks identified in a sample were detected at similar intensities in each of the three replicates,

demonstrating a strong similarity in the distribution of the peaks common in each set of replicates of either organic mat or permafrost DOM.

Four major differences were observed between whole water mass spectra of organic mat from permafrost DOM. Firstly, nearly half (49%) of the 2573 individual peaks detected were unique to either organic mat and permafrost DOM, with the remainder of peaks detected present in both organic mat and permafrost DOM. That is, 29% of the 2573 individual peaks detected were found only in organic mat DOM, and 20% were found only in permafrost DOM. Of the peaks common to organic mat and permafrost DOM (51% of all peaks), we expected significantly different distributions of these peaks between DOM sources. To test this hypothesis, we used we used Spearman's rank correlation to identify the degree to which peak intensities were ranked in the same order between organic mat and permafrost DOM. A direct comparison of absolute intensities between organic mat and permafrost DOM was not possible due to differences in DOM concentration and in the presence of salt ions. Spearman's rank correlation between the intensities of the peaks common to both sources of whole water DOM was weak, with coefficients ranging from 0.32 to 0.43 (Table 3.S1). Thus, nearly one quarter to one third of all peaks identified were unique to either organic mat or permafrost DOM, and the distribution of the 51% of peaks common to both DOM sources differed significantly between DOM sources.

Secondly, peak distributions and intensities within nominal masses indicated that organic mat whole water DOM was more oxidized and less saturated compared to permafrost whole water DOM. For instance, comparing peaks detected at nominal *m/z* 503 between whole waters of organic mat vs. permafrost DOM, the majority of peaks detected only in organic mat DOM exhibited more negative mass defects (< 0.1 *m/z*; blue peaks in Fig. 3.4), while the majority of peaks detected only in permafrost DOM exhibited more positive mass defects (> 0.1 *m/z*; red

peaks in Fig. 3.4). Because oxygen exhibits a negative mass defect (exact mass = 15.9949Da), and hydrogen exhibits a positive mass defect (exact mass = 1.0078 Da), peaks with lower mass defects in Fig. 3.4, such as those detected only in organic mat DOM, were more likely to contain oxygen and less likely to contain hydrogen. Thus, peaks unique to organic mat DOM were characterized by a lower mass defect and were thus oxidized and unsaturated compared to the higher mass defect peaks detected only in permafrost DOM. Additionally, of the peaks common to both DOM sources (i.e., black peaks in Fig. 3.4), those peaks with lower mass defects generally exhibited higher relative intensities in organic mat DOM spectra compared to permafrost DOM spectra. These patterns were evident across all odd nominal masses between 250 to 1000 *m/z*, demonstrating that the relative abundance of oxygen-rich and hydrogen-deficient peaks was higher in organic mat DOM compared to permafrost DOM.

Thirdly, formulas unique to organic mat DOM exhibited a higher average O/C ratio and lower average H/C ratio compared to permafrost DOM, demonstrating that the criteria used to convert peak masses to elemental formulas were consistent with the mass defect spacing patterns observed at nominal masses in each spectrum. Analysis in van Krevelen space revealed that formulas unique to organic mat whole water DOM were more oxidized (blue squares in Fig. 3.5a; mean O/C = 0.56) and less saturated (mean H/C = 0.87) compared to formulas unique to permafrost whole water DOM (red circles in Fig. 3.5a; mean O/C = 0.45, mean H/C = 1.39). Lastly, the average molecular weight of formulas in organic mat DOM was 23 Da higher compared to permafrost DOM (organic mat = 511 ± 7 Da; permafrost = 488 ± 3 Da; Table 3.2). Comparing between the subset of formulas unique to each DOM source, the average molecular weight of formulas unique to organic mat DOM was 32 Da higher than the average molecular

weight of formulas unique to permafrost DOM (organic mat = 509 Da, permafrost = 477 Da; Fig. 3.5a).

3.4.4 Optical characterization of SPE DOM

There were significant differences in the characteristics of chromophoric and fluorescent organic mat and permafrost SPE DOM (Table 1). Mean S_R of organic mat SPE DOM (0.64 ± 0.01) was lower than the mean S_R of permafrost SPE DOM (0.88 ± 0.10), suggesting that organic mat DOM exhibited a higher average molecular weight than permafrost DOM.[34] Average $SUVA_{254}$ was higher for organic mat SPE DOM (3.3 ± 0.1) compared to permafrost SPE DOM (1.1 ± 0.2), indicating that organic mat DOM contained more aromatic C than permafrost DOM.[33] EEM emission intensities were highest for the humic peaks C and A compared to protein-like peak T, and there were no differences in the ratio of peak C to peak A between organic mat and permafrost SPE DOM (Table 3.1). The emission maximum of peak C for organic mat SPE DOM was shifted to higher wavelengths by 11 ± 4 nm compared to permafrost SPE DOM, suggesting that organic mat DOM was more condensed than permafrost DOM.[51] Average FI was significantly lower for organic mat SPE DOM (1.42 ± 0.01) compared to permafrost SPE DOM (1.58 ± 0.01), indicating that organic mat DOM contained more aromatic C than permafrost DOM (Table 3.1; McKnight et al., 2001).

3.4.5 FT-ICR MS Characterization of SPE DOM

In contrast to mass spectra of whole water DOM, high resolution mass spectrometry analysis of the SPE fractions of organic mat and permafrost DOM did not exhibit interference from salt ions, that is, interfering ions did not contribute significantly to the peak distribution and

intensity. At a maximum, salt peaks, shown in black in Fig. 3.2, contributed 0.1 and 0.5% of total spectral magnitude in organic mat and permafrost SPE DOM, respectively. The two salt peaks in organic mat SPE DOM ranged in mass from 363 to 727 *m/z*, while the 36 salt peaks in permafrost SPE DOM ranged in mass from 295 to 727 *m/z*. On average, 4478 ± 153 and 3221 ± 22 non-salt ions were detected in organic mat and permafrost SPE DOM, respectively (excluding contributions from ^{13}C isotopes; Table 3.2).

Similar to the results from whole water DOM spectra, the reproducibility between mass spectra of SPE DOM from triplicate experimental leachates was high for both DOM sources. For instance, 71% of all peaks identified in any replicate leachate of organic mat SPE DOM were common to all replicates, while 73% of all peaks observed in permafrost SPE DOM were common to each of the three experimental replicates. As observed between replicate spectra of whole water DOM, peak intensities were strongly linearly correlated between replicates of SPE spectra for organic mat or permafrost DOM (Fig. 3.S1).

Similar to whole water fractions of both DOM sources, four mass spectral features distinguished organic mat from permafrost SPE DOM. Firstly, 57% of the 3868 individual peaks detected were unique to either organic mat or permafrost SPE DOM; 39% were unique to organic mat SPE DOM, and 18% were unique to permafrost SPE DOM. Of the 43% of peaks common to both organic mat and permafrost SPE DOM, Spearman's rank correlation between their intensities was weak, with coefficients ranging from 0.26 to 0.39 (Table 3.S1). Thus, while 43% of all peaks were common to both DOM sources, the intensities of these common peaks differed significantly between DOM sources, indicating that organic mat SPE DOM had a different distribution of the common peaks compared to permafrost SPE DOM.

As observed for whole water DOM, peak distributions and intensities within nominal masses indicated that organic mat SPE DOM was more oxidized and less saturated compared to permafrost SPE DOM. Again comparing within nominal *m/z* 503, the majority of peaks detected only in organic mat SPE DOM exhibited defects < 0.1 (blue peaks in Fig. 4), while the majority of peaks detected only in permafrost SPE DOM exhibited defects > 0.1 (red peaks in Fig. 3.4) Additionally, of the peaks common to SPE fractions of both DOM sources (black peaks in Fig. 3.4), those peaks with lower mass defects generally exhibited higher relative intensity in organic mat DOM spectra compared to permafrost DOM spectra, suggesting that the relative abundance of oxygen-rich and hydrogen-deficient peaks was higher in organic mat SPE DOM compared to permafrost SPE DOM.

Consistent with peak distribution patterns within nominal masses, formulas unique to organic mat SPE DOM also revealed that organic mat DOM exhibited a higher average O/C ratio and lower average H/C ratio compared to permafrost SPE DOM. Analysis in van Krevelen space revealed that formulas unique to organic mat SPE DOM were more oxidized (blue squares in Fig. 3.5b; mean O/C = 0.61) and less saturated (mean H/C = 0.81) compared to formulas unique to permafrost SPE DOM (red circles in Fig. 3.5b; mean O/C = 0.29, mean H/C = 1.20). Lastly, the average molecular weight of formulas in organic mat SPE DOM was 71 Da higher compared to permafrost SPE DOM (organic mat = 585 ± 6 Da; permafrost = 514 ± 9 Da; Table 3.2). The average molecular weight of formulas unique to organic mat SPE DOM was 86 Da higher than the average molecular weight of formulas unique to permafrost SPE DOM (organic mat = 592 Da, permafrost = 506 Da; Fig. 3.5b).

3.4.6 The effects of salt ions and isolation on FT-ICR MS characterization of DOM

Differences between mass spectra of whole water and SPE fractions of each DOM source were likely due to the effects of interfering salt ions and the SPE isolation process. For instance, compared to SPE DOM, spectra of whole water DOM contained 15 and 20% more salt ions, and 60 and 35% fewer non-salt peaks for organic mat and permafrost DOM, respectively (Table 2). Because salt ions suppress the ionization of organic compounds,[35] the increased presence of salt ions along with fewer organic peaks in whole water spectra (relative to SPE spectra) suggested that salt ions decreased the number of organic formulas detected in whole water DOM compared to SPE DOM. To determine the influence of salt ions on the distribution of peaks detected in the whole water DOM mass spectra, we used Spearman's rank correlation to test the similarities in peak intensities for the subset of peaks common to both whole water and SPE fractions of the same DOM source. This analysis showed that peak intensities were strongly correlated between whole water and SPE spectra for either organic mat or permafrost DOM, with coefficients ranging from 0.77 to 0.89 (Table 3.S1). To determine if new compositional information was gained from the "additional" peaks detected in the SPE spectra, we compared formulas detected only in the whole water fraction to formulas detected only in the SPE fraction of each DOM source (Figs. 5c and d) with the assumption that "additional" formulas unique to SPE were those that were quenched by salts, and thus undetected in the whole water fraction. There was large overlap in van Krevelen space between formulas unique to the whole water fraction, formulas unique to the SPE fraction, and formulas common to both fractions of each DOM source (Figs. 3.5c and d). This result indicated that while fewer formulas were detected in the whole water spectra of each DOM source due to the effect of salts, the additional formulas detected in the SPE fraction did not add new information on chemical composition because there was strong

overlap in the chemical composition of formulas detected in whole water and SPE DOM, for both organic mat and permafrost DOM.

In addition to the influence of interfering salt ions, it was likely that isolation of DOM by SPE resulted in lower detection of highly oxidized formulas by mass spectrometry because these formulas have been shown to exhibit poor retention on SPE resins.[36,52] Consistently, the whole water fraction of both DOM sources contained a cluster of highly oxidized formulas (O/C > 0.8; Figs. 3.5c and d) that were absent in the SPE fraction, suggesting that these compounds exhibited poor sorption affinity to the PPL solid phase during extraction.

3.4.7 ^{13}C NMR Characterization of SPE DOM

Integration of resonance spectra of SPE DOM according to dominant functional or structural groups revealed compositional differences between organic mat and permafrost DOM (Figure 3.6). Organic mat SPE DOM was enriched in aromatic C compared to permafrost SPE DOM; the ratio of aromatic to aliphatic C (i.e., resonance from 110 - 160 ppm divided by resonance from 0 - 110 ppm) was 29% higher for organic mat compared to permafrost SPE DOM. Organic mat SPE DOM was enriched in oxygen-containing functional groups compared to permafrost SPE DOM; containing higher carboxyl C, and ketone and aldehyde C by 4% each. Organic mat SPE DOM was depleted in carbohydrate C (60 - 90 ppm) by 10% compared to permafrost SPE DOM.

3.4.8 Principal component analysis of whole water and SPE DOM

Principal component analysis of average optical and mass spectrometry chemical characteristics reduced the dataset into two components that distinguished organic mat from

permafrost DOM and whole water from SPE DOM. Sample scores of experimental replicates were tightly grouped, and there was less sample score variability between replicates compared to the variability between DOM sources and fractions (Fig. 3.7). The first component (PC1) explained 71% of the sample variance, and was positively related to aromaticity. The second component (PC2) explained 21% of the sample variance, and was negatively related to oxygen content. Comparing organic mat to permafrost DOM, organic mat DOM was enriched in high molecular weight, low H/C, and high O/C formulas, as shown by positive PC1 scores and negative PC2 scores relative to permafrost DOM. Comparing whole water to SPE DOM, whole water DOM was enriched in low molecular weight, high H/C, and high O/C formulas, as shown by negative PC1 and PC2 scores relative to SPE DOM (Fig. 3.7).

Principal component analysis of the relative magnitude of all formulas detected in the twelve DOM spectra reduced the dataset into two components that distinguished formulas enriched in organic mat or permafrost DOM and formulas enriched in whole water or SPE DOM (Fig. 3.S2a). Similar to the principal component analysis of average characteristics (Fig. 3.7), sample scores of experimental replicates were tightly grouped, and there was less variability between replicates compared to the variability between DOM sources and fractions. The first component (PC1) explained 31% of the sample variance and separated the DOM source (organic mat vs. permafrost; Fig. 3.S2a). The second component explained 15% of the sample variance and separated whole water from SPE fractions of DOM (Fig. 3.S2a).

Using the results from the principal component analysis, formulas that were relatively enriched in each DOM source were identified by comparing sample and formula scores (Figs. 3.S2a and b). In total, six-color coded regions were identified based upon the co-location of sample and formula scores, corresponding to formulas that are relatively enriched in those

samples (Figs. 3.S2a and b). For example, formulas in the light blue box in Fig. 3.S2b had high PC1 scores (i.e., > 0.80), similar to organic mat SPE DOM replicates in Fig. 3.S2a that also had high PC1 scores. Thus, formulas in the light blue box were relatively enriched in organic mat SPE DOM compared to all other DOM spectra. Accordingly, the summed relative magnitude of formulas in the light blue box was at a minimum 4-fold higher in the organic mat SPE DOM replicates compared to all other spectra (Table 3.S2).

Plotting formulas enriched in each DOM source in van Krevelen space revealed the subset of all formulas that were most important in explaining differences between organic mat and permafrost DOM (i.e., blue squares vs. red circles in Fig. 3.8). For example, formulas of greater relative abundance in organic mat DOM were tightly clustered with low H/C that spanned O/C 0.45 - 0.8, while formulas of greater relative abundance (and thus more prominent) in permafrost DOM were clustered in the central region of the van Krevelen plot (Fig. 3.8). Additionally, the average molecular weight of formulas more prominent in organic mat DOM was 101 Da greater than the average molecular weight of formulas characteristic to permafrost DOM, further demonstrating the compositional differences between organic mat and permafrost DOM.

3.4.9 Dark bacterial respiration rates of organic mat and permafrost DOM

Volumetric rates of bacterial respiration, measured as O_2 consumption and CO_2 production per day, were higher for organic mat compared to permafrost DOM (organic mat DOM: O_2 consumption = 41.7 ± 4.9 μM-O_2 d^{-1}, CO_2 production = 30.5 ± 8.0 μM-CO_2 d^{-1}; permafrost DOM: O_2 consumption = 1.9 ± 0.3 μM-O_2 d^{-1}, CO_2 production = 1.6 ± 0.7 μM-CO_2 d^{-1}). Average volumetric rates of bacterial production were similar between organic mat and

permafrost DOM (organic mat DOM = 9.4 ± 4.3 μM-C d^{-1}; permafrost DOM = 6.2 ± 0.5 μM-C d^{-1}). When bacterial respiration and production rates were normalized to initial DOC concentration and cell abundance in organic mat and permafrost DOM (Table 3.1), respiration rates were similar between DOM sources, but production rates were significantly higher for permafrost compared to organic mat DOM (Fig. 3.9). Additionally, bacterial growth efficiency was significantly lower for organic mat DOM (20 ± 14%) compared to permafrost DOM (80 ± 7%; Fig. 3.9).

3.5 Discussion

3.5.1 FT-ICR MS reproducibility and the effects of interfering species, isolation, and instrumentation on DOM chemical composition

Based on the strong overlap in peak mass and intensity between replicate mass spectra, DOM composition as analyzed by FT-ICR MS was highly reproducible (Tables 3.2 and 3.S1, Figure 3.3). High reproducibility of DOM mass spectra has previously been reported,[46] where 70% of peaks detected in mass spectra of riverine SPE DOM were common to experimental replicates, similar to the 71 - 76% overlap in peak detection reported here for replicates of organic mat and permafrost SPE DOM. The degree of reproducibility between replicate spectra served as a baseline for evaluating the much larger differences in DOM composition observed between DOM fractions (whole water vs. SPE) and sources (organic mat vs. permafrost). For example, there were fewer common peaks detected between different fractions of the same DOM source (43 - 45% for whole water vs. SPE), or between the different DOM sources (43 - 51% for organic mat vs. permafrost), relative to the 71 - 76% detected among any set of replicate spectra. Furthermore, Spearman rank correlation of common peak intensities between experimental

replicates was significantly stronger compared to correlation between DOM fractions and sources; correlation coefficients between replicates ranged from 0.95 - 1.00, correlation coefficients between fractions ranged from 0.77 - 0.89, and correlation coefficients between sources ranged from 0.13 - 0.43 (Table 3.S1). These results demonstrated that the observed differences in chemical composition of DOM by fraction or by source were significant, consistent with the groupings in DOM composition by whole water vs. SPE or organic mat vs. permafrost DOM as separated by principal component analysis (Figs. 3.7 and 3.S2a).

Smaller compositional differences between whole water and SPE fractions of DOM compared to differences between DOM sources is consistent with studies of freshwater DOM.[48] Differences in DOM composition by FT-ICR MS between whole water and SPE were likely predominantly due to preferential loss of high O/C formulas during SPE isolation; by comparison, salts or other interfering species had minor influence on the mass spectra and thus DOM composition. Based on principal component analysis (Fig. 3.7), separation of DOM between whole water and SPE fractions occurred along the PC2 axis, which accounted for only 21% of the variability in DOM composition and suggested that the greater number of high O/C compounds in the whole water was the key distinction between whole water and SPE DOM. Fewer formulas with high O/C in the SPE fractions was likely due to preferential loss of highly oxidized formulas during SPE isolation, consistent with previous observations of incomplete recovery and fractionation of DOM during isolation.[36,37]

While salts resulted in the detection of fewer DOM formulas in the whole water spectra compared to the SPE spectra, the “additional” formulas detected by SPE had similar chemical composition as formulas detected in the whole water, as evidenced by their overlap in van Krevelen space (Fig. 3.5). This result together with the loss of high O/C formulas during SPE

isolation suggested that for DOM in soils similar to those studied here (i.e., low conductivity, relatively high DOM concentrations), SPE isolation may result in a stronger bias on DOM composition as analyzed by FT-ICR MS compared to the effects of salts when analyzing whole water DOM. However, independent of the fraction of DOM analyzed, FT-ICR MS analysis of DOM is "blind" to some compound classes, based on comparison to characterization by solid-state ^{13}C NMR.

Compared to compound class distributions measured by ^{13}C NMR, FT-ICR MS significantly overestimated aromatic C and underestimated carbohydrate C, which has previously been reported for freshwater and marine DOM.[25–27] For instance, compared to ^{13}C NMR, the fraction of aromatic C was 11 - 22% higher and the fraction of carbohydrate C (defined in Stubbins et al., 2010) was 22 - 33% lower when analyzed by FT-ICR MS (Figs. 3.5 and 3.6). Discrepancies in compound class distributions between ^{13}C NMR and FT-ICR MS have been attributed to greater ionization efficiency of aromatics compared to carbohydrates because the assumption is that ^{13}C NMR has less bias in compound class detection compared to FT-ICR MS.[25,26]

However, ^{13}C NMR is susceptible to biases that occur when DOM is isolated and concentrated from water prior to ^{13}C NMR analysis to remove interfering impurities (e.g., paramagnetics) present in water. For example, the presence of highly oxidized compounds in the whole water mass spectra (i.e., those that were not retained by the solid phase resin during extractions), suggested that the abundances of oxygen-containing functional groups detected by ^{13}C NMR were likely a minimum (i.e., carboxyl, aldehyde, and ketone; Fig. 3.6). Despite biases in absolute amounts of compound classes or functional groups of DOM depending on the technique used, the relative differences in organic mat and permafrost DOM chemical

composition were consistent across all methods and statistical analyses. The agreement in relative differences in DOM character across multiple characterization techniques has previously been reported for freshwater[15,25] and soil DOM.[53]

3.5.2 Compositional differences between organic mat and permafrost DOM

Examining either optical proxies for DOM composition or direct measurements of DOM composition by FT-ICR MS or ^{13}C NMR, all analyses indicated that DOM leached from the shallower organic mat contained higher molecular weight, more oxidized, and more unsaturated, aromatic species compared to DOM leached from the deeper permafrost layer (Tables 3.1, 3.2, and 3.S1 Figs. 3.4, 3.5, 3.6, and 3.7). These differences in DOM composition between organic mat and permafrost soil layers were consistent with previous observations in arctic [13,14,21] and sub-arctic soils.[53–56] For instance, Cory et al. (2013) used optical proxies to show that organic mat DOM contained higher aromatic C and higher average molecular weight compared to permafrost DOM. That is, Alaskan Arctic surface waters that primarily drained the shallower organic mat of soils exhibited higher $SUVA_{254}$, lower slope ratio, and lower fluorescence index compared to surface waters impacted by thermokarsts or hillslope failures that primarily drained deeper mineral-rich soils. In addition, DOM collected from a shallower active layer bog site in Swedish permafrost soils contained higher molecular weight, more oxidized, and more unsaturated species compared to DOM from a deeper active layer fen site.[21]

These differences in soil DOM chemical composition between the shallower organic mat and deeper permafrost layer were consistent with a conceptual model proposed for DOM processing in soils. This “downward cycling” model for DOM predicts a shift in DOM composition between surface organic layers and deeper mineral layers due to the net effects of

sorption to mineral phases, microbial degradation, and mobilization within the soil column.[57] Factors contributing to the downward cycling model include vegetation, soil acidity, and exchangeable iron and aluminum. Dominant vegetative species within the Imnavait Creek watershed include moss (S*phagnum*) and tussock (*Eriophorum vaginatum*), both of which trap moisture and release organic acids, contributing to increased soil acidity.[39] Consequently, lower soil pH significantly increases exchangeable iron and aluminum concentrations,[58] which likely increases the relative importance of DOM sorption to mineral phases compared to other controls on DOM composition with depth. Compounds enriched in organic mat DOM in this study, i.e., higher molecular weight compounds, aromatics, or compounds rich in carboxyl functionalities, exhibit higher sorption capacities to iron and aluminum oxides and thus are typically immobilized, protected from microbial degradation, and enriched in shallow soils.[57] Compounds enriched in permafrost DOM, i.e., lower molecular weight compounds, aliphatics, or compounds poor in carboxyl functionalities, exhibit lower sorption capacities, and thus are not protected from microbial degradation, leading to the accumulation of these compound classes and their degradation products in deeper soils.[57] Consistently, a study of DOM sorption processes in Siberian permafrost soils reported that hydrophobic, aromatic DOM was preferentially retained by shallower, acidic layers of the soil that were rich in iron oxides compared to deeper horizons.[59]

3.5.3 Bacterial degradation of DOM draining arctic permafrost soils

Given the importance of substrate quality on bacterial degradation in arctic surface waters,[11,12] we expected the substantial differences in chemical composition between organic mat and permafrost DOM to affect the bacterial degradation of DOM drained from these soil layers. However, there was no significant difference in rates of bacterial respiration (normalized to DOC

and bacterial cell concentrations) between organic mat and permafrost DOM (Fig. 9), and both were within the range of previously reported rates for DOM draining pan-arctic soils.[5,9,10,13] In contrast, bacterial production rates and growth efficiencies were significantly higher for permafrost compared to organic mat DOM (Fig. 3.9). Bacterial growth rate and efficiency have been strongly, inversely correlated to the oxidation state of DOM,[18–20] suggesting that compounds with a lower oxidation state may be used more efficiently by bacteria. Consistently, permafrost DOM had a lower average O/C and fewer compounds at the higher O/C range, and was more efficiently used by bacteria (i.e., less CO_2 respired per DOC consumed) compared to organic mat DOM (Fig. 3.9).

While not significant, higher respiration rates for permafrost DOM compared to organic mat DOM in this study were consistent with reported inverse correlations between proxies for aromatic C content and DOM lability in surface waters draining permafrost soils.[9,14] Mann et al. (2014) suggested that phenolic compounds, i.e., aromatics substituted with hydroxyl functional groups, inhibited bacterial activity and thus slowed the respiration of DOM drained from the organic mat compared to the deeper permafrost layer. Consistently, organic mat DOM in this study contained more aromatics and more oxygen-containing functional groups than permafrost DOM (Figures 3.6 and 3.8).

However, despite large differences in aromatic and phenolic content, no significant difference in respiration rates or relationship between aromatic C and respiration rates in some studies suggests that DOM degradation by aquatic bacteria is likely more complex than predicted based on aromatic or phenolic content alone (Cory et al., 2013 and this study). We offer two explanations for these contrasting relationships between aromatic C content and respiration rates. Firstly, aromatic compounds may concurrently inhibit and support bacterial respiration. An

alternative to the phenolic inhibition hypothesis[10,16] is that native bacterial communities degraded aromatics, including the phenolic fraction. Aromatic compounds are abundant in soil and surface waters in the Arctic (Cory et al., 2007; Waldrop et al., 2010; this study), the pathways used by microorganisms to metabolize aromatics (including phenolic compounds) are well characterized, [61] and aromatics have been found to support bacterial respiration in other waters where the dominant source of DOM is plant and soil organic matter rich in aromatic C.[15,30,62] Secondly, the content of aromatic C may not be a causal factor controlling rates of bacterial respiration. Other aspects of DOM composition that may co-vary with aromatic C may be important. For example, the distinguishing feature of permafrost DOM was low molecular weight, highly saturated aliphatic compounds depleted in oxygen (Fig. 3.8). Relative to aromatic compounds, these low molecular weight aliphatics are expected to be more labile to bacteria.[15,18–20] Thus, the abundance of relatively more labile oxygen-poor, aliphatic compounds may account for the observed increased bacterial growth efficiency or respiration of permafrost DOM once thawed and exported to surface waters (Mann et al., 2014; Abbott et al., 2014; this study).

3.5.4 Conclusions and implications

Several studies have demonstrated that warming surface temperatures in the Arctic is deepening hydrologic flow paths through soils and increasing the export of permafrost DOM to arctic surface waters.[3,8,63] The results from this study demonstrated that an increase in the export of permafrost DOM to surface waters will result in DOM that has a lower $SUVA_{254}$ (absorbs less light per DOC), and is comprised of smaller, more saturated, and less oxidized species compared to DOM currently flushed to surface waters. Permafrost DOM is more labile to bacteria, as indicated by the significantly higher bacterial production rates and growth efficiencies compared to organic mat DOM. Thus a shift in DOM source is expected to change the rates and pathways

of DOM degradation in surface waters compared to DOM currently draining the shallow active layer. However, conversion of permafrost DOM to CO_2 by bacterial respiration could be the same (this study) or up to 1.6 times greater[10] than respiration of DOM currently draining the organic mat of arctic soils. Taking the results from our study as a conservative estimate (i.e., no difference in rates of bacterial respiration between permafrost and organic mat DOM; Fig. 3.9), and assuming no changes in the lateral transfer of DOM with permafrost thaw, a shift in the composition of DOM from organic mat to permafrost character may not change the amount of DOM that is respired by bacteria to CO_2 in soil waters, surface waters, and aquatic sediments, and subsequently released from arctic surface waters to the atmosphere.[5–8,38]

Thus, bacterial respiration of permafrost DOM will continue to contribute significantly to the CO_2 fluxes from freshwaters that currently account for up to 40% of the net land surface C exchange with the atmosphere.[5,6,38] Given that bacterial respiration may increase by a factor of 1.6,[10] and conversion of DOM to CO_2 by sunlight was most often three to 10-fold greater than rates of bacterial respiration for DOM in the water column of arctic lakes and streams,[5] photo-mineralization of DOM may continue to dominate DOM degradation in the water column. However, "dark" bacterial respiration of DOM in soil waters and in aquatic sediments likely contributes more CO_2 released from surface waters to the atmosphere than photo-mineralization. Therefore, degradation of DOM by both bacteria and sunlight will continue to be important for DOM fate as more permafrost DOM is exported to surface waters,[5,13] and understanding the controls on both bacterial and photochemical degradation of permafrost DOM is critical for predicting changes in the magnitude of CO_2 released to the atmosphere as permafrost soils continue to thaw.

3.6 Acknowledgements

We thank J. Dobkowski, K. Harrold, A. Clinger, S. Michael, M. Stuart, S. Nalven, and researchers, technicians, and support staff of the Toolik Lake Arctic LTER for assistance in the field and laboratory. Thanks to B. C. Crump and G. W. Kling for contributing to the development and execution of the experimental design, and for feedback on earlier versions of this manuscript. FT-ICR MS and ^{13}C NMR analyses were performed at EMSL, a DOE Office of Science User Facility sponsored by the Office of Biological and Environmental Research and located at Pacific Northwest National Laboratory. Thanks to K. Roscioli and S. Burton for assisting with the FT-ICR MS and ^{13}C NMR analyses, respectively. Thanks to the anonymous reviewers whose comments improved the quality of this manuscript. Research was supported by NSF OPP–102327.

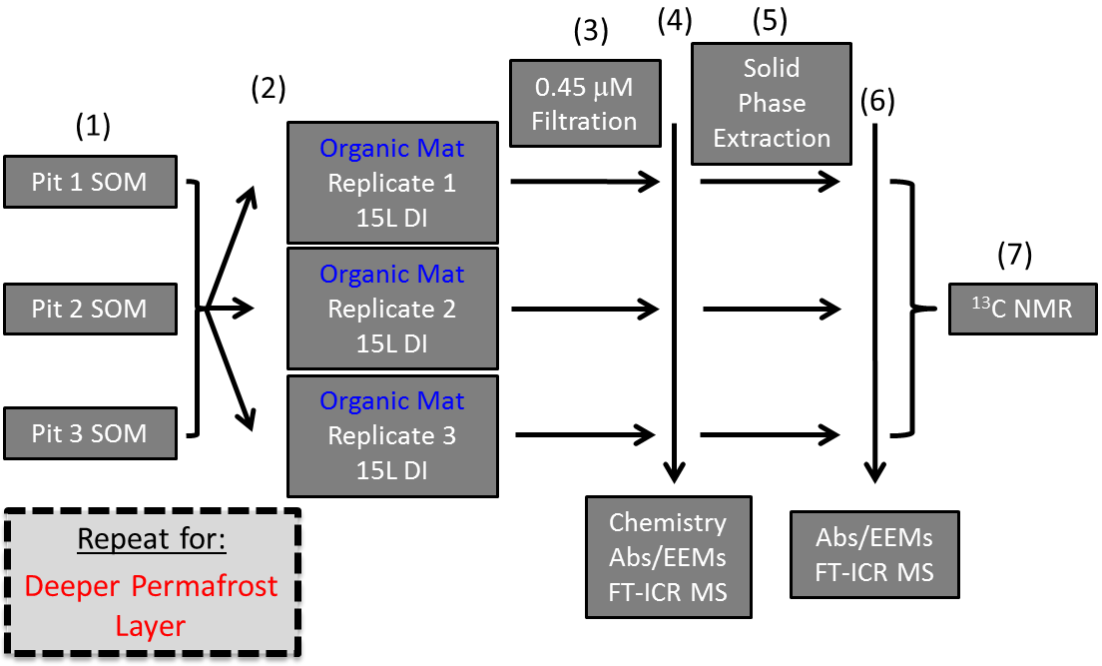

Figure 3.1. Experimental design for leaching and isolating DOM from the shallower organic mat and deeper permafrost layers of arctic soils.

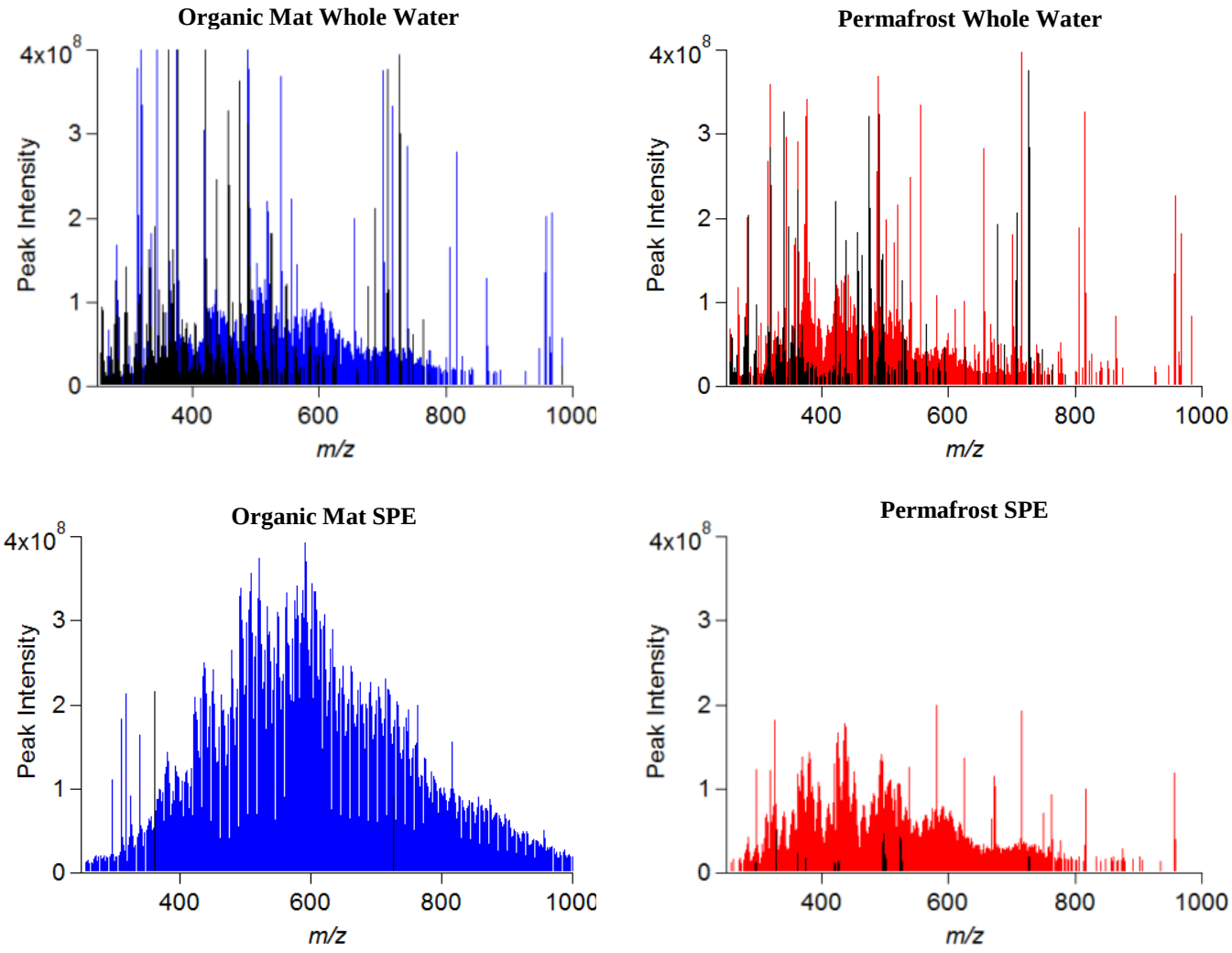

Figure 3.2. Mass spectra of whole water and solid phase extraction (SPE) organic mat and permafrost DOM. Black peaks are salt ions.

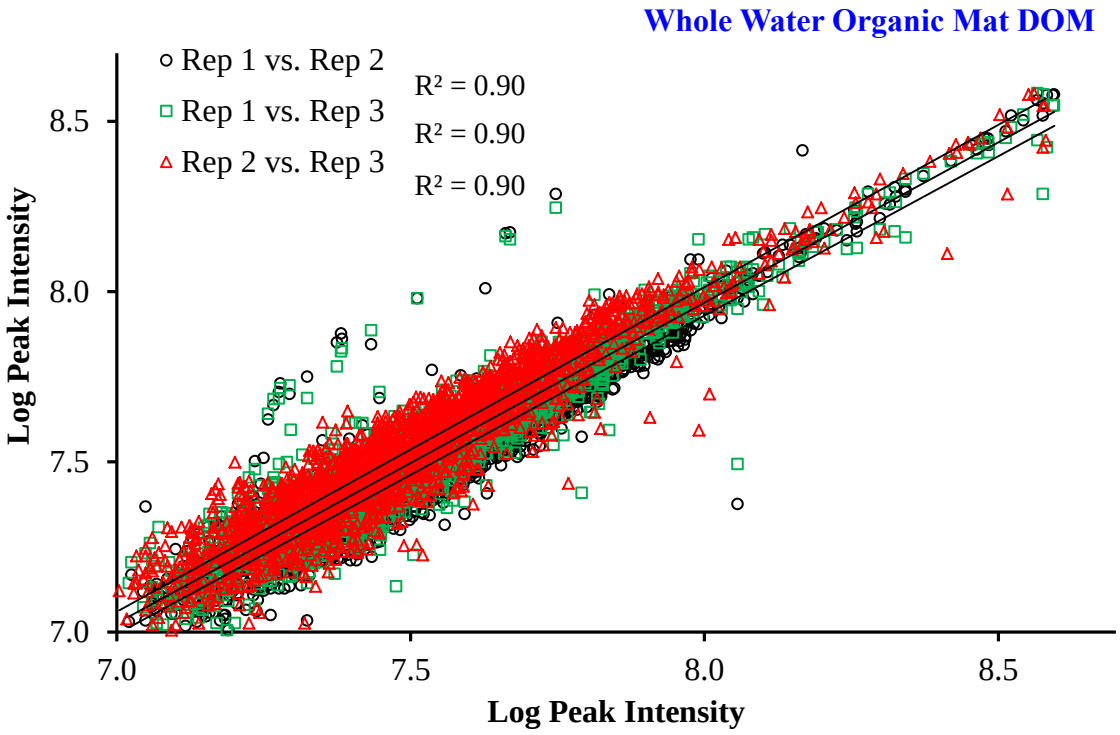

Figure 3.3. Linear correlations between FT-ICR MS peak intensities of experimental replicates of whole water organic mat DOM.

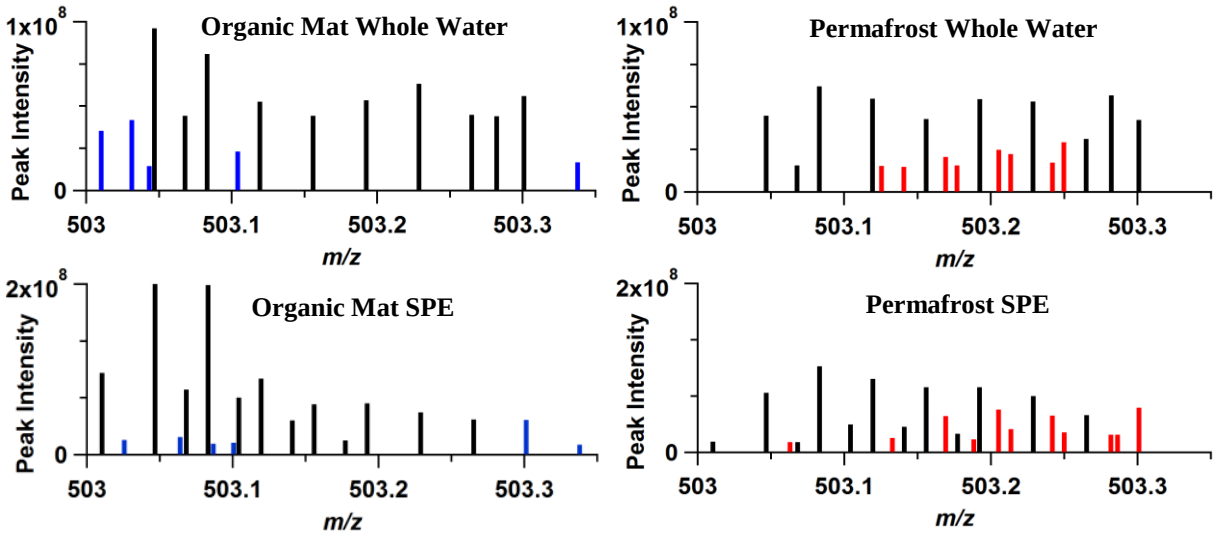

Figure 3.4. Nominal *m/z* 503, where blue peaks were detected only in organic mat DOM, red peaks were detected only in permafrost DOM, and black peaks were detected in organic mat and permafrost DOM.

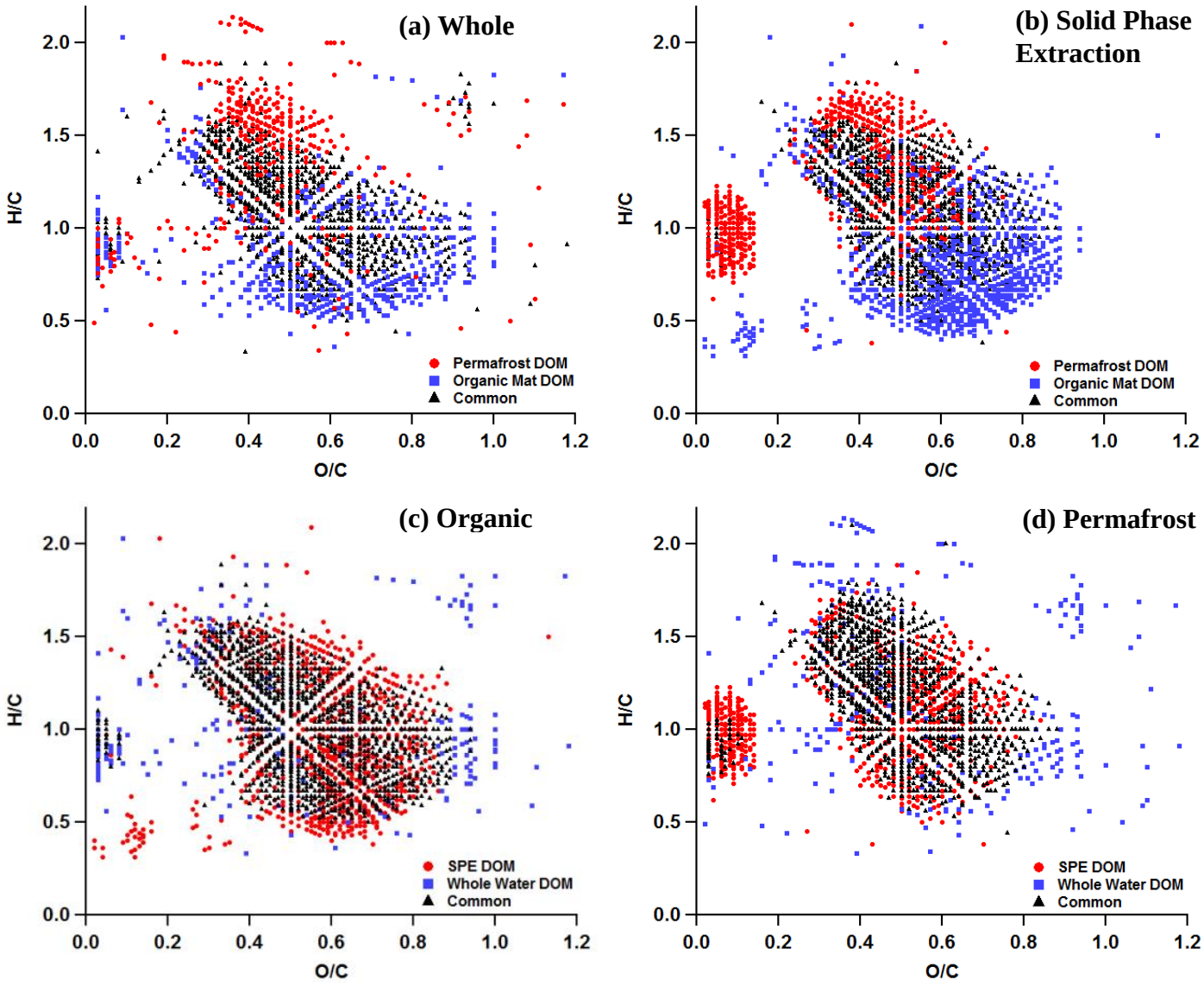

Figure 3.5. van Krevelen diagrams demonstrating differences between **a)** whole water fractions of organic mat and permafrost DOM, **b)** solid phase extraction fractions of organic mat and permafrost DOM, **c)** whole water and SPE fractions of organic mat DOM, and **d)** whole water and SPE fractions of permafrost DOM.

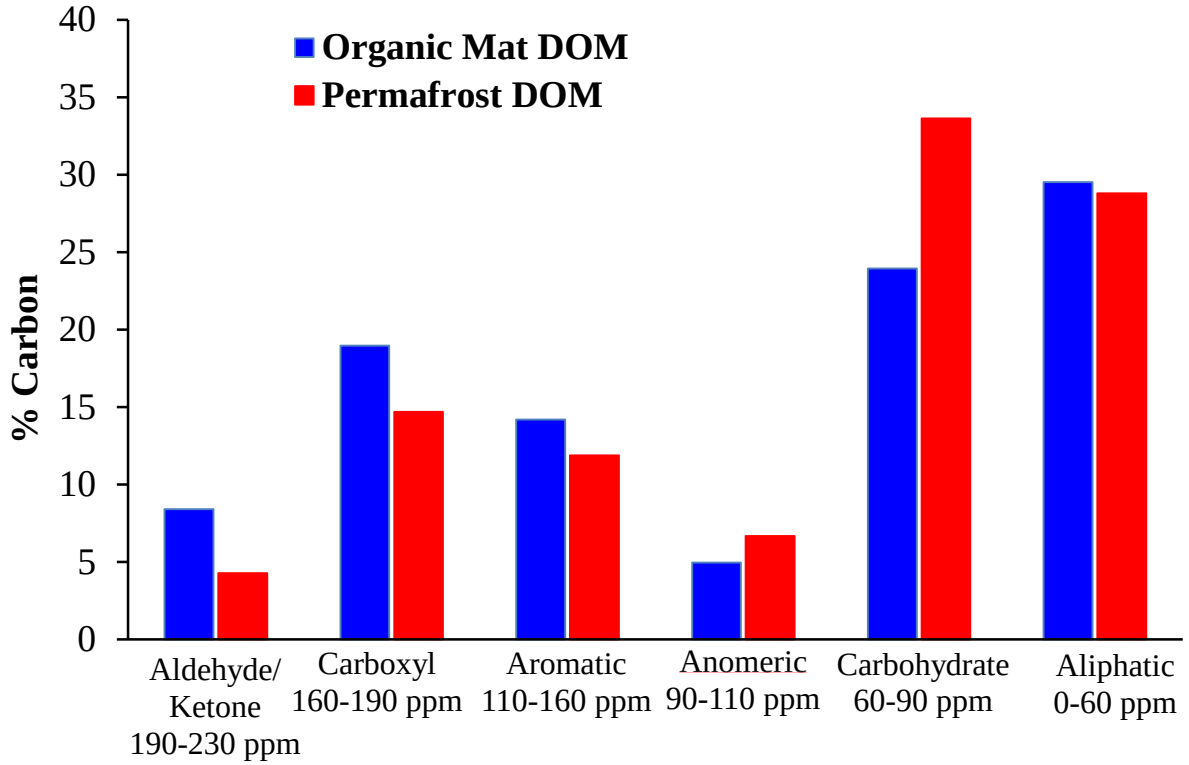

Figure 3.6. Functional group distributions of organic mat SPE DOM (blue bars) and permafrost SPE DOM (red bars) determined using ^{13}C NMR. Integration regions are listed below each functional group following Cory et al. (2007).

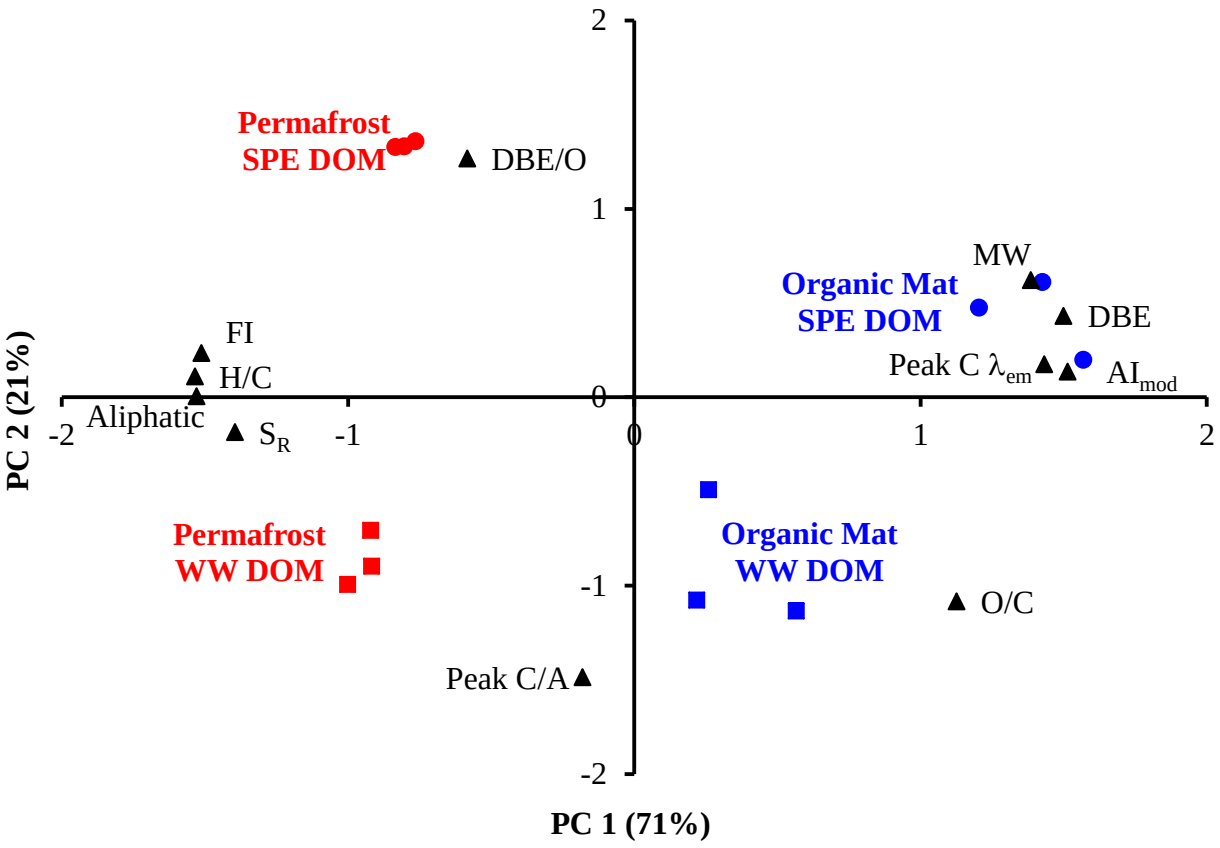

Figure 3.7. Bi-plot from principal component analysis of number-averaged chemical characteristics determined using optical spectroscopy and FT-ICR MS. Black triangles are variable loading scores.

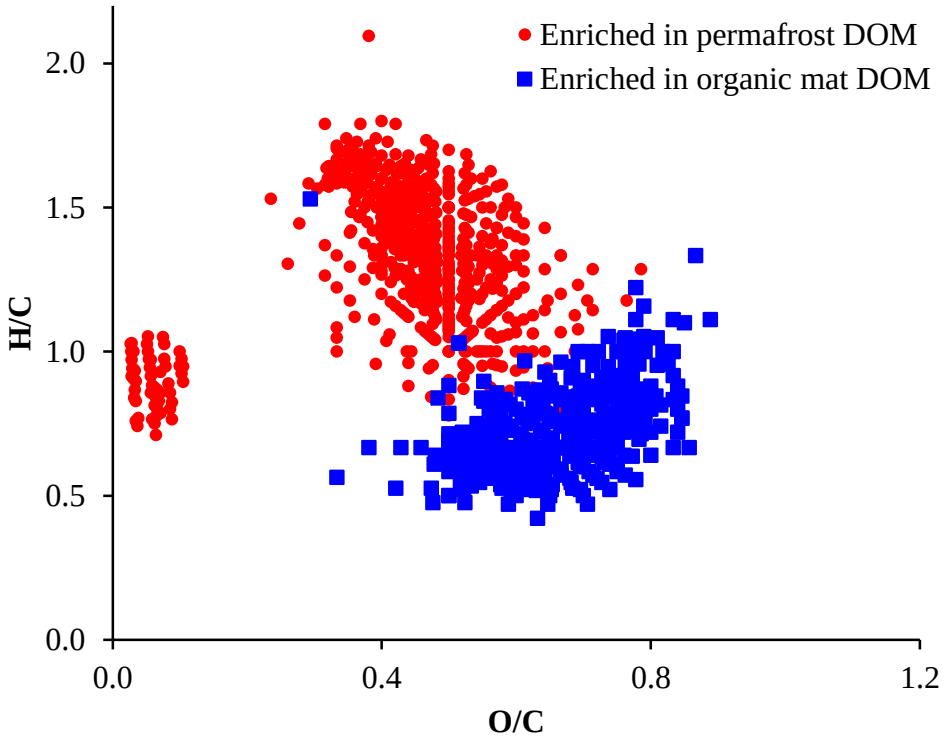

Figure 3.8. van Krevelen diagrams of formulas that were enriched in organic mat DOM (blue square on PCA loading plot; Fig. S2) and permafrost DOM (red square on PCA loading plot; Fig. S2). Summed spectral intensities of formulas are listed in Table S2.

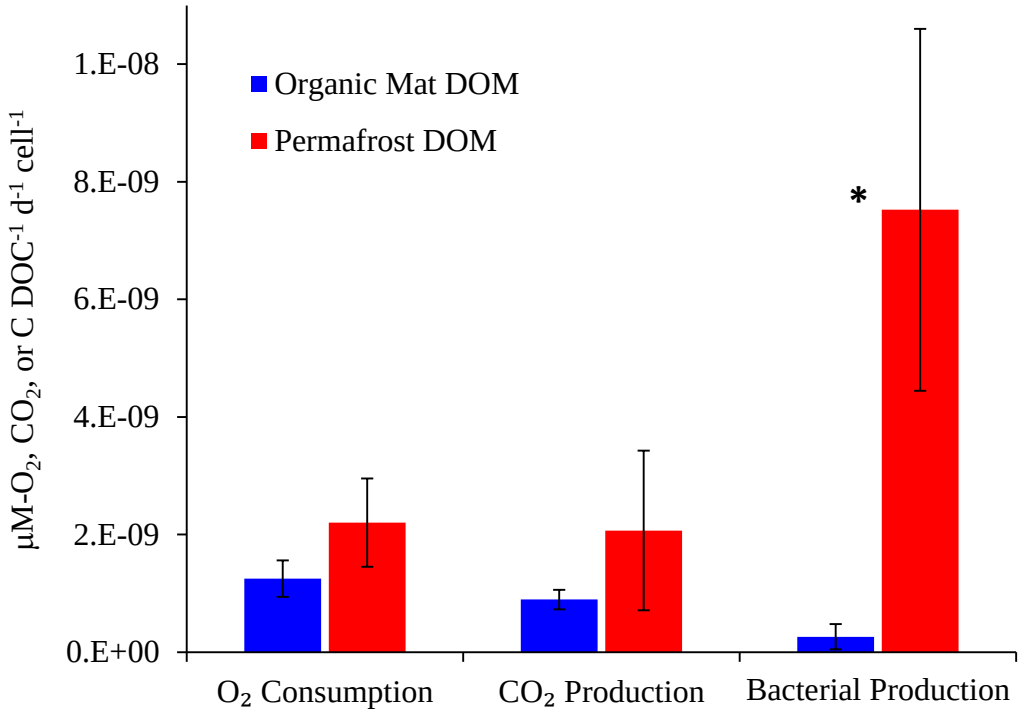

Figure 3.9. DOC and cell concentration normalized bacterial respiration (O_2 consumption and O_2 production), and bacterial production rates. Error bars indicate ± standard deviation from the mean of experimental triplicates. *****designates statistical significance at $\alpha = 0.05$.

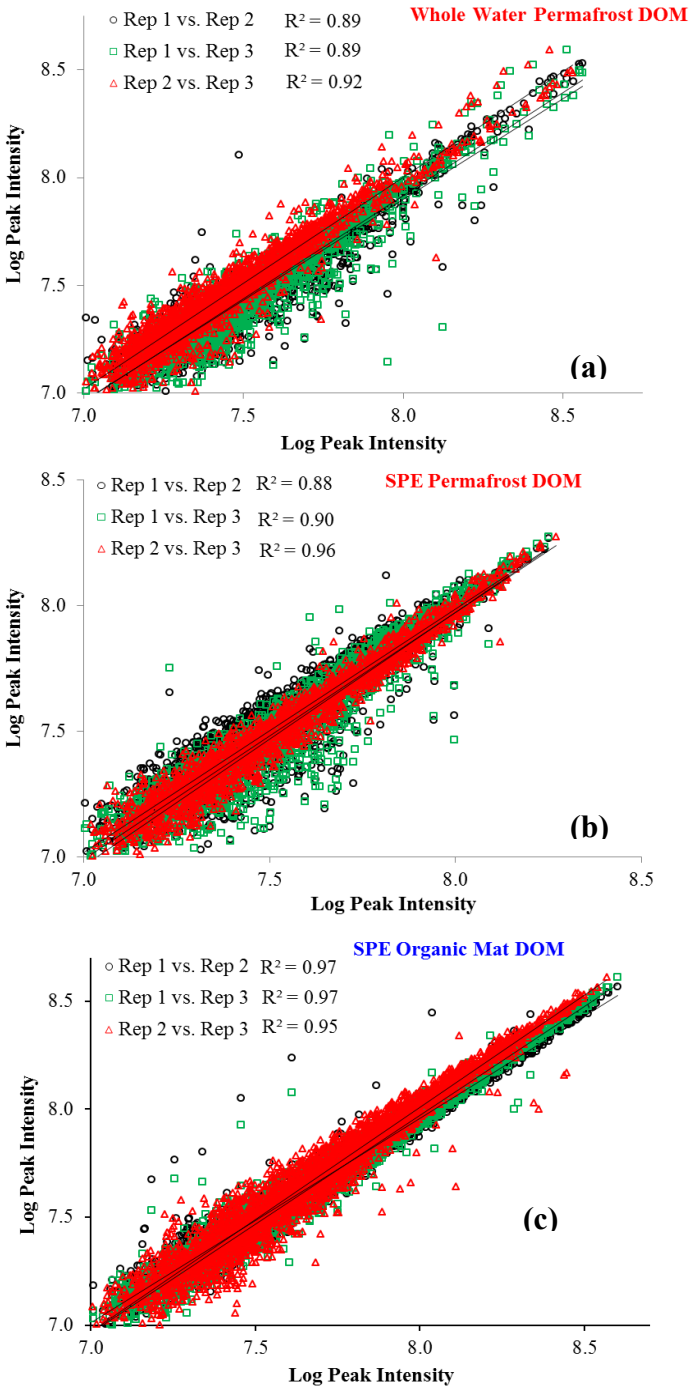

Figure S1: Linear correlations between FT-ICR MS peak intensities of experimental replicates of (a) whole water permafrost DOM, (b) SPE permafrost DOM, and (c) SPE organic mat DOM. Correlations between replicates of whole water organic mat DOM shown in Fig. 3.3 of main text.

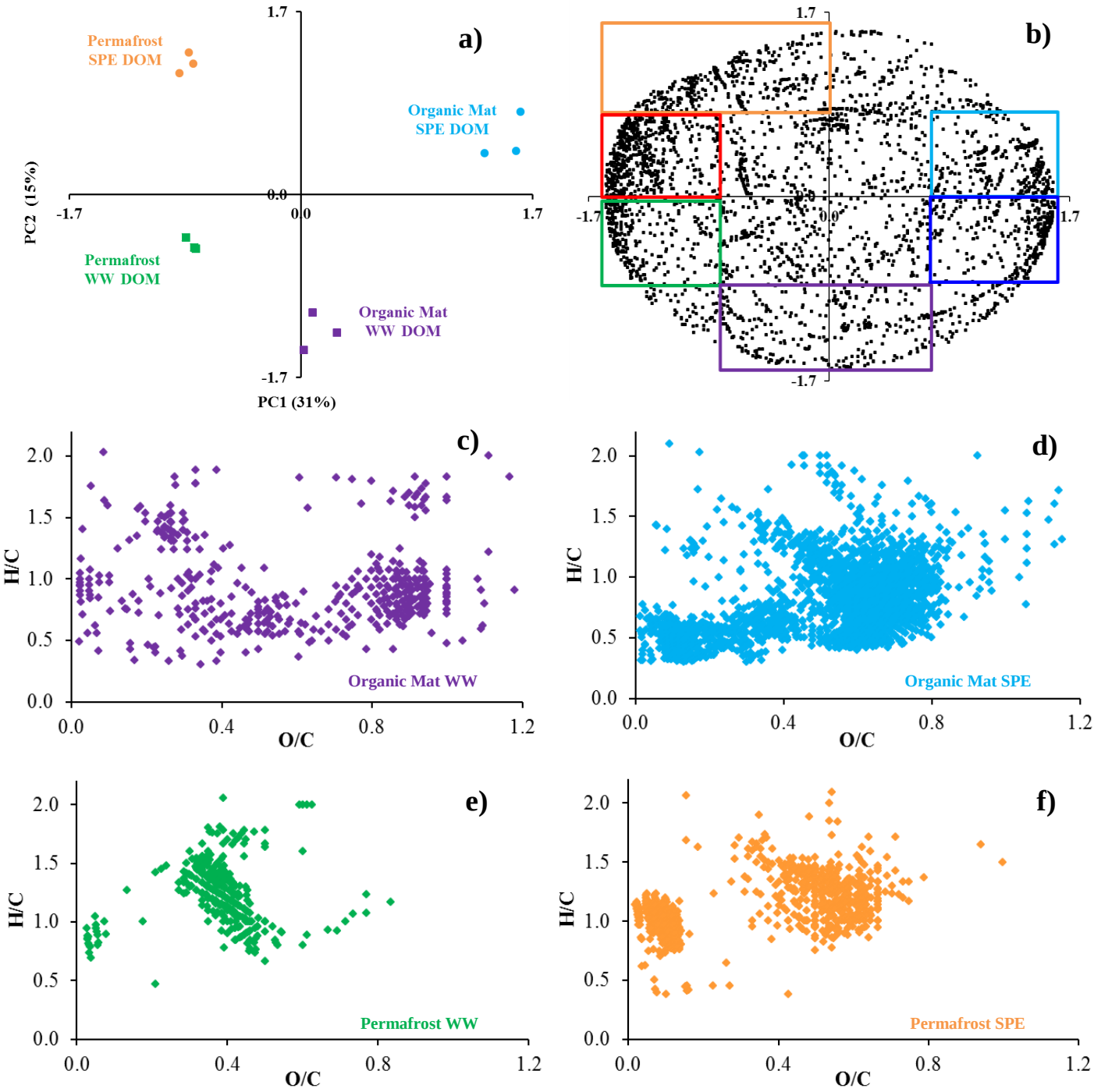

Figure 3.S2: Principal component analysis bi-plot showing **a**) factor scores of the 12 DOM spectra, and **b**) variable loadings, i.e., relative magnitude, of the 6,792 individual formulas included in the analysis. Formulas that fall into the colored boxes in Fig. S1b are enriched in the corresponding colored samples in Fig. S1a and are plotted on van Krevelen diagrams in Figs. 7 and S1c - f. Summed spectral intensities of these formula groupings are listed in Table S2.

Table 3.1. Summary of UV-visible and fluorescence spectroscopy data for organic mat and permafrost whole water and solid phase extraction (SPE) DOM[a]

DOM Source	Organic Mat		Permafrost	
DOM Fraction	whole water	SPE	whole water	SPE
DOC (μM)	3054 ± 181	450 ± 69	998 ± 27	164 ± 11
A_{254} (m^{-1})	100 ± 9	19 ± 2	15 ± 3	2 ± 1
$SUVA_{254}$ ($L\ mg\text{-}C^{-1}\ m^{-1}$)	2.7 ± 0.1	3.3 ± 0.1	1.2 ± 0.2	1.1 ± 0.2
Slope Ratio	0.72 ± 0.03	0.64 ± 0.01	0.96 ± 0.06	0.88 ± 0.10
Peak A (*RU*)	5.26 ± 0.36	1.75 ± 0.13	1.98 ± 0.51	0.49 ± 0.07
Peak C (*RU*)	2.32 ± 0.17	0.67 ± 0.06	0.83 ± 0.21	0.17 ± 0.01
Peak T (*RU*)	1.28 ± 0.05	0.25 ± 0.01	0.30 ± 0.08	0.08 ± 0.01
Peak C:A	0.44 ± 0.01	0.38 ± 0.01	0.42 ± 0.01	0.38 ± 0.01
Peak C λ_{ex} max (*nm*)	449 ± 2	456 ± 4	445 ± 1	445 ± 1
Fluorescence Index	1.49 ± 0.01	1.42 ± 0.01	1.55 ± 0.02	1.58 ± 0.01
Bacterial Cells ($cells\ mL^{-1}$)	$1.3 \pm 0.2*10^7$	-	$1.4 \pm 0.5*10^6$	-

[a] A_{254} = decadic absorbance at 254 nm; $SUVA_{254}$ = specific UV absorbance at 254 nm; Values show ± standard deviation from the mean of experimental triplicates.

Table 3.2. Summary of FT-ICR MS data for organic mat and permafrost whole water and solid phase extraction (SPE) DOM.[a]

DOM Source	Organic Mat		Permafrost	
DOM Fraction	Whole Water	SPE	Whole Water	SPE
# of peaks [a]	2794 ± 55	4478 ± 153	2390 ± 190	3221 ± 22
MW	511 ± 7	585 ± 6	488 ± 3	514 ± 9
O/C	0.53 ± 0.01	0.52 ± 0.01	0.49 ± 0.01	0.44 ± 0.01
H/C	1.01 ± 0.02	0.96 ± 0.01	1.16 ± 0.01	1.14 ± 0.01
DBE	13 ± 1	16 ± 1	11 ± 1	12 ± 1
AI_{MOD}	0.37 ± 0.01	0.40 ± 0.01	0.29 ± 0.01	0.32 ± 0.01
%Aliphatic	69 ± 1	65 ± 1	79 ± 2	77 ± 1
%Aromatic	31 ± 1	35 ± 1	21 ± 2	23 ± 1

[a] # of peaks excludes contributions from ^{13}C isotopes and salt ions; MW = molecular weight; DBE = double bond equivalents; AI_{MOD} = modified aromaticity index. Values show ± standard deviation from the number-averaged mean of experimental triplicates.

Table 3.S1. Spearmen correlation coefficients between common peak intensities of the whole water (WW) and solid phase extraction (SPE) fractions of organic mat and permafrost DOM. Red indicates strong correlations, while blue indicates weak correlations.

		Organic Mat DOM						Permafrost DOM					
		WW	WW	WW	SPE	SPE	SPE	WW	WW	WW	SPE	SPE	SPE
Organic Mat DOM	WW	1.00	0.96	0.97	0.84	0.87	0.83	0.37	0.43	0.38	0.38	0.41	0.35
	WW	0.96	1.00	0.96	0.76	0.80	0.76	0.36	0.41	0.37	0.33	0.35	0.31
	WW	0.97	0.96	1.00	0.85	0.88	0.85	0.32	0.39	0.33	0.32	0.35	0.29
	SPE	0.84	0.76	0.85	1.00	0.99	0.99	0.15	0.24	0.17	0.31	0.38	0.28
	SPE	0.87	0.80	0.88	0.99	1.00	0.99	0.16	0.26	0.19	0.32	0.39	0.29
	SPE	0.83	0.76	0.85	0.99	0.99	1.00	0.13	0.23	0.15	0.29	0.36	0.26
Permafrost DOM	WW	0.37	0.36	0.32	0.15	0.16	0.13	1.00	0.95	0.95	0.83	0.78	0.80
	WW	0.43	0.41	0.39	0.24	0.26	0.23	0.95	1.00	0.97	0.84	0.82	0.83
	WW	0.38	0.37	0.33	0.17	0.19	0.15	0.95	0.97	1.00	0.84	0.82	0.85
	SPE	0.38	0.33	0.32	0.31	0.32	0.29	0.83	0.84	0.84	1.00	0.96	0.96
	SPE	0.41	0.35	0.35	0.38	0.39	0.36	0.78	0.82	0.82	0.96	1.00	0.98
	SPE	0.35	0.31	0.29	0.28	0.29	0.26	0.80	0.83	0.85	0.96	0.98	1.00

Table 3.S2. The percentage of total spectral magnitude that is accounted for by each of the six boxes defined and presented in Figure S1b. SPE = solid phase extraction.

		Percentage of Total Spectral Magnitude					
DOM Source	**DOM Fraction**	**Light Blue**	**Purple**	**Blue**	**Orange**	**Green**	**Red**
Organic Mat	Whole Water	7%	**19%**	**18%**	3%	11%	17%
Organic Mat	Whole Water	5%	**22%**	**17%**	3%	12%	16%
Organic Mat	Whole Water	9%	**18%**	**19%**	3%	10%	14%
Organic Mat	SPE	**34%**	4%	**22%**	5%	5%	11%
Organic Mat	SPE	**26%**	5%	**23%**	5%	6%	12%
Organic Mat	SPE	**34%**	4%	**25%**	5%	5%	11%
Permafrost	Whole Water	3%	13%	5%	6%	**17%**	**32%**
Permafrost	Whole Water	3%	14%	6%	5%	**17%**	**34%**
Permafrost	Whole Water	3%	13%	6%	6%	**18%**	**36%**
Permafrost	SPE	4%	3%	6%	**16%**	14%	**33%**
Permafrost	SPE	5%	3%	7%	**17%**	13%	**33%**
Permafrost	SPE	4%	2%	5%	**16%**	13%	**31%**

References

1. C.-L. Ping, G. J. Michaelson, M. T. Jorgenson, J. M. Kimble, H. Epstein, V. E. Romanovsky, and D. A. Walker, *Nat. Geosci.*, 2008, **1**, 615–619.

2. C. Tarnocai, J. G. Canadell, E. A. G. Schuur, P. Kuhry, G. Mazhitova, and S. Zimov, *Global Biogeochem. Cycles*, 2009, **23**, GB2023.

3. X. Feng, J. E. Vonk, B. E. van Dongen, Ö. Gustafsson, I. P. Semiletov, O. V Dudarev, Z. Wang, D. B. Montluçon, L. Wacker, and T. I. Eglinton, *Proc. Natl. Acad. Sci. U. S. A.*, 2013, **110**, 14168–73.

4. J. E. Vonk and Ö. Gustafsson, *Nat. Geosci.*, 2013, **6**, 675–676.

5. R. M. Cory, C. P. Ward, B. C. Crump, and G. W. Kling, *Science*, 2014, **345**, 925–928.

6. G. W. Kling, G. W. Kipphut, and M. C. Miller, *Science*, 1991, **251**, 298–301.

7. P. S. Ramlal, R. H. Hesslein, R. E. Hecky, E. J. Fee, J. W. M. Rudd, and S. J. Guildford, *Biogeochemistry*, 1994, **24**, 145–172.

8. G. W. Kling, H. E. Adams, N. D. Bettez, W. B. Bowden, B. C. Crump, A. E. Giblin, K. E. Judd, K. Keller, G. W. Kipphut, E. R. Rastetter, G. R. Shaver, and M. Stieglitz, in *A Changing Arctic: Ecological Consequences for Tundra, Streams, and Lakes.*, eds. J. E. Hobbie and G. W. Kling, Oxford University Press, New York, 2014, pp. 143 – 172.

9. B. W. Abbott, J. R. Larouche, J. B. Jones, W. B. Bowden, and A. W. Balser, *J. Geophys. Res. Biogeosciences*, 2014, **119**, 2049–2063.

10. P. J. Mann, W. V Sobczak, M. M. Larue, E. Bulygina, A. Davydova, J. E. Vonk, J. Schade, S. Davydov, N. Zimov, R. M. Holmes, and R. G. M. Spencer, *Glob. Chang. Biol.*, 2014, **20**, 1089–100.

11. B. Crump, G. Kling, M. Bahr, and J. Hobbie, *Appl. Environ. Microbiol.*, 2003, **69**, 2253–2268.

12. K. E. Judd, B. C. Crump, and G. W. Kling, *Ecology*, 2006, **87**, 2068–79.

13. R. M. Cory, B. C. Crump, J. A. Dobkowski, and G. W. Kling, *Proc. Natl. Acad. Sci. U. S. A.*, 2013, **110**, 3429–3434.

14. P. J. Mann, A. Davydova, N. Zimov, R. G. M. Spencer, S. Davydov, E. Bulygina, S. Zimov, and R. M. Holmes, *J. Geophys. Res.*, 2012, **117**, G01028.

15. R. L. Sleighter, R. M. Cory, L. A. Kaplan, H. A. N. Abdulla, and P. G. Hatcher, *J. Geophys. Res. Biogeosciences*, 2014, **119**, 1520–1537.

16. C. Freeman, N. Ostle, and H. Kang, *Nature*, 2001, **409**, 149–150.

17. R. M. W. Amon and R. Benner, *Limnol. Oceanogr.*, 1996, **41**, 41 – 51.

18. L. Sun, E. Perdue, J. Meyer, and J. Weis, *Limnol. Oceanogr.*, 1997, **42**, 714–721.

19. J. Vallino, C. Hopkinson, and J. Hobbie, *Limnol. Oceanogr.*, 1996, **41**, 1591–1609.

20. J. L. Meyer, *Microb. Ecol.*, 1994, **28**, 195–199.

21. S. B. Hodgkins, M. M. Tfaily, C. K. McCalley, T. A. Logan, P. M. Crill, S. R. Saleska, V. I. Rich, and J. P. Chanton, *Proc. Natl. Acad. Sci. U. S. A.*, 2014, **111**, 5819–24.

22. A. C. Stenson, A. G. Marshall, and W. T. Cooper, *Anal. Chem.*, 2003, **75**, 1275–1284.

23. N. Hertkorn, M. Frommberger, M. Witt, B. P. Koch, P. Schmitt-Kopplin, and E. M. Perdue, *Anal. Chem.*, 2008, **80**, 8908–8919.

24. C. K. Remucal, R. M. Cory, M. Sander, and K. McNeill, *Environ. Sci. Technol.*, 2012, **46**, 9350–9.

25. W. C. Hockaday, J. M. Purcell, A. G. Marshall, J. a. Baldock, and P. G. Hatcher, *Limnol. Oceanogr. Methods*, 2009, **7**, 81–95.

26. N. Hertkorn, M. Harir, B. P. Koch, B. Michalke, and P. Schmitt-Kopplin, *Biogeosciences*, 2013, **10**, 1583–1624.

27. R. Jaffé, Y. Yamashita, N. Maie, W. T. Cooper, T. Dittmar, W. K. Dodds, J. B. Jones, T. Myoshi, J. R. Ortiz-Zayas, D. C. Podgorski, and A. Watanabe, *Geochim. Cosmochim. Acta*, 2012, **94**, 95–108.

28. A. Stubbins, J. F. Lapierre, M. Berggren, Y. T. Prairie, T. Dittmar, and P. A. del Giorgio, *Environ. Sci. Technol.*, 2014, **48**, 10598 – 10606.

29. R. M. Cory and D. M. McKnight, *Environ. Sci. Technol.*, 2005, **39**, 8142–9.

30. R. M. Cory and L. A. Kaplan, *Limnol. Oceanogr.*, 2012, **57**, 1347–1360.

31. R. G. M. Spencer, G. R. Aiken, K. P. Wickland, R. G. Striegl, and P. J. Hernes, *Global Biogeochem. Cycles*, 2008, **22**.

32. D. M. McKnight, E. W. Boyer, P. K. Westerhoff, P. T. Doran, T. Kulbe, and D. T. Andersen, *Limnol. Oceanogr.*, 2001, **46**, 38–48.

33. J. L. Weishaar, G. R. Aiken, B. A. Bergamaschi, M. S. Fram, R. Fujii, and K. Mopper, *Environ. Sci. Technol.*, 2003, **37**, 4702–8.

34. J. R. Helms, A. Stubbins, J. D. Ritchie, E. C. Minor, D. J. Kieber, and K. Mopper, *Limnol. Oceanogr.*, 2008, **53**, 955–969.

35. R. King, R. Bonfiglio, C. Fernandex-Metzler, C. Miller-Stein, and T. Olah, *J. Am. Soc. Mass Spectrom.*, 2000, **11**, 942 – 950.

36. R. L. Sleighter and P. G. Hatcher, *Mar. Chem.*, 2008, **110**, 140–152.

37. T. Dittmar, B. Koch, N. Hertkorn, and G. Kattner, *Limnol. Oceanogr. Methods*, 2008, **6**, 230–235.

38. A. D. McGuire, L. G. Anderson, T. R. Christensen, S. Dallimore, L. Guo, D. J. Hayes, M. Heimann, T. Lorenson, R. W. Macdonald, and N. Roulet, *Ecol. Monogr.*, 2009, **79**, 523–555.

39. M. D. Walker, T. D. Hamilton, H. A. Maier, A. M. Corinne, and M. K. Raynolds, in *A Changing Arctic: Ecological Consequences for Tundra, Streams, and Lakes.*, eds. J. E. Hobbie and G. W. Kling, Oxford University Press, New York, 2014, vol. 89 (7), pp. 61 – 80.

40. W. R. Eisner, *Arctic*, 1991, **44**, 279–282.

41. L. Hinzman, D. Kane, R. Gieck, and K. Everett, *Cold Reg. Sci. …*, 1991, **19**, 95 –110.

42. G. W. Kling, G. W. Kipphut, M. M. Miller, and J. W. O'Brien, *Freshw. Biol.*, 2000, **43**, 477–497.

43. M. P. Miller, B. E. Simone, D. M. McKnight, R. M. Cory, M. W. Williams, and E. W. Boyer, *Aquat. Sci.*, 2010, **72**, 269–275.

44. P. G. Coble, *Mar. Chem.*, 1996, **51**, 325–346.

45. R. L. Sleighter, G. A. McKee, Z. Liu, and P. G. Hatcher, *Limnol. Oceanogr. Methods*, 2008, **6**, 246–253.

46. R. L. Sleighter, H. Chen, A. S. Wozniak, A. S. Willoughby, P. Caricasole, and P. G. Hatcher, *Anal. Chem.*, 2012, **84**, 9184–91.

47. A. Stubbins, R. G. M. Spencer, H. Chen, P. G. Hatcher, K. Mopper, P. J. Hernes, V. L. Mwamba, A. M. Mangangu, J. N. Wabakanghanzi, and J. Six, *Limnol. Oceanogr.*, 2010, **55**, 1467–1477.

48. R. L. Sleighter, Z. Liu, J. Xue, and P. G. Hatcher, *Environ. Sci. Technol.*, 2010, **44**, 7576–82.

49. R. M. Cory, D. M. McKnight, Y.-P. Chin, P. Miller, and C. L. Jaros, *J. Geophys. Res.*, 2007, **112**, 1–14.

50. B. Crump, J. Baross, and C. Simenstad, *Aquat. Microb. Ecol.*, 1998, **14**, 7–18.

51. C. Stedmon and R. Cory, *Biological Origins and Fate of Fluorescent Dissolved Organic Matter in Aquatic Environments*, Cambridge University Press, New York, 2014.

52. I. Perminova, I. Dubinenkov, A. Kononikhin, A. Konstantinov, A. Zherebker, M. Andzhushev, V. Lebedev, E. Bulygina, and Holmes, *Environ. Sci. Technol.*, 2014, **48**, 7461 – 7468.

53. M. M. Tfaily, R. Hamdan, J. E. Corbett, J. P. Chanton, P. H. Glaser, and W. T. Cooper, *Geochim. Cosmochim. Acta*, 2013, **112**, 116–129.

54. R. M. Cory, S. A. Green, and K. S. Pregitzer, *Biogeochemistry*, 2004, **67**, 269–288.

55. J. D'Andrilli, T. Dittmar, B. P. Koch, J. M. Purcell, A. G. Marshall, and W. T. Cooper, *Rapid Commun. Mass Spectrom.*, 2010, **24**, 643–650.

56. K. Kaiser, G. Guggenberger, L. Haumaier, and W. Zech, *Eur. J. Soil Sci.*, 1997, 301–310.

57. K. Kaiser and K. Kalbitz, *Soil Biol. Biochem.*, 2012, **52**, 29–32.

58. C.-L. Ping, J. Bockheim, J. M. Kimble, G. J. Michaelson, and D. A. Walker, *J. Geophys. Res.*, 1998, **103**, 917 – 928.

59. M. Kawahigashi, K. Kaiser, A. Rodionov, and G. Guggenberger, *Glob. Chang. Biol.*, 2006, **12**, 1868–1877.

60. M. P. Waldrop, K. P. Wickland, R. White III, A. A. Berhe, J. W. Harden, and V. E. Romanovsky, *Glob. Chang. Biol.*, 2010, **16**, 2543–2554.

61. G. Fuchs, M. Boll, and J. Heider, *Nat. Rev. Microbiol.*, 2011, **9**, 803–16.

62. N. D. Ward, R. G. Keil, P. M. Medeiros, D. C. Brito, A. C. Cunha, T. Dittmar, P. L. Yager, A. V. Krusche, and J. E. Richey, *Nat. Geosci.*, 2013, **6**, 530–533.

63. K. Keller, J. D. Blum, and G. W. Kling, *Chem. Geol.*, 2010, **273**, 76–81.

Chapter 4

Complete and partial photo-oxidation of DOM draining permafrost soils.

4.1 Abstract

In northern latitudes, the carbon (C) fluxes from freshwaters may account for up to 40% of the net land surface C exchange with the atmosphere.[1] These large fluxes of carbon dioxide (CO_2) to the atmosphere are supported mainly by the movement of dissolved organic matter (DOM) from land and its subsequent complete oxidation to CO_2 in freshwaters.[2–5] The remaining DOM may be partially oxidized to compounds that remain in the DOM pool and are exported in rivers to oceans. Photochemical processing of DOM to CO_2 and partially-oxidized DOM exported to the ocean accounts for 70-95% of total DOM processed in the water column of arctic lakes and rivers. Given that the chemical composition of DOM is an expected control on the susceptibility of DOM to complete and partial photo-oxidation, this balance of DOM fate may change with increased inputs of chemically distinct DOM from deeper permafrost soil layers to sunlit surface waters. Thus, we measured the susceptibility of DOM draining the shallow organic mat and the deeper permafrost soil to complete and partial photo-oxidation, and related differences in their susceptibilities to their chemical composition before and after sunlight exposure. Despite lower initial aromatic and carboxyl content, DOM from permafrost soils was as susceptible to complete photo-oxidation to CO_2 as was organic mat DOM. Concurrent losses of carboxyl moieties and shifts in DOM chemical composition during photo-degradation indicated that photo-decarboxylation was likely an important photo-mineralization pathway for

both DOM sources. Highly oxidized, tannin-like formulas were more susceptible to photo-mineralization compared to other formulas that comprise organic mat and permafrost DOM, suggesting that these formulas may control the photo-mineralization of DOM in arctic surface waters. Permafrost DOM was significantly more susceptible to partial photo-oxidation compared to DOM leached from the organic mat, potentially owing to the depletion of phenolic moieties with antioxidant properties in permafrost relative to organic mat DOM. Increased permafrost thaw may increase photochemical DOM processing rates in surface waters that drain permafrost soils and shift the dominant DOM processing pathway from complete to partial photo-oxidation.

4.2 Introduction

Carbon dioxide (CO_2) emissions from inland surface waters to the atmosphere are as large as the net carbon (C) transfer from the atmosphere to Earth's surface (~ 2 Pg-C yr^{-1}).[3,6–8] In northern latitudes, the C fluxes from freshwaters may account for up to 40% of the net land surface C exchange with the atmosphere.[1] These large fluxes of CO_2 to the atmosphere are mainly supported by the movement of dissolved organic matter (DOM) from land and its subsequent complete oxidation to CO_2 in freshwaters.[2–5] The remaining DOM may be unprocessed, flocculated and buried in sediments, or partially oxidized and exported in rivers to oceans. Thus a critical component of the global C cycle is the fate of DOM drained from soils into inland waters.

This fate of DOM, that is, either complete or partial oxidation, is usually attributed to bacterial respiration. However, we recently showed that in the shallow, unshaded water column of streams, rivers, and lakes of the Arctic photochemical oxidation of DOM to CO_2 equals or exceeds bacterial respiration by 5-10 fold.[4] Furthermore, we found that photochemical

processing of DOM to CO_2 and partially-oxidized DOM exported to the ocean accounts for 70-95% of total DOM processed in the water column of arctic lakes and rivers.[4]

This balance of DOM fate may change as active surface layers deepen and permafrost thaws, more soil volume will be leached to produce DOM, and thermokarst failures will expose more soil C to light.[9–14] Several studies have shown that DOM from deeper permafrost soil has a distinct chemical composition and thus different susceptibility to degradation compared to DOM draining the organic mat dominated surface active layer.[13,15–18] For instance, permafrost DOM has been consistently reported to contain lower amounts of light-absorbing aromatic compounds, and given that near-surface rates of light absorption increase with increasing concentrations of light-absorbing DOM, some have proposed that permafrost DOM will undergo less photo-degradation compared to DOM with higher aromatic C content that drains the surface organic mat.[16] In contrast, the chromophoric or light-absorbing fraction of permafrost DOM (CDOM) was more susceptible to photo-degradation than CDOM draining the surface organic layer.[13]

Despite this evidence that CDOM draining permafrost layers may be more susceptible to photo-degradation than CDOM draining the active layer, no study has related these differences in susceptibility to the production of CO_2 or the production of partially oxidized compounds that remain in the DOM pool. This is because we have an incomplete understanding of (i) the pathways that are most important for complete and partial photo-oxidation, (ii) the moieties or compounds most susceptible to complete or partial photo-oxidation, or (iii) the composition and reactivity of partially oxidized DOM.

The photo-decarboxylation of DOM, or the breakdown of organic acids to CO_2, has been proposed as an important pathway for the photo-mineralization of DOM.[19–22] This suggests that the composition and reactivity of carboxylic acids within the DOM pool may control the lability

of DOM to photo-mineralization. For instance, esterification of carboxyl groups decreased photochemical O_2 consumption by 50%, and although the extent of esterification was no quantified the general result provides support for photo-decarboxylation as an important pathway for the photo-mineralization of DOM to CO_2.[19] Despite evidence for photo-decarboxylation reactions contributing to the photo-mineralization of DOM, the one study that has attempted to quantify their contribution concluded that carboxyl C must have been photo-chemically regenerated throughout the experiment to account for the measured CO_2 production by sunlight.[21]

Several studies have reported that the ratio of photochemical O_2 consumption to CO_2 production by DOM is > 1, suggesting that the "extra" O_2 consumed is incorporated into molecules that remain in the DOM pool after photo-degradation.[4,21,23] However, we do not know the composition of the molecules into which this extra O_2 is incorporated, which in turn limits our ability to predict the susceptibility of DOM to partial photo-oxidation. A recent study proposed that the antioxidant capacity of DOM may be related to its abundance of plant-derived aromatic, phenolic moieties.[24] These aromatic lignin and tannin-like compounds are hypothesized to act as antioxidants by quenching oxidants (e.g., •OH) and by protecting functional groups from oxidation,[24] thereby slowing or preventing the oxidation of DOM. It follows that DOM sources enriched or depleted in aromatic, phenolic moieties may be less or more susceptible to partial photo-oxidation, respectively. However, no study has related the composition of DOM, specifically the abundance of lignin and tannin-like compounds, to its susceptibility to partial photo-oxidation.

Thus, the objective of this study was to understand relationships between the chemical composition of DOM draining permafrost soils and the DOM susceptibility to complete and

partial photo-oxidation in arctic surface waters. We measured the susceptibility of DOM draining the shallow organic mat and the deeper permafrost layer to complete and partial photo-oxidation, and related differences in susceptibility to the chemical composition of DOM before and after sunlight exposure. Finally, we suggest that the balance of DOM fate (i.e., complete photo-oxidation to CO_2 vs. partial photo-oxidation to compounds that remain in the DOM pool) may change as inputs of chemically distinct, permafrost DOM to arctic surface waters increase.

4.3 Methods

4.3.1 Experimental Design

Soils were collected from moist acidic tundra at a mid-slope location in the Imnavait Creek watershed (68.62˚ N, 149.28˚ W; elevation ~ 900 m) at two depths, the shallow organic mat (5 - 15 cm) and the deeper permafrost layer (95 - 105 cm; Fig. 4.1). Average thaw depth in late summer (mid-August) in the Imnavait basin is ~44 cm, with a maximum of ~52 cm; therefore, the deep sample is well below the deepest thaw for this location.[25] Triplicate soil samples from each layer were leached overnight in laboratory grade DI at room temperature. Particles > 0.45 μm were filtered from the leachate and the operationally defined dissolved fractions are from here on referred to as organic mat DOM and permafrost DOM. Splits of DOM were taken for water chemistry (i.e., pH, conductivity, dissolved organic carbon (DOC)), and the remaining water was used in the photochemical experiments. Organic mat and permafrost DOM were exposed to natural sunlight at Toolik Lake Field Station in June and July 2013.[4,13] Following sunlight exposure, splits of dark-control and light-exposed DOM were taken for UV-visible and fluorescence spectroscopy, and high resolution Fourier transform ion cyclotron resonance mass spectrometry (FT-ICR MS). Using solid phase extraction (SPE), the remaining

DOM was concentrated and inorganic impurities were minimized.[26] SPE eluate from each replicate leachate was reserved for spectroscopic and FT-ICR MS analyses. Finally, functional group distributions of pooled, freeze-dried SPE eluates were measured by solid-state ^{13}C NMR. This experimental design was repeated for DOM drained from the organic mat and the permafrost soil horizon (Fig. 4.1).

4.3.2 Effect of sunlight on the chemical composition of organic mat and permafrost DOM

Changes in the chemical composition of organic mat and permafrost DOM after exposure to sunlight were characterized using UV-visible and fluorescence spectroscopy, FT-ICR MS, and solid-state ^{13}C NMR. Dark-control and light-exposed treatments were handled similarly throughout all analyses, and all experimental details and parameters were identical to those previously described.[18]

As expected, differences in compositional characteristics, determined by optical spectroscopy and FT-ICR MS, between dark-control and light-exposed treatments of organic mat and permafrost DOM were consistent for the whole water (0.45 μm filtered soil leachate) and solid phase extraction (SPE) fractions.[18] Because the trends in optical characteristics were similar between the whole water and SPE DOM fractions, the whole water optical results are used due to higher signal to noise ratios compared to the SPE optical results. It follows that the SPE mass spectra are used because this fraction was less susceptible to interfering species (e.g., salts) that limit the number of peaks and thus assigned molecular formulas in each spectrum.[18] Initial bulk compositional data for both fractions of each DOM source are presented in Table 4.S1.

4.3.2.1 Effect of sunlight on the light absorbing and emitting fraction of organic mat and permafrost DOM

UV-visible absorption spectra were collected using a 1-cm pathlength UV-visible spectrophotometer (Aqualog; Horiba Scientific). Napierian absorption coefficients were calculated by multiplying absorbance (A) by 2.303 and dividing by the pathlength (m) of the quartz cuvette. Spectral slope ratio (S_R) was calculated from the absorption spectra as the ratio of the slope from 275 to 295 nm to the slope from 350 to 400 nm.[27] Specific UV-visible absorbance as 254 nm ($SUVA_{254}$; L mg-C^{-1} m^{-1}) was calculated as decadic absorbance at 254 nm divided by the pathlength (m) and by the DOC concentration (mg-C L^{-1}).[28]

Fluorescence excitation-emission matrices (EEMs) of whole water and SPE DOM were collected over excitation and emission ranges of 240 to 600 nm by excitation/emission increments of 5 nm/1.64 nm, respectively, using integration times ranging from 3 to 4 s (Aqualog; Horiba Scientific). When necessary, DOM was diluted to less than 0.6 absorbance units (A) at 254 nm prior to analysis.[29] EEMs were corrected for inner-filter and instrument specific excitation and emission effects in Matlab (version 2013b). Blank EEMs were collected using fluorescence free, laboratory-grade DI water, and were subtracted from sample EEMs to minimize the influence of water Raman peaks. Intensities of corrected sample EEMs were converted to Raman units. The fluorescence index (FI) was calculated as the ratio of emission intensity at 470 nm to emission intensity at 520 nm at an excitation wavelength of 370 nm.[30]

4.3.2.2 Effect of sunlight on high resolution mass spectra of organic mat and permafrost DOM

DOM was diluted to give a final sample composition of 50:50 (v/v) MeOH:H_2O. Additionally, SPE extracts were diluted to less than 50 mg-C L^{-1} to minimize charge competition during ionization. DOM was continuously injected into an Apollo II ESI ion source of a Bruker Daltonics 12 Tesla Apex Qe FT-ICR MS housed at the William R. Wiley Environmental Molecular Sciences Laboratory, Pacific Northwest National Laboratory (PNNL). Accumulation of ions in the hexapole ranged from 0.4 - 3s before being transferred to the ICR cell, where 300 scans, collected with a 4 MWord time domain, were co-added for each sample. The summed free induction decay signal was zero-filled once and Sine-Bell apodized prior to fast Fourier transformation and magnitude calculation using Bruker Daltonics Data Analysis software. Similarly, a 50:50 (v/v) MeOH:H_2O blank spectrum was collected to test for contamination.

Mass spectra were externally calibrated using a polyethylene glycol standard and internally calibrated using fatty acids and other CH_2 homologous series naturally present in the sample.[31] Peaks from 250 to 1000 *m/z* with a signal to noise ratio ≥ 4 were added to mass lists, and those peaks detected in the blank spectrum were discarded prior to formula assignments. The presence or absence of peaks between spectra was quantified, where common peaks were defined as *m/z* values that agree within 0.5 mDa of each other.[32] A molecular formula calculator (Molecular Formula Calc v.1.0 ©NHMFL, 1998) generated formulas using carbon, hydrogen, oxygen, nitrogen, and sulfur. Only formulas that agreed within an error of $\leq \pm 1$ ppm to the calculated exact mass of the formula were considered. All formula assignments were screened to meet the criteria described by Stubbins et al. (2010).

Formulas susceptible to photo-degradation were distinguished from formulas resistant to photo-degradation by comparing differences in relative peak magnitudes across experimental triplicates. A formula was considered susceptible to photo-degradation if the 95% confidence

interval (CI) of triplicate light-exposed minus dark-control peak intensities was < 0. Similarly, if the 95% CI of triplicate light-exposed - dark-control peak intensities was > 0, the formula was categorized as resistant to degradation by sunlight. While we interpreted peaks that increased in intensity following sunlight exposure as resistant to photo-degradation, it was not possible to rule out the possibility that these species increased in intensity because they were produced by sunlight.[22,33]

4.3.2.3 Effect of sunlight on ^{13}C NMR spectra of organic mat and permafrost DOM

Solid-state ^{13}C NMR spectra of the powdered DOM were obtained using a Varian Infinity CMX 300 MHz spectrometer at PNNL. Powdered DOM was packed into 4 mm zirconia rotors fitted with Teflon spacers and caps. A ramped (^{13}C pulse) cross polarization magic angle spinning (CPMAS) pulse sequence was used. The contact time was 1 ms, the spinning rate was 14 kHz, and the decoupling field was 71 kHz. The ^{13}C chemical shifts were referenced to tetramethylsilane (0 ppm) using an external reference, hexamethylbenzene (methyl C; 17.36 ppm). Functional group distributions were quantified using Mnova NMR software (Metrelab Research).

4.3.3 Measurement of complete and partial photo-oxidation

Protocols for measurements of photochemical CO_2 production and O_2 consumption have previously been described in detail.[4,23] Briefly, organic mat and permafrost DOM were pre-equilibrated with air in the dark at room temperature, transferred to DI rinsed, pre-combusted, air-tight borosilicate vials (Labco Limited), and exposed to natural sunlight at Toolik Lake Field Station. Organic mat DOM was exposed to 6.7 kW m^{-2} (UVA + UVB) over 25 hours, while permafrost DOM was exposed to 5.8 kW m^{-2} over 16 hours. Dark-controls were wrapped in

aluminum foil. Average air temperature, measured every 5 minutes throughout the irradiation period, was 8.2 ± 4.0°C (N = 300) for organic mat DOM and 13.0 ± 1.5°C for permafrost DOM (N = 189). Following the experiment, the light-exposed and dark-control treatments were equilibrated at room temperature in the dark, and then analyzed for their dissolved oxygen concentration (O_2) using a membrane inlet mass spectrometer (Bay Instruments LLC), and dissolved inorganic carbon (DIC) concentration using a DIC analyzer (Apollo SciTech). Photochemical CO_2 production (μM) was quantified as the light minus dark difference in DIC concentration, while photochemical O_2 consumption (μM) was quantified as the dark minus light difference in O_2 concentration.

The contribution of H_2O_2 to photochemical O_2 consumption was quantified as the change in photochemical O_2 consumption upon addition of catalase (200 units mL^{-1}; Sigma Aldrich).[34] The capacity for catalase to disproportionate H_2O_2 was measured as a quality control check on the H_2O_2 measurements by adding catalase (200 units mL^{-1}) to vials spiked with known quantities of H_2O_2 and measuring changes in dissolved O_2 (Fig. 4.S1). As expected, H_2O_2 disproportionation produced 0.5 mol O_2 per mol H_2O_2 consumed. H_2O_2 measurements were conducted on organic mat and permafrost DOM that was stored in the dark at 4 ˚C for 18 months prior to irradiation. Because flocculation occurred during storage, the solutions were re-filtered (GF/F) prior to irradiation. Given that DOM chemistry is not a strong control on the apparent quantum yields for the production of H_2O_2,[35] it is unlikely that changes to the chemical composition of organic mat and permafrost DOM during storage significantly influenced the production of H_2O_2.

4.4 Results

4.4.1 Photo-mineralization and photo-oxidation of organic mat and permafrost DOM

Exposing organic mat DOM to sunlight produced more CO_2 than did permafrost DOM (organic mat = 161 ± 10 μM-CO_2, permafrost = 34 ± 1 μM-CO_2; Fig. 4.2). The production of CO_2 by sunlight consumed 5.2 ± 0.5% and 3.4 ± 0.3% of the initial C in organic mat and permafrost DOM. When normalized to mol photons absorbed by each DOM source (organic mat = 6.0 ± 0.2 mol photons m^{-2}; permafrost = 0.9 ± 0.1 mol photons m^{-2}; Table 4.S2), and assuming that apparent quantum yields for photochemical CO_2 production decay exponentially from 280 to 600 nm,[36] the apparent quantum yield for photochemical CO_2 production at 350 nm was similar for each DOM source (Fig. 4.3; organic mat = 0.90 ± 0.06 mmol CO_2 mol $photons^{-1}$, permafrost = 1.25 ± 0.12 CO_2 mol $photons^{-1}$; p = 0.075).

Similar to CO_2 production, organic mat DOM consumed more O_2 due to light exposure compared to permafrost DOM (organic mat = 146 ± 23 μM-O_2, permafrost = 55 ± 4 μM-O_2; Fig. 4.2). However, in contrast to CO_2 production, normalized to photons absorbed, apparent quantum yields for photochemical O_2 consumption at 350 nm were significantly lower for organic mat DOM compared to permafrost DOM (organic mat = 0.82 ± 0.09 mmol O_2 mol $photons^{-1}$, permafrost = 1.94 ± 0.13 mmol O_2 mol $photons^{-1}$, $p < 0.001$; Fig. 4.3). It follows that the ratio of photochemical O_2 consumption to CO_2 production was significantly lower for organic mat DOM compared to permafrost DOM (Fig. 4.2; organic mat = 0.90 ± 0.04, permafrost = 1.60 ± 0.12; $p < 0.001$); in other words, partial photo-oxidation was more prevalent in the permafrost soil DOM.

4.4.2 The effects of sunlight on the light-absorbing and emitting fractions of organic mat and permafrost DOM

As expected, sunlight exposure degraded the aromatic fraction of all DOM studied, quantified as loss and shifts in the chromophoric and fluorescent fraction of DOM (CDOM and FDOM, respectively. For example, there was a 27 ± 3and 4 ± 1 decrease in CDOM (per m), quantified as the decrease in the absorption coefficient at 305 nm (a_{305}) for organic mat and permafrost DOM, respectively (Table 4.S2). When normalized to mol photons absorbed by each DOM source from 280 - 600 nm, the loss in a_{305} was similar for each DOM source (organic mat = 4.5 ± 0.4 m^{-1} mol photons m^{-2}; permafrost = 4.2 ± 0.4 m^{-1} mol photons m^{-2}). Sunlight exposure also decreased the average molecular weight of each DOM source, as measured by an increase in the slope ratio (S_R). The absolute increase in S_R was 1.5-fold higher for organic mat compared to permafrost DOM. However, when normalized to light absorbed by each DOM source, the increase in S_R was significantly higher for permafrost compared to organic mat DOM (Table 4.S2; $p < 0.001$). Similarly, absolute changes in the fluorescence index (FI) were 1.2-fold higher for organic mat compared to permafrost DOM, while light-normalized changes were significantly higher for permafrost compared to organic mat DOM (Table 4.S2; $p < 0.001$).

4.4.3 High resolution mass spectra of organic mat and permafrost DOM

The FT-ICR mass spectra were generally similar to those previously reported for DOM leached from arctic[18,37] and sub-arctic soils.[38,39] Thousands of ions were detected across a mass range of 250 - 1000 Da, with dozens of ions detected at each nominal mass. Assignments of molecular formulas to individual ions revealed that DOM leached from the shallower organic mat contained higher molecular weight, more oxidized, and more unsaturated, aromatic species compared to DOM leached from the deeper permafrost layer.[18] The average molecular weight of formulas detected only in organic mat DOM was 86 Da higher than the average molecular weight of formulas detected only in permafrost DOM (organic mat = 592 Da, permafrost = 506

Da).[18] Additionally, formulas unique to organic mat DOM were more oxidized (mean O/C = 0.61) and less saturated (mean H/C = 0.81) compared to formulas unique to permafrost DOM (mean O/C = 0.29, mean H/C = 1.20).[18]

4.4.4 The effect of sunlight on high resolution mass spectra of organic mat and permafrost DOM

There was strong overlap between peaks in mass spectra of dark-control and light-exposed treatments of each DOM source, as expected given that less than 10% of the DOM was consumed or altered during light exposure (as discussed above in CO_2 production and O_2 consumption). On average, 70 - 79% of peaks identified in dark-control treatments of organic mat DOM were also detected in light-exposed treatments. Similarly, 72 - 81% of peaks were common to replicate dark-control and light-exposed treatments of permafrost DOM. However, photochemical production of CO_2, consumption of O_2, and the concurrent loss and alteration of CDOM and FDOM suggested substantial alteration of DOM during light exposure. To test the magnitude of this alteration, we used Spearman's rank correlation to identify the degree to which peak intensities were ranked in the same order between dark-control and light-exposed treatments of each DOM source. The rank analysis indicated that the distribution of the common peak intensities was significantly altered after exposure to sunlight. Spearman's rank correlation coefficients between the intensities of the peaks common to dark-control and light-exposed organic mat DOM spectra ranged from 0.77 - 0.91, less than coefficients within triplicate dark-control spectra (0.96 - 0.99) or triplicate light-exposed spectra (0.95 - 0.99; Table 4.S3). Spearman's rank correlation between the intensity of peaks in mass spectra of permafrost DOM exhibited a similar decrease after sunlight exposure (Table 4.S3). Thus, while the number of

peaks common to dark-control and light-exposed treatments of each DOM source was similar, the distribution of these common peak intensities was substantially different after exposure to sunlight.

Formulas in mass spectra of organic mat and permafrost DOM that exhibited a decrease in relative peak intensity following sunlight exposure were interpreted to be photo-degraded, while formulas that exhibited a relative increase in peak intensity were interpreted to be resistant to degradation by sunlight (see methods section 4.3.2.2). Formulas that were broken down or altered by sunlight exhibited (i) higher molecular weight, (ii) higher O:C ratios, and (iii) lower H:C ratios compared to formulas resistant to degradation by sunlight. The percent loss in peak intensity between dark-control and light-exposed DOM was greater at higher masses compared to lower masses. In contrast, the percent increase in peak intensity between light-exposed and dark-control DOM was greater at lower masses compared to higher masses. For example, the molecular weight of formulas in organic mat and permafrost DOM that were degraded by sunlight (red squares; Fig. 4.4) was on average 106 and 62 Da higher, respectively, than formulas that increased in intensity following light exposure (black squares; Figure 4.4), suggesting that sunlight broke down larger compounds into smaller compounds.

Analysis of organic mat and permafrost DOM in van Krevelen space revealed that formulas susceptible to photo-degradation exhibited higher O/C and lower H/C ratios compared to formulas resistant to photo-degradation (Fig. 4.5). In each DOM source, there were two clusters of formulas susceptible to degradation. One cluster of species had high O/C ratios (> 0.5) and spanned a range of H/C from 0.5 - 1.2, while another cluster of species had lower O/C ratios (0.3 - 0.5) and spanned a range of H/C from 1.0 - 1.5. Compared to formulas susceptible to photo-degradation, formulas resistant to degradation by sunlight exhibited higher lower O/C and

higher H/C ratios. For instance, the average O/C of formulas in organic mat and permafrost DOM that were resistant to photo-degradation was 0.11 and 0.23 lower, respectively, while the average H/C of formulas resistant to photo-degradation in each DOM source was 0.14 higher compared to formulas degraded by sunlight.

Despite large overlap between the composition of formulas degraded by sunlight in organic mat and permafrost DOM, the composition of formulas that increases in abundance following light exposure was different for each DOM source (Fig. 4.5). Formulas resistant to degradation in organic mat DOM formed one cluster ranging in O/C from 0.4 - 0.7 and H/C from 0.6 - 1.5. In contrast, formulas resistant to photo-degradation in permafrost DOM formed two clusters: one ranging in O/C from 0.4 - 0.6 and H/C from 1.2 - 1.6 and a second ranging in O/C from 0.05 - 0.15 and H/C from 0.75 - 1.1.

4.4.5 Effect of photo-degradation on functional group distribution

Integration of resonance spectra of DOM according to dominant functional or structural groups revealed compositional differences between dark-control and light-exposed treatments of organic mat and permafrost DOM (Figure 4.6). In both DOM sources, sunlight exposure decreased the aromatic C content. For example, compared to the dark-controls, the ratio of aromatic to aliphatic C in the light-exposed treatments was 15 and 39% lower for organic mat and permafrost DOM, respectively. Relative to treatments kept in the dark, sunlight exposure decreased oxygen containing functional groups (i.e., the sum of carboxyl, ketone, and aldehyde C) by 4% each for organic mat and permafrost DOM. Compared to dark-controls, carbohydrate carbon increased in the light-exposed treatments of organic mat and permafrost DOM by 4% each.

4.5. Discussion:

4.5.1 The effects of sunlight on the bulk chemical composition of DOM

The effects of sunlight on bulk compositional characteristics of organic mat and permafrost DOM were generally consistent with previous studies of DOM photo-degradation and with the current understanding that sunlight breaks down larger, more aromatic compounds into smaller, less aromatic compounds.[16,40] For example, sunlight exposure decreased the average molecular weight of organic mat and permafrost DOM as indicated by a significant increase in the S_R, and as the preferential degradation of higher molecular weight formulas in the FT-ICR mass spectra for both DOM sources (Table 4.S2; Fig 4.4). In addition, sunlight decreased CDOM and FDOM, the light-absorbing and emitting fractions of DOM, respectively, suggesting that aromatic moieties within the DOM pool were degraded (Table 4.S2). Consistently, the ratio of aromatic to aliphatic C within each DOM source decreased after exposure to sunlight, as measured by ^{13}C NMR (Fig. 4.6).

While many changes in DOM composition after sunlight exposure were generally consistent with the current understanding of photo-degradation, there were several findings in this study that were different and unexpected. Most notably, permafrost DOM had less aromatic C, but had higher susceptibility to photo-degradation compared to organic mat DOM (i.e., complete + partial photo-oxidation; Fig. 4.2). This finding contrasts the expectation that DOM with higher aromatic C is more susceptible to photo-degradation,[16,33] and suggests that aromatic C content may not be a strong control of the susceptibility of DOM to photo-degradation.[13,41,42] In following sections, we advance our understanding of DOM photo-degradation by relating changes in DOM composition following photo-exposure to (i) the pathways that are most

important for complete and partial photo-oxidation, (ii) the moieties or compounds most susceptible to complete or partial photo-oxidation, or (iii) the composition of partially oxidized DOM.

4.5.2 Photo-mineralization of organic mat and permafrost DOM: evidence for photo-decarboxylation

The results strongly support photo-decarboxylation as an important pathway for photochemical production of CO_2 from DOM. Generally, photo-decarboxylation is described as the breakdown of organic acids (R-COOH) to hydrocarbons (R-H) and CO_2 by sunlight:[43]

$$R\text{-}COOH + ({}_XO_2) \rightarrow R\text{-}H + CO_2 \qquad (1)$$

Where X is the mol of O_2 consumed per mol CO_2 produced, which likely ranges from zero to 0.5.[43,44] Consistently, in this study (i.e., organic mat DOM) and others, photochemical ratios of O_2/CO_2 were < 1,[4,21] suggesting that photo-decarboxylation contributed to the photo-mineralization of DOM. However, there were distinct differences in the importance of this process between the organic mat and permafrost soils. For example, the loss of carboxyl C after sunlight exposure could account for 37 ± 2% of the CO_2 produced by the organic mat, but up to 89 ± 4% of the CO_2 produced by permafrost DOM. These calculations were made based on the observed loss of carboxyl C following exposure to sunlight (≤ 3%, Figure 4.6). For example, the 2% loss of carboxyl C in organic mat DOM after exposure to sunlight represents 59 ± 2 μM-C (based on an initial [DOC] of 3054 ± 74 μM-C), which is 37 ± 2% of the CO_2 produced. These estimates for the contribution of photo-decarboxylation to the photo-mineralization of organic mat and permafrost DOM may be a minimum given that sunlight exposure has been reported to simultaneously increase and decrease carboxyl carbon content,[20,21] suggesting that the observed

decrease in carboxyl C content reported here may be a net loss (i.e., carboxylation - decarboxylation). To our knowledge, this is the first estimate of the contribution of photo-decarboxylation reactions to the photo-mineralization of DOM leached from soils, and demonstrates that photo-decarboxylation contributes significantly (40 - 90%) of chemically distinct DOM source that are mineralized to CO_2 by sunlight.

Furthermore, we observed shifts in the chemical composition of DOM that were consistent with photo-decarboxylation reactions. Compounds with carboxyl groups are more likely to have high O/C ratios, and thus photo-decarboxylation should result in a preferential loss of high O/C compounds following exposure of DOM to sunlight. Consistently, a majority of the photo-degraded formulas in organic mat and permafrost DOM (77 and 68% respectively), exhibited high O/C ratios (> 0.5) were classified as highly oxidized, tannin-like formulas (Fig 4.5).[33] Because organic acids are photo-decarboxylated to primarily form hydrocarbons and CO_2,[43] there is a loss of O and C at a 2:1 ratio without a change in the number of H atoms between the parent acid and the produced hydrocarbon. Thus, new compounds produced by photo-decarboxylation should have lower O/C and higher H/C ratios compared to compounds degraded by sunlight, as observed in studies of riverine[33] and marine DOM.[22] In these artic soils, both the organic mat and the permafrost horizon DOM had that were most susceptible to degradation by sunlight, while the intensity of lower O/C and higher H/C species increased upon exposure to sunlight (Fig. 4.5).

Similar susceptibilities to photo-mineralization and similar shifts in chemical composition after photo-exposure between two chemically distinct sources of DOM (i.e., organic mat and permafrost DOM), raise the possibility that a small pool of high O/C formulas are disproportionately susceptible to photo-decarboxylation and thus control for the photo-

mineralization of DOM in waters draining permafrost soils in the arctic. Despite large differences in chemical composition,[18] 77 and 68% of photo-degraded formulas in organic mat and permafrost DOM, respectively, exhibited O/C ratios greater than 0.5. Approximately 20% of these high O/C, photo-degraded formulas were common to both DOM sources (17% in organic mat DOM, 19% in permafrost DOM). Thus, these highly oxidized, tannin-like formulas were more susceptible to photo-mineralization compared to other formulas that comprise organic mat and permafrost DOM, and may control for the photo-mineralization of DOM in inland waters.

An alternative pathway for the photochemical mineralization of organic mat and permafrost DOM could be reaction with hydroxyl radical (•OH). This is because the absorption of sunlight by CDOM is the primary source and sink of •OH in arctic surface waters[45] and reactions of •OH with DOM yield CO_2.[46] However, a recent study of surface waters draining the same soils as studied here concluded that the production of CO_2 due to oxidation of DOM by •OH accounted for less than 5% of the measured photo-mineralization.[45] Previous work has also suggested that •OH accounted for a small fraction of CO_2 produced in temperate surface waters.[46] Thus, the mineralization of organic mat and permafrost DOM by •OH was likely not an important photochemical pathway.

4.5.3 Evidence for partial photo-oxidation of organic mat and permafrost DOM

Multiple lines of evidence strongly suggested that O_2 was incorporated into DOM during photo-degradation, and that permafrost DOM was more susceptible to partial photo-oxidation than was organic mat DOM (Figs. 4.2, 4.4, Appendix 4.1). For example, organic mat DOM did not consume O_2 in excess of CO_2 produced, while permafrost DOM consumed significantly more O_2 per mol CO_2 produced (20 ± 3 μM more O_2 than CO_2 produced during light exposure).

Assuming ≤ 1 mol O_2 needed for every mol CO_2 produced, the "extra" O_2 consumed was likely incorporated into the molecules that comprise the permafrost DOM pool. Given the strong evidence for photo-decarboxylation discussed above, which consumes less than 1 mol O_2 for every mol CO_2 produced (see section 4.5.2), the estimate of partial photo-oxidation and oxygen incorporation into permafrost DOM are likely conservative (low). For example, assuming that the estimates above of the CO_2 produced by photo-decarboxylation reactions are correct, then the estimated partial photo-oxidation increased from zero in organic mat DOM (i.e., no excess O_2 consumption) to 31 ± 16 μM-C. Similarly, assuming that 89 ± 4% of CO_2 was produced through photo-decarboxylation reactions in permafrost DOM, the amount of partially oxidized C increased from 40 ± 7 to 71 ± 6 μM-C.

Phenolic moieties within the DOM pool have been proposed to slow the oxidation of DOM.[24] That is, aromatic lignin and tannin-like compounds can act as antioxidants by quenching oxidants (e.g., •OH) and by protecting functional groups from oxidation,[24] thus slowing or preventing the oxidation of DOM. In the present study, DOM drained from the deeper permafrost layer was depleted in aromatic, phenolic moieties derived from lignin and tannin-like plant precursors compared to organic mat DOM.[18] Based on these compositional differences, permafrost DOM likely exhibited a lower antioxidant capacity compared to organic mat DOM, consistent with the increased susceptibility of permafrost DOM to partial photo-oxidation relative to organic mat DOM.

Multiple lines of evidence indicated that organic mat and especially permafrost DOM were partially oxidized by sunlight. However, we observed no trend of increasing O/C ratios following photo-degradation, as would be expected for oxidative processes that incorporate O_2 into organic compounds.[34] Possibilities for not detecting partially photo-oxidized organic mat

and permafrost DOM include first, consumption of O_2 by formation of hydrogen peroxide or other inorganic compounds, second, production of partially oxidized photoproducts with low masses outside the ranged detected by FT-ICR MS (250 - 1000 m/z), or third, partially oxidized photoproducts exhibited decreased ionization affinity compared to other compounds in the DOM pool, as discussed in this and the next two paragraphs. First, hydrogen peroxide (H_2O_2) production in these experiments was less than the limit of detection of O_2 by membrane inlet mass spectrometry (~1μM), suggesting that the measured photochemical O_2 consumption and estimates for partial photo-oxidation were likely not overestimated due to the photochemical production of H_2O_2 (Fig. 4.S1).

Second, evidence for the production of low molecular weight species included an increase in slope ratio and the preferential degradation of higher molecular weight species in the FT-ICR mass spectra of both DOM sources (Table 4.S2, Fig. 4.4). However, there was no evidence for significant production of highly oxidized low molecular weight species from organic mat and permafrost DOM, as measured by Orbitrap MS (100 - 250 m/z; Table 4.S4). Thus, low molecular weight oxidized species were either not a major product of the partial photo-oxidization of organic mat and permafrost DOM, or the low molecular weight partially photo-oxidized species were not easily ionized by (-) ESI and thus not detected by Orbitrap or FT-ICR MS.

Third, several studies have demonstrated that (-) ESI is unable to detect some fractions of DOM, including carbohydrate-like compounds (i.e., formulas sharing O/C and H/C ratios with carbohydrates in van Krevelen space).[18,47–49] For example in this study, the fraction of carbohydrate-like C in permafrost DOM was 33% lower when analyzed by FT-ICR MS compared to ^{13}C NMR, likely due to the suppressed ionization affinity of carbohydrate-like

species relative to other compound classes. Photo-degradation of both DOM sources increased the proportion of carbohydrate-like C by 4%, as measured by ^{13}C NMR (Figure 4.6), although there was no detectable production of carbohydrate-like C in the van Krevelen analysis of organic mat and permafrost DOM (Fig. 4.5). A similar result was found where photo-degradation of marine DOM led to a small increase (2%) in polyols or polyhydroxylated carbohydrates (detected by ^{1}H NMR) that were not detected via (-) ESI FT-ICR MS.[22] In the present study, the small increase in carbohydrate-like C following photo-degradation (4%) could account for any excess O_2 consumed by organic mat DOM and 56 - 99% of the excess O_2 consumed from permafrost DOM, suggesting that carbohydrate-like species, with poor ionization affinities, may be an important product of the partial photo-oxidation of DOM.

4.5.4 Conclusions and implications: how will the balance of DOM degradation change as more permafrost DOM is exported to arctic surface waters?

The amount of DOM oxidized completely to CO_2 by sunlight and released to the atmosphere, versus partially oxidized by sunlight and exported to oceans, will likely change with climate warming and increased thawing of permafrost soils. This is because DOM draining deeper permafrost soils is chemically distinct compared to DOM draining the shallower organic mat,[13,15,16,18] and the chemical composition of DOM is an important control for its susceptibility to complete and partial photo-oxidation. The nature of this degradation susceptibility is characterized and constrained by several results from this study. First, our results strongly suggested that photo-decarboxylation was an important pathway for the photo-mineralization of DOM draining the surface, organic mat and the deeper, permafrost layer. Second, in DOM from both organic mat and permafrost soil, highly oxidized, tannin-like formulas were more

susceptible to photo-mineralization compared to other formulas, suggesting that these formulas may control the photo-mineralization of DOM in arctic surface waters. Third, permafrost DOM was more susceptible to partial photo-oxidation compared to organic mat DOM, potentially due to an decreased abundance of phenolic moieties with antioxidant properties that have been proposed to slow the oxidation of DOM.[24] Finally, highly oxidized carbohydrate-like species may be an important product of the partial photo-oxidation of organic mat and permafrost DOM.

Assuming similar concentrations of DOM are laterally transferred from soils to surface waters with increased permafrost thaw, and thus the only change is in the character of DOM, then the importance of DOM photochemical processing pathways will likely increase with greater inputs of deeper, permafrost DOM to arctic surface waters. While organic mat and permafrost DOM exhibited similar susceptibilities to photo-mineralization, several studies have consistently shown that DOM from deeper permafrost soils has a lower concentration of chromophoric (CDOM) relative to DOM draining from the shallower organic mat.[13,15–17] Because CDOM is the main light absorbing constituent in most arctic surface waters,[4,50] this lower amount of CDOM draining permafrost soils will increase the penetration of ultraviolet light in surface waters, thereby increasing the fraction of DOM in a water column exposed to ultraviolet light. This suggests that the role of sunlight in the evasion of CO_2 from surface waters of the Arctic may increase as inputs of permafrost DOM depleted in light-absorbing aromatics comprises a larger fraction of the DOM exported from permafrost soils to sunlit surface waters. Furthermore, permafrost DOM was significantly more susceptible to partial photo-oxidation compared to organic mat DOM. Taken together, increased permafrost thaw may increase photochemical DOM processing rates in surface waters that drain permafrost soils and shift the dominant DOM processing pathway from complete to partial photo-oxidation, thereby increasing

the production of compounds with unknown susceptibilities to further oxidation by sunlight or bacteria. In turn, photochemical oxidation processes could become more important in shaping the composition and reactivity of DOM exported downstream to the Arctic Ocean.[40]

4.6 Acknowledgements

We thank J. Dobkowski, K. Harrold, A. Clinger, S. Michael, and researchers, technicians, and support staff of the Toolik Lake Arctic LTER for assistance in the field and laboratory. Thanks to B. C. Crump and G. W. Kling for contributing to the development and execution of the experimental design. Thanks to S. Page for discussions about partial photo-oxidation. FT-ICR and Orbitrap MS, and ^{13}C NMR analyses were performed using EMSL, a DOE Office of Science User Facility sponsored by the Office of Biological and Environmental Research and located at Pacific Northwest National Laboratory. Thanks to K. Roscioli and S. Burton for assisting with the MS and NMR analyses, respectively. Research was supported by NSF OPP–1023270.

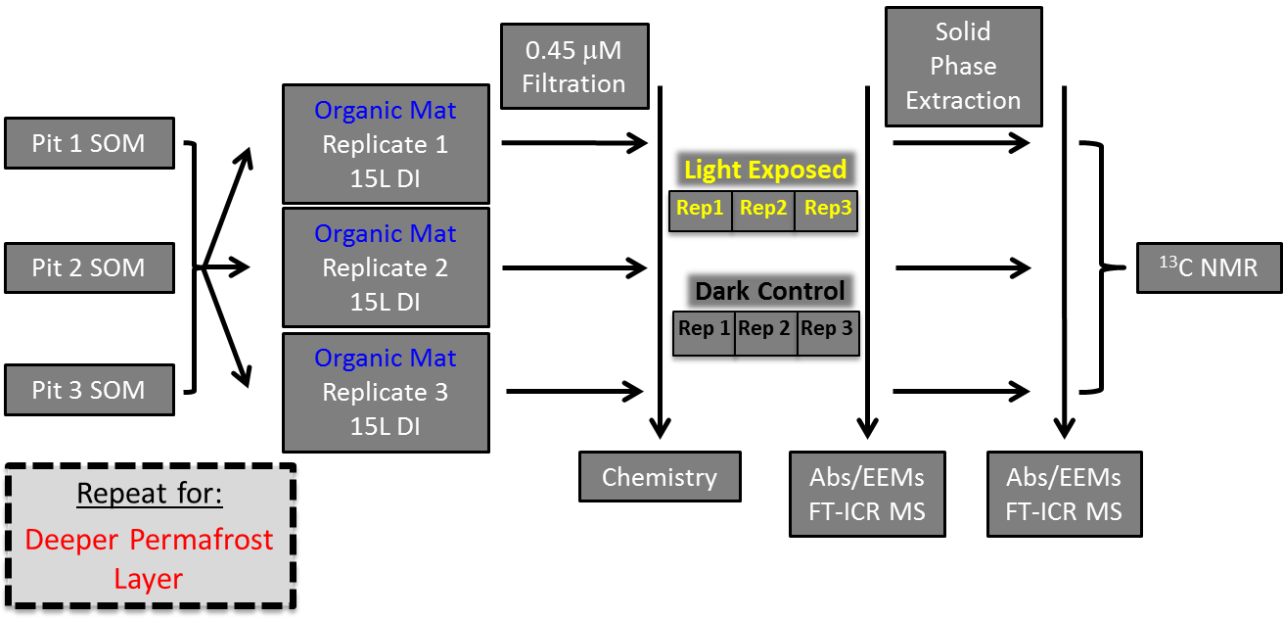

Figure 4.1. Experimental design for photochemical oxidation experiments of DOM leached from the shallower organic mat and deeper permafrost layers of arctic soils.

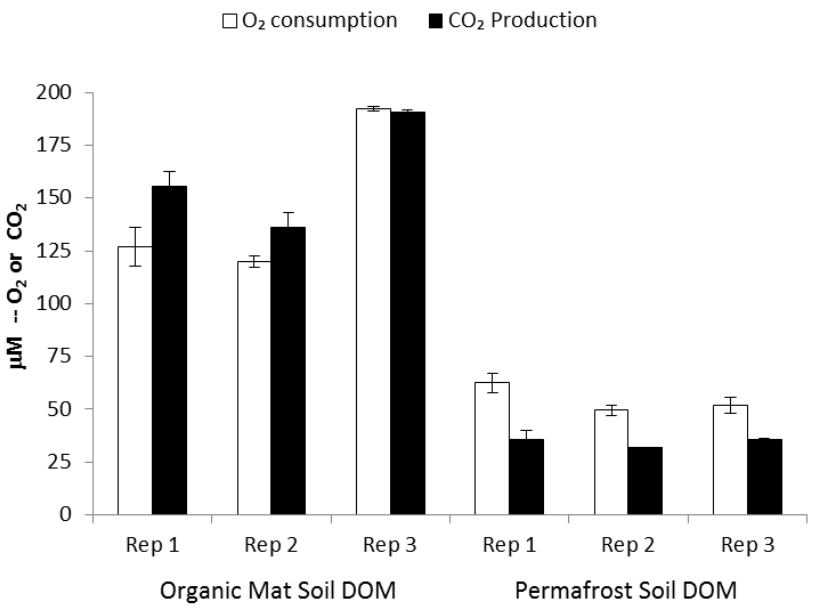

Figure 4.2. Photochemical oxidation (clear bars) and mineralization (filled bars) of organic mat and permafrost DOM.

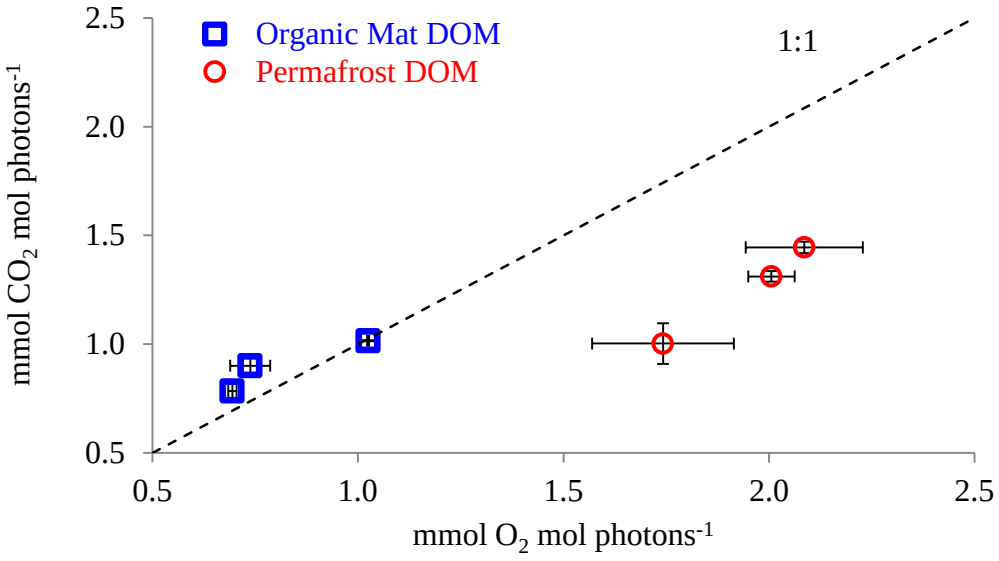

Figure 4.3. Apparent quantum yields at 350 nm for photochemical oxidation (x-axis) and mineralization (y-axis) of organic mat (blue squares) and permafrost (red circles) DOM.

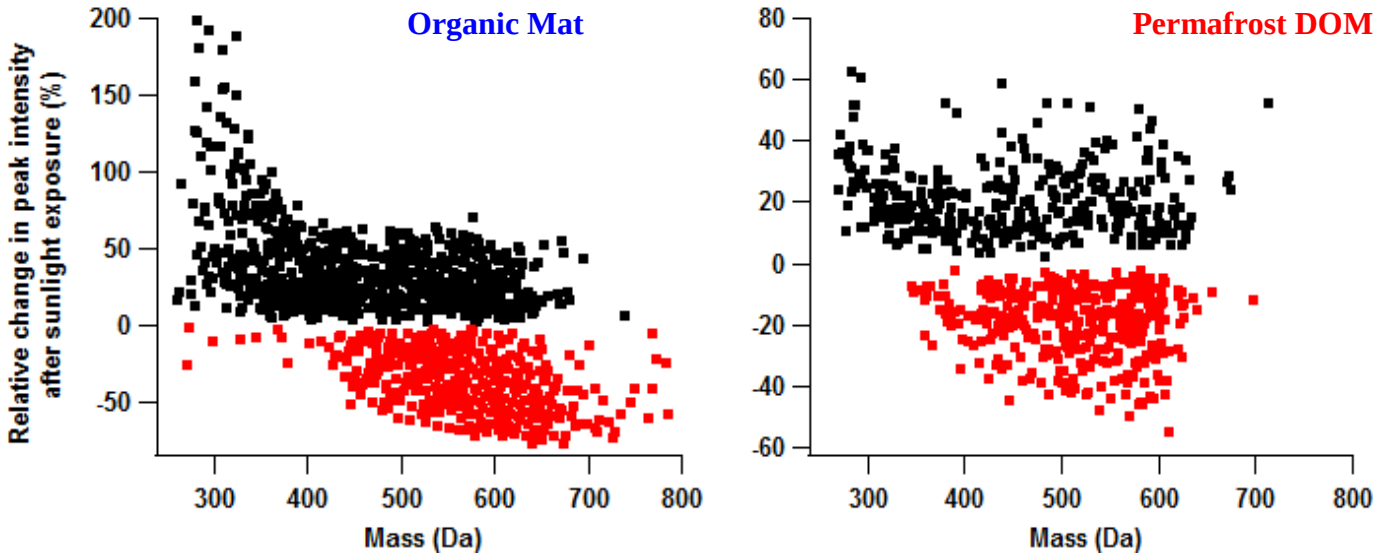

Figure 4.4. Change in relative peak intensity after sunlight exposure of species from 250 - 800 Da that were common to dark-control and light-exposed organic mat or permafrost DOM.

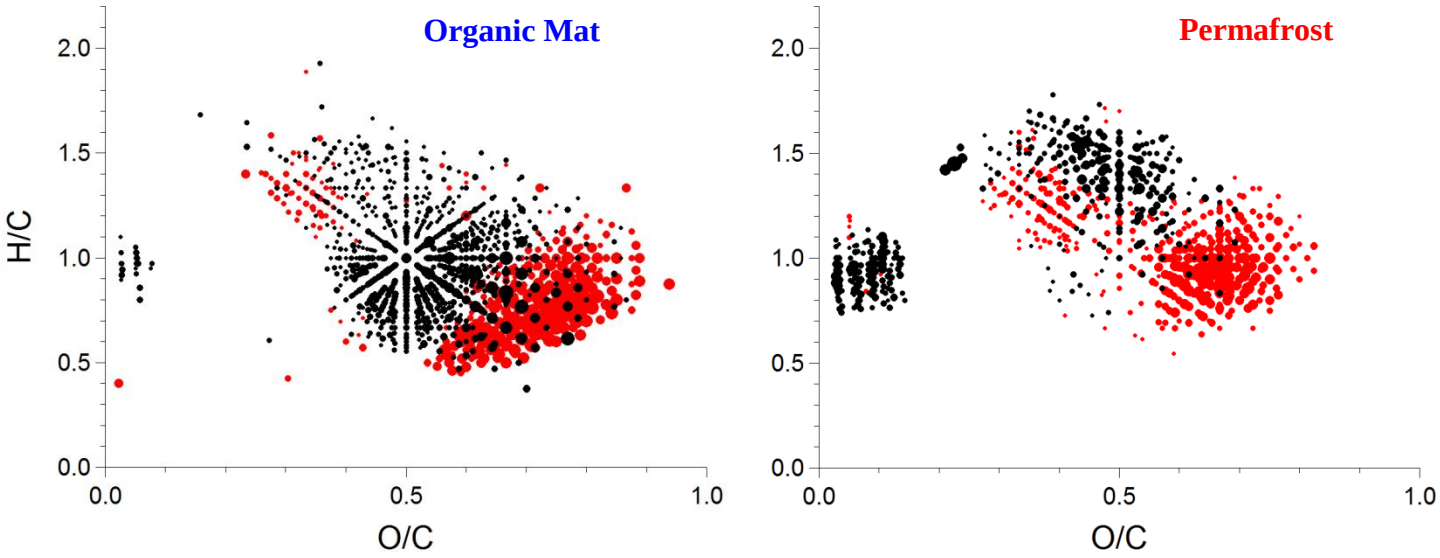

Figure 4.5. Van Krevelen diagrams of formulas that decreased (red) or increased (black) in abundance after sunlight exposure. Bubble size is proportional to the change in relative peak intensity after sunlight exposure.

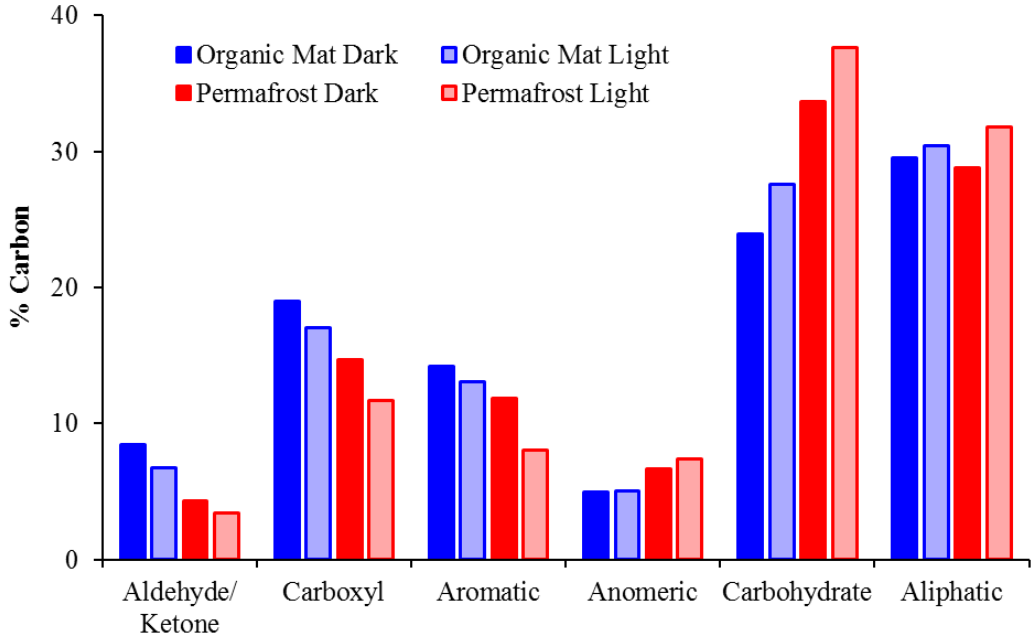

Figure 4.6. Functional group distributions of dark-control and light-exposed organic mat DOM (dark and light blue bars) and permafrost SPE DOM (dark and light red bars) determined using ^{13}C NMR. Integration regions are listed below each functional group following Cory et al. (2007).

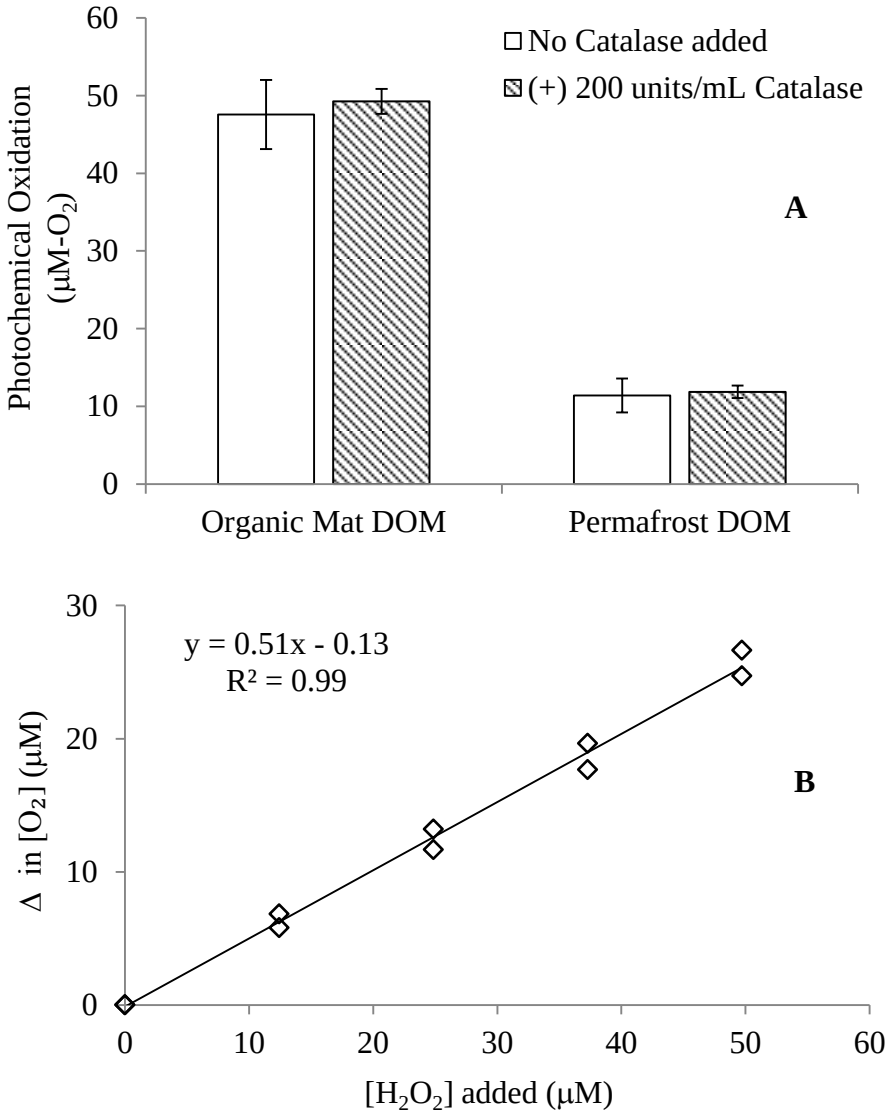

Figure 4.S1: A: Photochemical O_2 consumption in the presence and absence of catalase, a quencher of H_2O_2. **B:** Increase in dissolved O_2 concentration after addition of catalase solution to vials spiked with known amounts of H_2O_2.

DOM Source	Organic Mat		Permafrost	
DOM Fraction	Whole Water	SPE	Whole Water	SPE
pH	5.7 ± 0.1	-	5.8 ± 0.1	-
Conductivity ($\mu S\ cm^{-1}$)	37 ± 3	-	9 ± 1	-
DOC (μM)	3054 ± 181	450 ± 69	998 ± 27	164 ± 11
A_{254} (m^{-1})	100 ± 9	19 ± 2	15 ± 3	2 ± 1
$SUVA_{254}$ ($L\ mg\text{-}C^{-1}\ m^{-1}$)	2.7 ± 0.1	3.5 ± 0.2	1.2 ± 0.2	1.3 ± 0.2
Slope Ratio	0.72 ± 0.03	0.64 ± 0.01	0.96 ± 0.06	0.88 ± 0.10
Fluorescence Index	1.49 ± 0.01	1.42 ± 0.01	1.55 ± 0.02	1.58 ± 0.01
MW	511 ± 7	585 ± 6	488 ± 3	514 ± 9
O/C	0.53 ± 0.01	0.52 ± 0.01	0.49 ± 0.01	0.44 ± 0.01
H/C	1.01 ± 0.02	0.96 ± 0.01	1.16 ± 0.01	1.14 ± 0.01
%Aromatic	31 ± 1	35 ± 1	21 ± 2	23 ± 1

A_{254} = decadic absorbance at 254 nm; $SUVA_{254}$ = specific UV absorbance at 254 nm; MW = molecular weight; Values show ± standard deviation from the mean of experimental triplicates.

Table 4.S1: Summary of optical and FT-ICR MS data for the initial composition of organic mat and permafrost, whole water and solid phase extraction (SPE) DOM. All data previously reported in Ward and Cory, *In Review*.

DOM Source	Light vs. Dark Δ	[1]Decrease in *a*CDOM (m^{-1}) 280 - 700 nm	Decrease in *a*CDOM (m^{-1}) 305 nm	[2]Increase in SR	[3]Decrease in FI	[4]Qa (mol photons m^{-2})
Organic mat	Absolute Δ	2230 ± 138	27 ± 3	0.26 ± 0.01	0.23 ± 0.02	6.0 ± 0.2
	Q_a normalized Δ	372 ± 20	4.5 ± 0.4	0.04 ± 0.01	0.04 ± 0.01	
Permafrost	Absolute Δ	406 ± 126	4 ± 1	0.17 ± 0.01	0.19 ± 0.01	0.9 ± 0.1
	Q_a normalized Δ	411 ± 86	4.2 ± 0.8	0.18 ± 0.01	0.20 ± 0.02	

[1]Integrated loss in aCDOM from 280 - 700 nm; [2]SR = slope ratio (Helms et al., 2008); [3]FI = fluorescence index (McKnight et al., 2001); [4]Total integrated light absorption by CDOM during photo-exposure from 280 - 700 nm.

Table 4.S2: Absolute and light normalized changes in chromophoric and fluorescent DOM (CDOM and FDOM, respectively) properties after exposure to sunlight.

Organic Mat DOM

		Whole water						Solid-Phase Extraction (SPE)					
		Light R1	Light R2	Light R3	Dark R1	Dark R2	Dark R3	Light R1	Light R2	Light R3	Dark R1	Dark R2	Dark R3
Whole water	Light R1	1.000	.960	.957	0.809	.780	.772	0.754	.831	.753	0.652	.672	.632
	Light R2	.960	1.000	.951	.809	0.816	.781	.687	0.774	.694	.597	0.632	.583
	Light R3	.957	.951	1.000	.807	.791	0.807	.796	.841	0.805	.695	.719	0.690
	Dark R1	0.809	.809	.807	1.000	.958	.960	0.684	.701	.678	0.774	.805	.766
	Dark R2	.780	0.816	.791	.958	1.000	.948	.598	0.623	.599	.691	0.737	.690
	Dark R3	.772	.781	0.807	.960	.948	1.000	.699	.687	0.702	.793	.829	0.799
SPE	Light R1	0.754	.687	.796	0.684	.598	.699	1.000	.955	.992	0.922	.905	.911
	Light R2	.831	0.774	.841	.701	0.623	.687	.955	1.000	.959	.855	0.858	.843
	Light R3	.753	.694	0.805	.678	.599	0.702	.992	.959	1.000	.915	.907	0.913
	Dark R1	0.652	.597	.695	0.774	.691	.793	0.922	.855	.915	1.000	.988	.991
	Dark R2	.672	0.632	.719	.805	0.737	.829	.905	0.858	.907	.988	1.000	.990
	Dark R3	.632	.583	0.690	.766	.690	0.799	.911	.843	0.913	.991	.990	1.000

Permafrost DOM

		Whole water						Solid-Phase Extraction (SPE)					
		Light R1	Light R2	Light R3	Dark R1	Dark R2	Dark R3	Light R1	Light R2	Light R3	Dark R1	Dark R2	Dark R3
Whole water	Light R1	1.000	.918	.926	0.916	.852	.880	0.787	.746	.751	0.742	.664	.689
	Light R2	.918	1.000	.948	.895	0.888	.915	.810	0.804	.806	.772	0.740	.757
	Light R3	.926	.948	1.000	.882	.862	0.901	.791	.802	0.813	.741	.704	0.737
	Dark R1	0.916	.895	.882	1.000	.931	.936	0.767	.691	.692	0.787	.712	.724
	Dark R2	.852	0.888	.862	.931	1.000	.959	.781	0.739	.730	.815	0.792	.796
	Dark R3	.880	.915	0.901	.936	.959	1.000	.794	.773	0.774	.814	.795	0.814
SPE	Light R1	0.787	.810	.791	0.767	.781	.794	1.000	.940	.928	0.948	.906	.915
	Light R2	.746	0.804	.802	.691	0.739	.773	.940	1.000	.983	.878	0.900	.921
	Light R3	.751	.806	0.813	.692	.730	0.774	.928	.983	1.000	.861	.881	0.912
	Dark R1	0.742	.772	.741	0.787	.815	.814	0.948	.878	.861	1.000	.947	.948
	Dark R2	.664	0.740	.704	.712	0.792	.795	.906	0.900	.881	.947	1.000	.980
	Dark R3	.689	.757	0.737	.724	.796	0.814	.915	.921	0.912	.948	.980	1.000

Table 4.S3: Spearman's rank correlation coefficients of peak intensities between light-exposed and dark-control, whole water and solid phase-extraction, organic mat and permafrost DOM. All correlations are significant at $\alpha = 0.05$.

DOM Source	Treatment	Replicate	N	MW	O:C	H:C	DBE
Organic Mat	Dark-control	#1	312	177	0.41	1.10	5.2
Organic Mat	Dark-control	#2	315	179	0.41	1.09	5.3
Organic Mat	Dark-control	#3	311	176	0.40	1.08	5.3
Organic Mat	Light-exposed	#1	357	179	0.40	1.07	5.4
Organic Mat	Light-exposed	#2	363	180	0.41	1.08	5.3
Organic Mat	Light-exposed	#3	340	179	0.41	1.06	5.4
Light - Dark Average			41	2	0.003	-0.019	0.1
Light -Dark SD			10	0.7	0.008	0.011	0.1
DOM Source	**Treatment**	**Replicate**	**N**	**[a]MW**	**O:C**	**H:C**	**[b]DBE**
Permafrost	Dark-control	#1	302	184	0.37	1.21	4.9
Permafrost	Dark-control	#2	280	186	0.37	1.16	5.2
Permafrost	Dark-control	#3	242	185	0.37	1.14	5.2
Permafrost	Light-exposed	#1	307	182	0.39	1.18	5.0
Permafrost	Light-exposed	#2	300	184	0.40	1.17	5.0
Permafrost	Light-exposed	#3	315	183	0.39	1.20	4.9
Light - Dark Average			33	-2	0.020	0.009	-0.2
Light -Dark SD			36	0.3	0.002	0.041	0.2

[a] MW = molecular weight; [b] DBE = double bond equivalents. All values are number-weighted.

Table 4.S4: Summary of dark-control and light-exposed organic mat and permafrost DOM chemical composition as detected by ESI (-) Orbitrap-MS.

References

1. A. D. McGuire, L. G. Anderson, T. R. Christensen, S. Dallimore, L. Guo, D. J. Hayes, M. Heimann, T. Lorenson, R. W. Macdonald, and N. Roulet, *Ecol. Monogr.*, 2009, **79**, 523–555.

2. G. W. Kling, G. W. Kipphut, and M. C. Miller, *Science*, 1991, **251**, 298–301.

3. A. K. Aufdenkampe, E. Mayorga, P. A. Raymond, J. M. Melack, S. C. Doney, S. R. Alin, R. Aalto, and K. Yoo, *Front. Ecol. Environ.*, 2011, **9**, 53–60.

4. R. M. Cory, C. P. Ward, B. C. Crump, and G. W. Kling, *Science*, 2014, **345**, 925–928.

5. P. A. Raymond, J. Hartmann, R. Lauerwald, S. Sobek, C. McDonald, M. Hoover, D. Butman, R. Striegl, E. Mayorga, C. Humborg, P. Kortelainen, H. Dürr, M. Meybeck, P. Ciais, and P. Guth, *Nature*, 2013, **503**, 355–9.

6. J. J. Cole, Y. T. Prairie, N. F. Caraco, W. H. McDowell, L. J. Tranvik, R. G. Striegl, C. M. Duarte, P. Kortelainen, J. A. Downing, J. J. Middelburg, and J. Melack, *Ecosystems*, 2007, **10**, 171–184.

7. P. A. Raymond, J. W. McClelland, R. M. Holmes, A. V. Zhulidov, K. Mull, B. J. Peterson, R. G. Striegl, G. R. Aiken, and T. Y. Gurtovaya, *Global Biogeochem. Cycles*, 2007, **21**.

8. T. J. Battin, L. A. Kaplan, S. Findlay, C. S. Hopkinson, E. Marti, A. I. Packman, J. D. Newbold, and F. Sabater, *Nat. Geosci.*, 2008, **1**, 95–100.

9. D. Olefeldt and N. T. Roulet, *J. Geophys. Res. Biogeosciences*, 2012, **117**.

10. J. C. Rowland, C. E. Jones, G. Altmann, R. Bryan, B. T. Crosby, G. L. Geernaert, L. D. Hinzman, D. L. Kane, D. M. Lawrence, A. Mancino, P. Marsh, J. P. McNamara, V. E. Romanovsky, H. Toniolo, B. J. Travis, E. Trochim, and C. J. Wilson, *Eos (Washington. DC).*, 2010, **91**.

11. W. B. Bowden, M. N. Gooseff, a. Balser, a. Green, B. J. Peterson, and J. Bradford, *J. Geophys. Res.*, 2008, **113**, G02026.

12. Y. Zhang, W. Chen, and D. W. Riseborough, *J. Geophys. Res.*, 2006, **111**, D22103.

13. R. M. Cory, B. C. Crump, J. A. Dobkowski, and G. W. Kling, *Proc. Natl. Acad. Sci. U. S. A.*, 2013, **110**, 3429–3434.

14. M. T. Jorgenson, Y. L. Shur, and E. R. Pullman, *Geophys. Res. Lett.*, 2006, **33**, L02503.

15. B. W. Abbott, J. R. Larouche, J. B. Jones, W. B. Bowden, and A. W. Balser, *J. Geophys. Res. Biogeosciences*, 2014, **119**, 2049–2063.

16. P. J. Mann, A. Davydova, N. Zimov, R. G. M. Spencer, S. Davydov, E. Bulygina, S. Zimov, and R. M. Holmes, *J. Geophys. Res.*, 2012, **117**, G01028.

17. P. J. Mann, W. V Sobczak, M. M. Larue, E. Bulygina, A. Davydova, J. E. Vonk, J. Schade, S. Davydov, N. Zimov, R. M. Holmes, and R. G. M. Spencer, *Glob. Chang. Biol.*, 2014, **20**, 1089–100.

18. C. P. Ward and R. M. Cory, *Geochim. Cosmochim. Acta*, In Review.

19. C. Miles and P. Brezonik, *Environ. Sci. Technol.*, 1981, **15**, 1089–1095.

20. P. Schmitt-Kopplin, N. Hertkorn, H.-R. Schulten, and A. Kettrup, *Environ. Sci. Technol.*, 1998, **32**, 2531–2541.

21. H. Xie, O. C. Zafiriou, W.-J. Cai, R. G. Zepp, and Y. Wang, *Environ. Sci. Technol.*, 2004, **38**, 4113–9.

22. M. Gonsior, N. Hertkorn, M. H. Conte, W. J. Cooper, D. Bastviken, E. Druffel, and P. Schmitt-Kopplin, *Mar. Chem.*, 2014, **163**, 10–18.

23. C. P. Ward, R. L. Sleighter, P. G. Hatcher, and R. M. Cory, *Environ. Sci. Process. Impacts*, 2014, 721–731.

24. M. Aeschbacher, C. Graf, R. P. Scwarzenbach, and M. Sander, *Environ. Sci. Technol.*, 2012, **46**, 4916–4925.

25. G. W. Kling, H. E. Adams, N. D. Bettez, W. B. Bowden, B. C. Crump, A. E. Giblin, K. E. Judd, K. Keller, G. W. Kipphut, E. R. Rastetter, G. R. Shaver, and M. Stieglitz, in *A Changing Arctic: Ecological Consequences for Tundra, Streams, and Lakes.*, eds. J. E. Hobbie and G. W. Kling, Oxford University Press, New York, 2014, pp. 143 – 172.

26. T. Dittmar, B. Koch, N. Hertkorn, and G. Kattner, *Limnol. Oceanogr. Methods*, 2008, **6**, 230–235.

27. J. R. Helms, A. Stubbins, J. D. Ritchie, E. C. Minor, D. J. Kieber, and K. Mopper, *Limnol. Oceanogr.*, 2008, **53**, 955–969.

28. J. L. Weishaar, G. R. Aiken, B. A. Bergamaschi, M. S. Fram, R. Fujii, and K. Mopper, *Environ. Sci. Technol.*, 2003, **37**, 4702–8.

29. M. P. Miller, B. E. Simone, D. M. McKnight, R. M. Cory, M. W. Williams, and E. W. Boyer, *Aquat. Sci.*, 2010, **72**, 269–275.

30. D. M. McKnight, E. W. Boyer, P. K. Westerhoff, P. T. Doran, T. Kulbe, and D. T. Andersen, *Limnol. Oceanogr.*, 2001, **46**, 38–48.

31. R. L. Sleighter, G. A. McKee, Z. Liu, and P. G. Hatcher, *Limnol. Oceanogr. Methods*, 2008, **6**, 246–253.

32. R. L. Sleighter, H. Chen, A. S. Wozniak, A. S. Willoughby, P. Caricasole, and P. G. Hatcher, *Anal. Chem.*, 2012, **84**, 9184–91.

33. A. Stubbins, R. G. M. Spencer, H. Chen, P. G. Hatcher, K. Mopper, P. J. Hernes, V. L. Mwamba, A. M. Mangangu, J. N. Wabakanghanzi, and J. Six, *Limnol. Oceanogr.*, 2010, **55**, 1467–1477.

34. R. M. Cory, K. McNeill, J. P. Cotner, A. Amado, J. M. Purcell, and A. G. Marshall, *Environ. Sci. Technol.*, 2010, **44**, 3683–9.

35. D. J. Kieber, G. W. Miller, P. J. Neale, and K. Mopper, *Environ. Sci. Process. Impacts*, 2014, **16**, 777–91.

36. A. V. Vähätalo, M. Salkinoja-Salonen, P. Taalas, and K. Salonen, *Limnol. Oceanogr.*, 2000, **45**, 664–676.

37. S. B. Hodgkins, M. M. Tfaily, C. K. McCalley, T. A. Logan, P. M. Crill, S. R. Saleska, V. I. Rich, and J. P. Chanton, *Proc. Natl. Acad. Sci. U. S. A.*, 2014, **111**, 5819–24.

38. J. D'Andrilli, J. P. Chanton, P. H. Glaser, and W. T. Cooper, *Org. Geochem.*, 2010, **41**, 791–799.

39. M. M. Tfaily, R. Hamdan, J. E. Corbett, J. P. Chanton, P. H. Glaser, and W. T. Cooper, *Geochim. Cosmochim. Acta*, 2013, **112**, 116–129.

40. R. M. Cory, D. M. McKnight, Y.-P. Chin, P. Miller, and C. L. Jaros, *J. Geophys. Res.*, 2007, **112**, 1–14.

41. L. C. Powers and W. L. Miller, *Mar. Chem.*, 2015, **171**, 21–35.

42. S. C. Johannessen and W. L. Miller, *Mar. Chem.*, 2001, **76**, 271–283.

43. D. Budac and P. Wan, *J. Photochem. Photobiol. A Chem.*, 1992, **67**, 135–166.

44. C. H. Langford, M. Wingham, and V. S. Sastri, *Environ. Sci. Technol.*, 1973, **7**, 820–823.

45. S. E. Page, J. R. Logan, R. M. Cory, and K. McNeill, *Environ. Sci. Process. Impacts*, 2014, **16**, 807–22.

46. J. V. Goldstone, M. J. Pullin, S. Bertilsson, and B. M. Voelker, *Environ. Sci. Technol.*, 2002, **36**, 364–372.

47. R. Jaffé, Y. Yamashita, N. Maie, W. T. Cooper, T. Dittmar, W. K. Dodds, J. B. Jones, T. Myoshi, J. R. Ortiz-Zayas, D. C. Podgorski, and A. Watanabe, *Geochim. Cosmochim. Acta*, 2012, **94**, 95–108.

48. W. C. Hockaday, J. M. Purcell, A. G. Marshall, J. a. Baldock, and P. G. Hatcher, *Limnol. Oceanogr. Methods*, 2009, **7**, 81–95.

49. N. Hertkorn, M. Harir, B. P. Koch, B. Michalke, and P. Schmitt-Kopplin, *Biogeosciences*, 2013, **10**, 1583–1624.

50. J. A. L. Gareis, L. F. W. Lesack, and M. L. Bothwell, *Water Resour. Res.*, 2010, **46**, W09516.

51. S. Andrews, S. Caron, and O. Zafiriou, *Limnol. Oceanogr.*, 2000, **45**, 267–277.

52. B. M. Peterson, *Probing the Photochemistry of Humic Substances*, Dissertation Thesis. ETH Zurich, 2012.

Appendix 4.1: Evaluating the assumptions taken to estimate the partial photo-oxidation of DOM

Recent work has suggested that partial photo-oxidation of DOM in sunlit surface waters is more important than previously recognized.[4] Estimates for the production of partially oxidized DOM are calculated as the difference between photochemical O_2 consumption and CO_2 production. For instance, in cases where DOM photochemically consumes more O_2 than it produces CO_2, the "excess" O_2 consumption is interpreted to be incorporated into molecules that remain in the DOM pool after sunlight exposure. Based on these assumptions, organic mat was not susceptible to partial photo-oxidation because it did not consume more O_2 than CO_2 produced (Fig. 4.2). In contrast, permafrost DOM consumed 20 ± 3 μM more O_2 than CO_2 produced during light exposure, suggesting that the excess O_2 was incorporated into the molecules that comprise the permafrost DOM pool. However, there is potentially large uncertainty underlying the assumptions taken to calculate partial photo-oxidation. Here we evaluate these major assumptions to further constrain our estimates for the susceptibility of organic mat and permafrost DOM to partial photo-oxidation: (i) the photochemical production of species that consume O_2 but do not directly partially oxidize DOM accounted for an insignificant fraction of the measured photochemical O_2 consumption, (ii) one mol of O_2 is consumed per mol of CO_2 produced when DOM is mineralized by sunlight, and (iii) one mol of O is consumed per mol of partially oxidized C produced.[51]

The absorption of sunlight by DOM can produce species that consume O_2 but do not directly oxidize DOM. Significant production of these species, such as H_2O_2, by organic mat and permafrost DOM could have resulted in an overestimate of photochemical O_2 consumption and thus partial photo-oxidation. However, there was no detectable difference in photochemical

oxygen consumption between light-exposed treatments with and without the addition of catalase (a quencher of H_2O_2) after sunlight exposure (Fig. 4.S1), suggesting that H_2O_2 production in these experiments was less than the limit of detection of O_2 by membrane inlet mass spectrometry (~1μM). These results were consistent with photochemical studies of temperate riverine DOM where H_2O_2 production accounted for < 5% of total photochemical O_2 consumption.[34] Thus, the measured photochemical O_2 consumption and estimates for partial photo-oxidation were likely not significantly overestimated due to the production of H_2O_2.

Some photochemical pathways consume less than one mol O_2 per mol CO_2 produced, suggesting that the estimates for partial photo-oxidation reported here are likely conservative. For instance, photo-decarboxylation reactions are hypothesized to consume 0.5 mol O_2 per mol CO_2.[19] The strong evidence that photo-decarboxylation reactions accounted for a significant fraction of the measured photo-mineralization of organic mat and permafrost DOM (see section 4.5.2) suggests that the O_2 consumption:CO_2 production was not equal to 1, and therefore our estimates for partial photo-oxidation were low. For instance, when assuming 1:1 O_2 consumption:CO_2 production stoichiometry, organic mat DOM was not susceptible to partial photo-oxidation. However, when accounting for the 37 ± 2% of CO_2 that was produced through photo-decarboxylation reactions in organic mat DOM, the estimated partial photo-oxidation increased from zero to 31 ± 16 μM-C. Similarly, when accounting for 89 ± 4% of CO_2 that was produced through photo-decarboxylation reactions in permafrost DOM, the amount of partially oxidized C increased from 40 ± 7 to 71 ± 6 μM-C. Thus, assuming 1 mol O_2 consumed per mol CO_2 produced is conservative, and the calculated production of partially photo-oxidized C is highly sensitive to photochemical pathways that require less than 1 mol O_2 per mol CO_2 produced (e.g., photo-decarboxylation).

Despite that few studies have characterized the composition of partially photo-oxidized compounds that remain in the DOM pool after sunlight exposure (Cory et al., 2010; Peterson 2012), assuming that 1 mol of O is consumed per mol oxidized C is likely conservative. Under conditions selective for the partial photo-oxidation of DOM by singlet O_2 ($^1O_2$), Cory et al. (2010) reported that partially oxidized formulas in the DOM pool exhibited an O/C range from 0.2 - 0.7, while Peterson (2012) reported a range that extended to higher O/C values (0.2 - 1.0).[52] These estimates highlight the need for further characterization of partially-oxidized DOM, but also indicate that assuming 1 mol of O is consumed per mol of oxidized C is O_2 demanding and thus conservative, as suggested by Andrews et al. (2000). For instance, if we assumed that the majority of partially oxidized DOM were carboxylic-rich alicyclic molecules with an average O/C of ~ 0.4,[34] and the contribution of photo-decarboxylation reactions to CO_2 production was negligible (i.e., one mol O_2 consumed per mol CO_2 produced), the estimated production of partially oxidized C in permafrost DOM would increase 2.5-fold from 40 ± 7 to 101 ± 17 μM-C. Thus, assuming 1 mol of O is consumed per mol of oxidized C is likely conservative, and the calculated production of partially photo-oxidized C is highly sensitive to the stoichiometry of partially oxidized molecules that remain in the DOM pool after sunlight exposure.

Appendix 4.2: Quantitative estimates for changes to water column carbon processing rates as inputs of permafrost DOM increase with permafrost thaw

If inputs of permafrost DOM to Imnavait Creek increased from 1 to 50%, C processing rates would increase by 5 - 8 mmol-C m^{-2} d^{-1} or 72 - 95%, with the majority of this increase attributed to partial photo-oxidation (71 - 81%; Fig. 4.A.1). As discussed in section 4.5.3, and demonstrated by comparing the trajectory of solid blue and dashed blue lines in Fig. A.4.1, the rates of partial photo-oxidation were highly sensitive to the assumed stoichiometry of mol O_2 required per CO_2 produced. When inputs of permafrost and organic mat DOM are equal, the rate of partial photo-oxidation is two-fold higher when assuming that 0.5 mol O_2 is required per mol CO_2 produced via photo-decarboxylation reactions (dashed blue line) compared to the rate of partial photo-oxidation where 1.0 mol O_2 is consumed per mol CO_2 produced (solid blue line). Summed mineralization rates (i.e, photo-mineralization + bacterial respiration) increased by 1.6 mmol-C m^{-2} d^{-1} or 21%, although this is likely a minimum given that exposure of permafrost DOM to sunlight is expected to stimulate bacterial respiration,[13] and the response of bacteria to sunlight-exposed DOM was not considered. Despite that summed mineralization rates increased by 21%, the relative importance of mineralization pathways that release CO_2 to the atmosphere vs. partial photo-oxidation to compounds that remain in the DOM pool decreased by 29 - 32%. Thus, increased permafrost thaw will likely increase C processing rates in surface waters that drain permafrost soils and shift the dominant C processing pathway from complete to partial photo-oxidation, thereby increasing the export of presumably recalcitrant DOM to the Arctic Ocean.

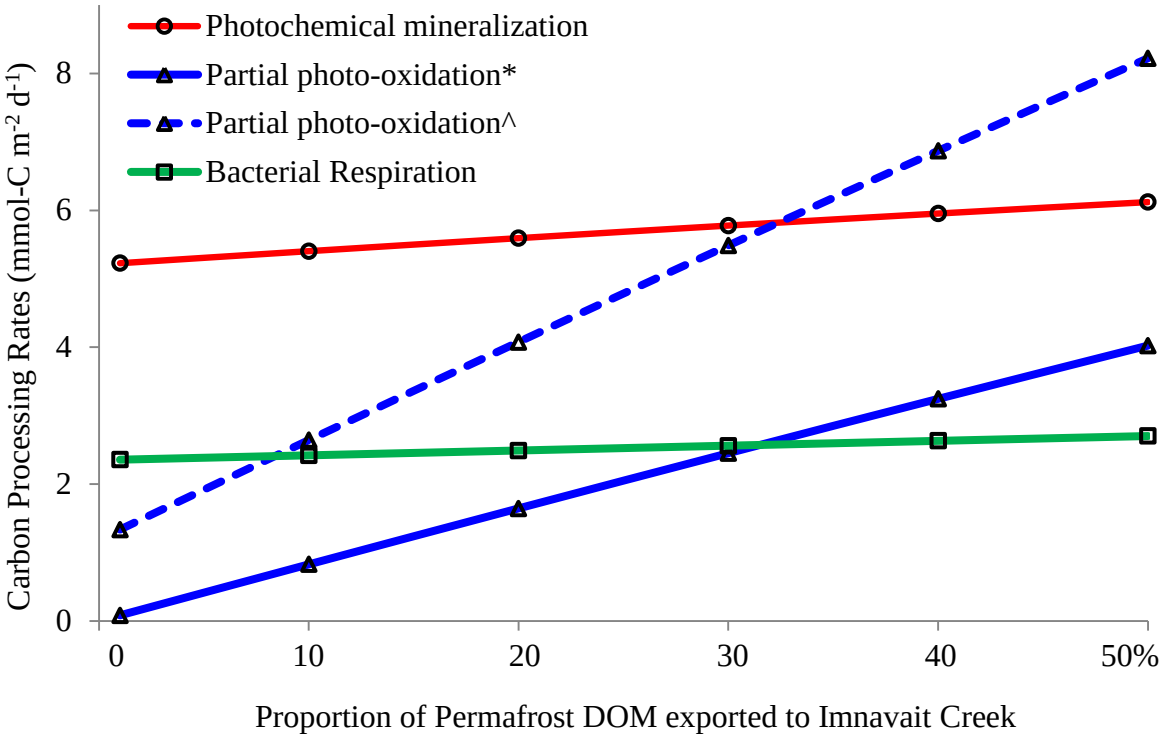

Figure 4.A.1. Water column C processing rates as the proportion of permafrost DOM exported to Imnavait Creek increases from 1 to 50%. *assuming 1 mol O_2 per mol CO_2 produced (Andrews et al., 2000; solid blue); ^assuming 0.5 mol O_2 per mol CO_2 (Miles and Brezonic 1981; dashed blue).

Chapter 5[6]

Apparent quantum yield spectra for the photo-mineralization of dissolved organic matter

5.1. Introduction:

Globally, about 50% of organic carbon (C) that is transferred from land to surface waters is mineralized to CO_2.[1,2] In arctic lakes and rivers, conversion of dissolved organic matter (DOM) to CO_2 by sunlight accounts for one-third of the total CO_2 released to the atmosphere.[3,4] Despite that the yield and thus the rate of this sunlight-driven reaction is dependent on the wavelength of light at Earth's surface, few studies have measured the spectrum of this yield in inland waters,[5,6] and no study has measured the spectrum of this yield in arctic surface waters. Thus, the objective of this study was to quantify the apparent quantum yield spectrum for the conversion of DOM to CO_2 by sunlight. The apparent quantum yield spectra of eight inland waters comprising a wide range of initial chemical compositions were measured using the wavelength band subtraction method.[7]

[6] The results presented here are a contribution to an inter-lab comparison study for measures of AQY spectrum in inland waters. The comparison study is being coordinated by Birgit Koehler at Uppsala University. Other contributors to this study include: Bill Miller and Leanne Powers (University of Georgia), Anssi Vähätalo (University of Helsinki), Lars Tranvik and Karolina Einarsdottir (Uppsala University), Leena Siitonen and Koistinen Mervi (University of Jyväskylä), and Rose Cory (University of Michigan).

5.2. Methods:

5.2.1 General approach

Rates of the photo-mineralization of dissolved organic matter (DOM) are the product of three spectra: the apparent quantum yield spectrum of photo-mineralization (Φ_λ; mol CO_2 per mol photons absorbed), the spectrum of photon flux absorbed by the water column ($Q_{a\lambda}$; mol photons absorbed m^{-2} d^{-1}), and the spectrum of the ratio of absorption by chromophoric DOM (CDOM) to total light absorption by the water column (i.e., $a_{CDOM\lambda} / a_{tot\lambda}$):

$$Photo-mineralization\ (mol\ CO_2\ m^{-2}\ s^{-1}) = \int_{\lambda_{min}}^{\lambda_{max}} \phi_\lambda\ Q_{a\lambda}\ \frac{aCDOM_\lambda}{atot_\lambda}\ d\lambda \qquad (1)$$

where λ_{min} and λ_{max} are the minimum and maximum wavelengths of light contributing to the photo-degradation of DOC (e.g., 280 and 700 nm, respectively).

By measuring the rate of photo-mineralization, the rate of light absorption by the water column, and the contribution of light absorption by CDOM to total light absorption by the water column, we can solve for Φ_λ. The goal of this study is to determine the wavelength dependence of Φ_λ, thus we implemented the previously described wavelength band subtraction method, which allowed for the measurement of Φ_λ at discrete wavebands.[7]

5.2.2 DOM sources

The Φ_λ spectra of eight DOM sources were measured in this study. Two waters were collected from the Alaskan Arctic (Imnavait Creek and Toolik Lake), while six waters were collected from Swedish Lakes (3 - 8). Shortly after collection (September - October 2014), the

waters were GF/F filtered and sent to the University of Michigan, where they were stored in the dark at 4˚C until the photochemical experiments were conducted (January - February 2015).

5.2.3 Quantifying the rate of photochemical mineralization

The rate of photochemical mineralization (left side of Eq. 1; mol CO_2 m^{-2} s^{-1}) was quantified as the light - dark difference in DIC concentration divided by the incubation time, following previously described protocols.[4,8] Briefly, DOM was pre-equilibrated with air in the dark at room temperature (20 ± 1°C) and transferred to DI rinsed air-tight quartz tubes (15 mm OD; 12 mm ID; 110 mm L; Robson Scientific). Equilibrated samples were analyzed for pH prior to irradiation (Table 5.1). Duplicate vials were placed in a custom built Delrin® housing underneath longpass filters (295, 320, 345, 370, 295, 420 nm) as shown in Fig. 5.1. Duplicate housing units were required to accommodate the number of filter treatments. The units were placed into a custom built circulating water bath housed in the exposure chamber of a solar simulator (Suntest XLS+; Atlas Materials Inc.). Depending on the rate of photochemical CO_2 production, the samples were exposed to simulated sunlight for 5 - 24 hours. Dark controls were wrapped in aluminum foil. Temperature of the samples measured at the end of the incubation ranged from 16 - 23 °C (Table 5.1). Following the experiment, the light exposed and dark control treatments were equilibrated to room temperature in the dark and analyzed for their dissolved inorganic carbon (DIC) concentration using a DIC analyzer (Apollo SciTech). For one DOM source (Toolik Lake), the production of CO_2 at wavelengths > 345 nm was below the limit of detection. In this case, photochemical O_2 consumption was measured rather than CO_2 production, assuming 1 mol O_2 consumed per mol CO_2 produced.[9]

5.2.4 Quantifying light absorption by the water column and CDOM

Light absorption by the water column was measured following equation 2:

$$Q_{a\lambda}\ (mol\ photons\ m^{-2}\ d^{-1}) = Q_{o\lambda}(1 - e^{-K_{d\lambda}z}) \quad (2)$$

where $Q_{o\lambda}$ is the photon flux at the surface (the vials were not completely submerged in water, thus reflection was not considered), $K_{d\lambda}$ is the attenuation coefficient of light in the photo-vial, and z is the pathlength of the vial (12 mm). The photon flux of the simulated sunlight was measured using a spectral radiometer at 305, 313, 320, 340, 380, 395, and 412 nm and linearly interpolated to 1-nm increments (Fig. 5.2; Biospherical Instruments, Inc.). Irradiance underneath each longpass filter was calculated by multiplying the photon flux of the simulated sunlight by the measured transmission of each filter (Fig. 5.2; DRA-Cary 300 Agilent Technologies). Interior surfaces of the solar simulator chamber were covered with black matted aluminum foil to minimize light reflectivity. We tested for the spatial variability of the simulated light source by measuring photochemical O_2 consumption of Suwannee River fulvic acid in eight different positions within the experimental chamber. There was no detectable difference in photochemical O_2 consumption between any of the measured positions, suggesting that the spatial variability of the simulated light source was likely not a significant source of error (Fig. 5.3).

Because light absorbing and scattering particles were filtered from all waters prior to irradiation, the attenuation coefficient of light in the vial was assumed to be equal to light absorption by CDOM ($a_{CDOM\lambda}$). Accordingly, the ratio of light absorption by CDOM to the total absorption by the water column (i.e., $a_{CDOM\lambda}$/ $a_{tot\lambda}$) was assumed to be equal to 1. UV-visible absorption spectra were collected using a 1-cm pathlength UV-visible spectrophotometer

(Aqualog Horiba Scientific). Naperian absorption coefficients were calculated by multiplying absorbance (A) by 2.303 and dividing by the pathlength (m) of the quartz cuvette.

5.2.5 Calculation of apparent quantum yield (Φ_λ) for the photo-mineralization of DOM

The Φ_λ for the photo-mineralization of DOM was calculated at discrete wavelengths by dividing the difference in the rate of CO_2 production under adjacent longpass filters by the difference in the rate of light absorption by CDOM under adjacent longpass filters. For example, equation 3 describes the calculation for Φ_λ at 333 nm (Φ_{333}):

$$\phi_{333} = \frac{\frac{d[CO_2]}{d[t]}(320\ nm\ filter) - \frac{d[CO_2]}{d[t]}(345\ nm\ filter)}{Q_{a\lambda}\ aCDOM_\lambda\ (320\ nm\ filter) - Q_{a\lambda}\ aCDOM_\lambda\ (345\ nm\ filter)} \quad (3)$$

The calculated Φ_λ is plotted at 333 nm, half-way between the "cut-off" filter wavelengths where the measured light transmission of each filter is equal to 0.5 (i.e., (323 nm + 343 nm) / 2 = 333 nm). This method was conducted for all adjacent longpass filter treatments to calculate Φ_λ at five discrete wavebands (311, 333, 359, 388, 410 nm).

5.2.6 Optical proxies for DOM chemical composition

Due to the analytical difficulty associated with measuring Φ_λ for the photo-mineralization of DOM in sunlit surface waters, there is growing interest in developing proxies for Φ_λ. Given that the composition of DOM is a hypothesized control for the magnitude of Φ_λ,[7,10] we measured several optical proxies for the chemical composition of chromophoric and fluorescent DOM (CDOM and FDOM, respectively) and developed relationships between these proxies and Φ_λ. Dominant peaks in the corrected EEMs were identified following Coble (1996): Peak A (λ_{ex} = 250 nm; λ_{em} = 380 - 460 nm), Peak C (λ_{ex} = 350; λ_{em} = 420 - 480 nm), and Peak T (λ_{ex} = 275

nm; λ_{em} = 340 nm). The fluorescence index (FI; McKnight et al., 2001) was calculated as the ratio of emission intensity at 470 nm to emission intensity at 520 nm at an excitation wavelength of 370 nm.

5.3. Results:

5.3.1 Reproducibility of waveband subtraction method

The reproducibility of the waveband subtraction method was high. Average Φ_λ of experimental duplicates of Suwannee River fulvic acid (8 mg-C L^{-1}) agreed strongly across different exposure and analysis dates (R^2 = 0.99; Fig. 5.4). The average coefficient of variation of Φ_λ between experimental duplicates was 7 ± 4% (N = 5). Within the same set of experiments, the average coefficient of variation of Φ_λ between instrumental duplicates was higher than experimental duplicates (39 ± 7%; N =10).

5.3.2 Trends in Φ_λ and light absorption and emission between DOM sources

All DOM sources exhibited decreasing Φ_λ with increasing wavelength (Fig. 5.5, Table 1). Imnavait Creek DOM exhibited the highest Φ_λ across all measured wavelengths, ranging from 0.72 mmol CO_2 mol $photons^{-1}$ at 311 nm to 0.29 at 410 nm. Swedish Lakes 4 and 5 exhibited the lowest Φ_λ at 311 nm (~0.2 mmol CO_2 mol $photons^{-1}$), while the Φ_λ of Swedish Lake 3 at 410 nm was an order of magnitude lower (~0.02 mmol CO_2 mol $photons^{-1}$). The range in Φ_λ narrowed moving from lower to higher wavelengths. For instance, the range in Φ_λ decreased from 0.7 mmol CO_2 mol $photons^{-1}$ at 311 nm to 0.3 mmol CO_2 mol $photons^{-1}$ at 410 nm.

Absorption spectra of all DOM sources decreased exponentially with increasing wavelength (Fig. 5.6). Initial absorption by DOM at 305 nm varied by a factor of nine. Swedish

Lake 6 DOM exhibited an absorption coefficient at 305 nm of 133 m^{-1}, while Toolik Lake DOM exhibited a coefficient of 14 m^{-1}. There was no significant correlation between initial light absorption or fluorescence index and Φ_λ (Fig. 5.7). However, significant relationships were observed between fluorescent peak ratios (A/T and C/T) and Φ_λ (Fig. 5.7).

5.4. Discussion:

5.4.1 Comparison of measured Φ_λ spectra to previously reported Φ_λ spectra

The trends and magnitude of Φ_λ spectra for the photo-mineralization of DOM reported here were similar to the few previously reported spectra for inland waters. All DOM sources exhibited decreasing Φ_λ with increasing wavelength, which is consistent with boreal lake waters.[5,6] The magnitude of Φ_λ was also similar to those previously reported. For instance, Φ_λ at 333 nm reported here ranged from 0.1 to 0.7 mmol CO_2 mol $photons^{-1}$, while Φ_λ at 333 nm reported by Koehler et al. (2014) ranged from ~ 0.4 - 1.0 mmol CO_2 mol $photons^{-1}$.

Differences in Φ_λ between modelled spectra (i.e., linear vs. exponential) were significantly less than differences in Φ_λ between DOM sources, indicating that Φ_λ was most sensitive to the initial DOM chemistry. The "best-fit" spectra varied between DOM source, where "best-fit" was quantified by higher R^2 values between a two component exponential decay model and a linear regression model. Five of the eight DOM sources were "best-fit" with an exponential decay model, while the other three DOM sources had higher R^2 values when fit with a linear regression model (Table 5.1). Both exponential and linear models have previously been fit to Φ_λ spectra for DOM photo-mineralization,[7] with the authors concluding that fitting Φ_λ spectra with a linear model did not result in higher R^2 values than an exponential decay model. While our data supported the conclusion of Johannessen and Miller (2001), our data also

indicated that differences in Φ_λ between modelled spectra were significantly less than differences in Φ_λ between DOM sources. For instance, at 320 nm (the approximate wavelength of peak water column photo-mineralization rates)[4,5] the linear and exponential modelled Φ_λ agreed favorably ($R^2 = 0.94$; Fig. 5.8). The average difference between Φ_λ modelled linearly vs. exponentially was 0.03 ± 0.01 mmol CO_2 mol photons^{-1}. In comparison, the range in Φ_λ at 320 nm between DOM sources was 0.49 mmol CO_2 mol photons^{-1} (Fig.5.8). Thus, differences between modelled Φ_λ values were significantly smaller than differences between DOM sources, indicating that Φ_λ was most sensitive to the initial DOM chemical composition.

5.4.2 Aromatic C content vs. light exposure history as an important control for the susceptibility of DOM to photo-mineralization

The insignificant relationships between initial light absorption (CDOM) or fluorescence index (FI) and Φ_λ was not consistent with the hypothesis that higher aromatic C content results in higher lability of DOM to photo-mineralization.[13] Light absorption at 305 nm (a_{305}) is positively correlated to aromatic C content, while FI is inversely correlated to aromatic C content. Thus, if aromatic C content were an important control for the lability of DOM photo-mineralization, we would expect Φ_λ to be positively and negatively correlated to a_{305} and FI, respectively. However, no significant relationship was observed between a_{305} or FI and Φ_λ, suggesting that the amount of aromatic C alone was not a strong proxy for the lability of DOM to photo-mineralization (Fig. 5.7). Consistent with this result, the initial aromatic C content of DOM drained from deeper permafrost soil layers was significantly less than aromatic C in DOM drained from shallow horizons (see Chapter 3), and both sources exhibited similar susceptibility to photo-mineralization (see Chapter 4).

The significant relationship observed between FDOM peak ratios and Φ_λ suggest that the composition of aromatics within the DOM pool, rather than the absolute amount of aromatic C, may be a control on the susceptibility of DOM to photo-mineralization. The ratio of peaks A/T and C/T were strongly correlated to Φ_λ (Fig. 5.7), indicating that molecules comprising peaks A and C were more susceptible to photo-mineralization compared to molecules comprising peak T. In boreal lakes, peak A was comprised of condensed aromatics,[14] which previously have been reported to be susceptible to photo-mineralization.[8,15] Peak C was enriched in oxidized plant-derived aromatics,[14] which could be susceptible to photo-decarboxylation reactions (Chapter 4). Despite the strong relationships between FDOM peak ratios and Φ_λ, the interpretation of these relationships should be cautious. While the advantages of using FDOM peak ratio as a proxy for Φ_λ are clear, more data are needed with increased spatial and temporal diversity in DOM chemistry to vet these relationships.

The findings reported here provide additional support for the conceptual model proposed by Cory et al. (2014), which suggested that light exposure history strongly controls the susceptibility of DOM to photo-mineralization. Imnavait Creek is a headwater stream, and its DOM has experienced little light exposure prior to its experimental irradiation, and its susceptibility to photo-mineralization was higher than all other DOM sources (Fig. 5.5; Table 5.1). In contrast, Toolik Lake is a 1.5 km^2 tundra lake with a residence time > 1 year, and Toolik Lake DOM had the lowest Φ_λ at 333 nm, nearly an order of magnitude less than Imnavait Creek DOM. Consistently, Imnavait Creek had the highest peak A/T and C/T ratios, while Toolik Lake had the lowest peak A/T and C/T ratios, indicating that aromatic structures with increased susceptibility to photo-mineralization become depleted with increased residence time in sunlit surface waters. Thus, it appears that light exposure history and the chemical composition of

aromatics within the DOM pool may govern the susceptibility of a wide range of DOM sources collected from arctic and sub-arctic surface waters.

5.5 Acknowledgements:

Bill Miller provided invaluable advice that improved our overall experimental design. Thanks to Katie Harrold for help with the DIC measurements and for building the water bath. Thanks to Noah Attal and Grace Hilbert for help with the optical measurements. DJ and Glenn at the UNC ESE Design Center built the Delrin housing. Roy Wentz at the UM glass shop was instrumental in helping to design the quartz tubes. Rackham Graduate School provided funding to CPW to purchase materials used to conduct the waveband subtraction method.

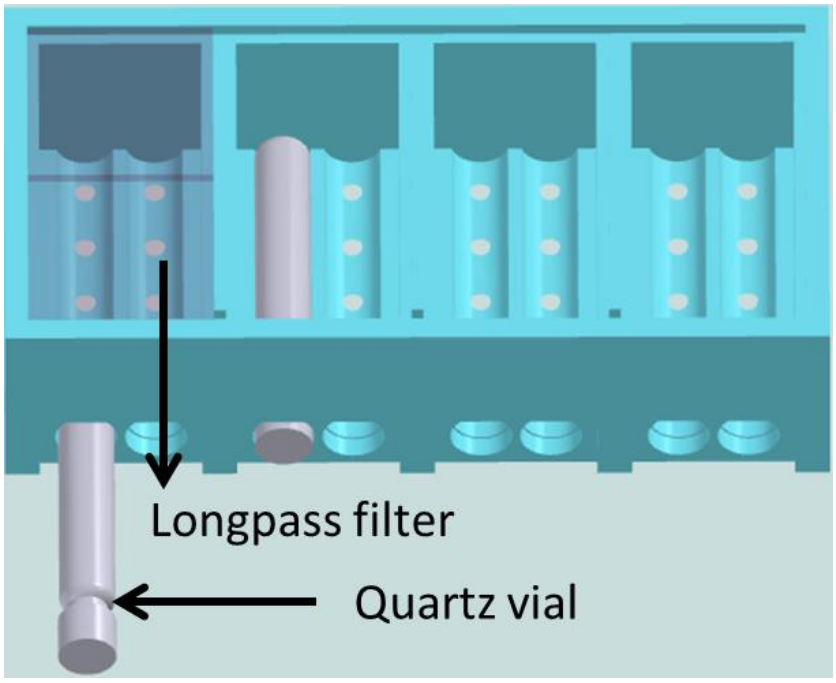

Figure 5.1: Custom built Delrin® housing used to conduct waveband subtraction method. Air-tight quartz tubes filled with DOM were placed underneath longpass filters (295, 320, 345, 370, 295, 420 nm), and photochemical CO_2 production was measured in all treatments.

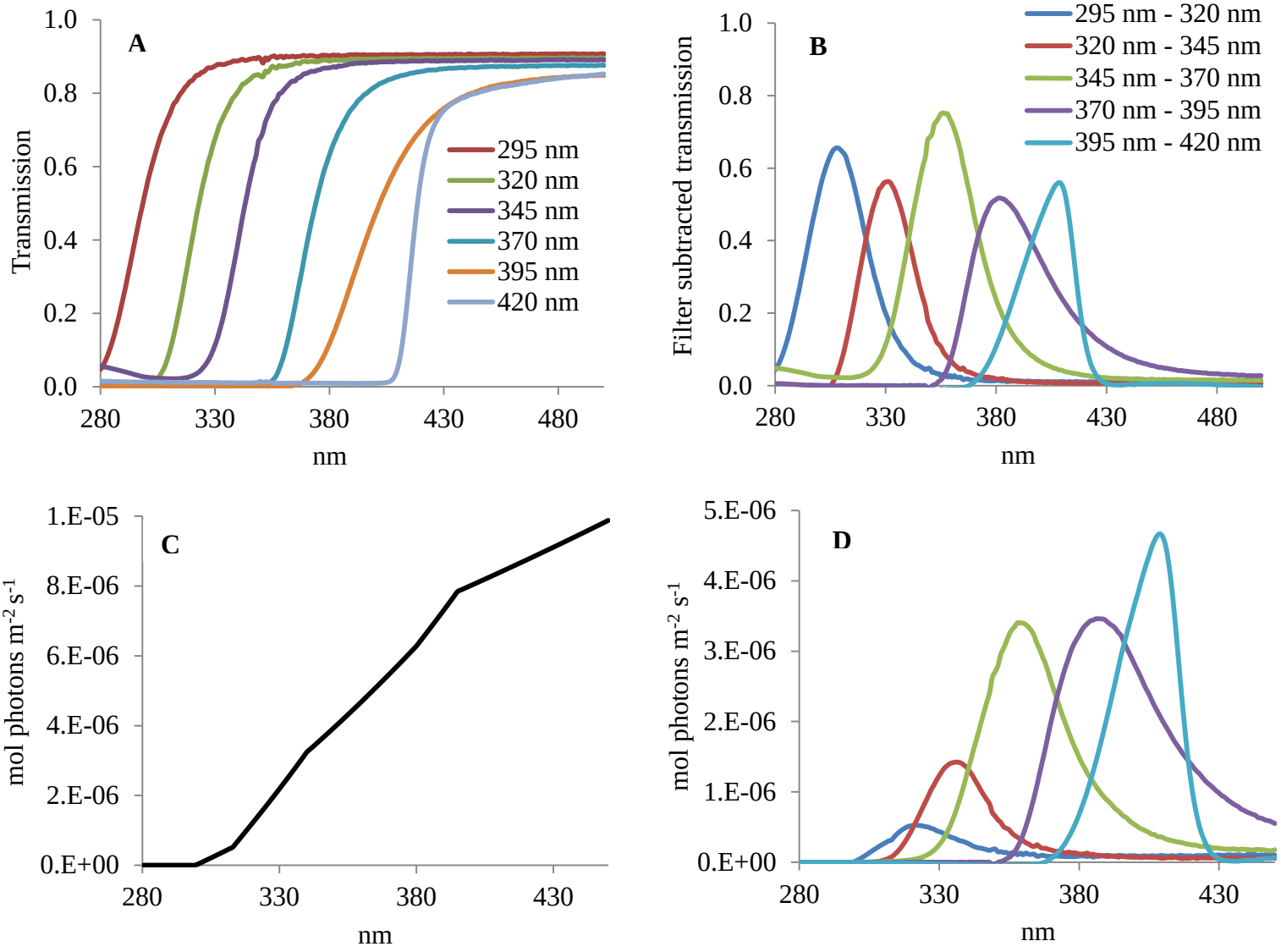

Figure 5.2: A: Transmission of longpass filters measured using a diffuse reflectance accessory equipped to a spectrophotometer. **B**: Filter subtracted transmission calculated by subtracting transmission of adjacent longpass filters reported in **A**. **C**: Photon flux of simulated sunlight measured using a spectral radiometer. **D**: Photon flux of filter subtracted sunlight spectra calculated by multiplying **B** and **C**.

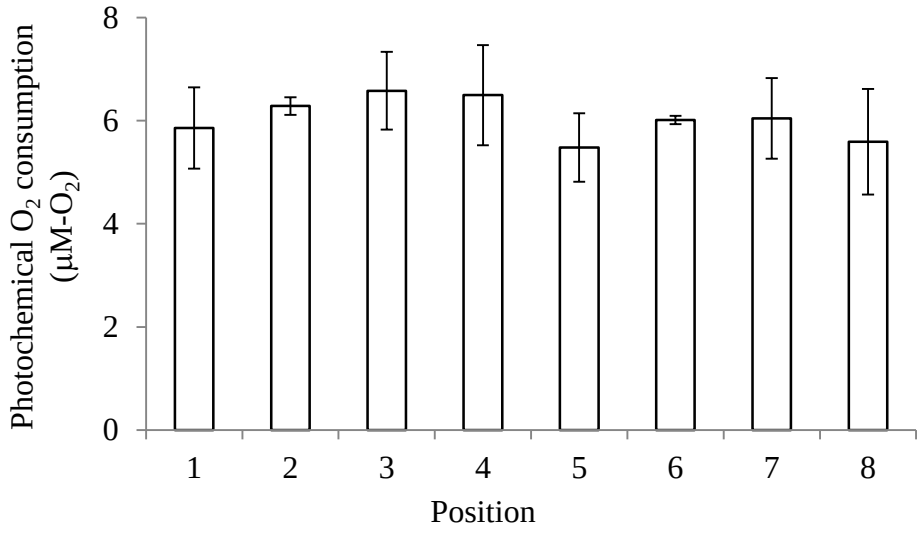

Figure 5.3: Photochemical O_2 consumption (μM-O_2) at eight different positions in the Suntest experimental chamber.

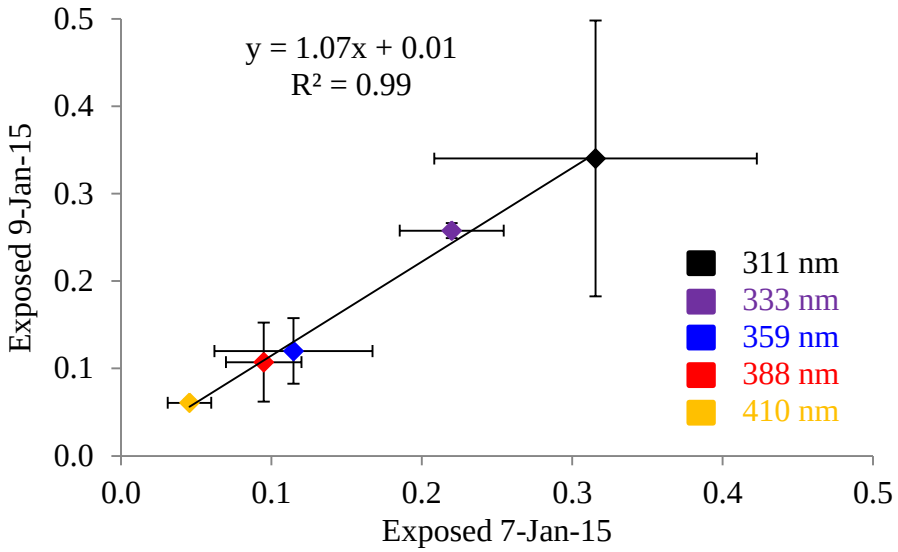

Figure 5.4: Average Φ_λ of experimental duplicates of Suwannee River fulvic acid (8 mg-C L^{-1}) across different exposure and analysis dates (7 and 9-January-2015).

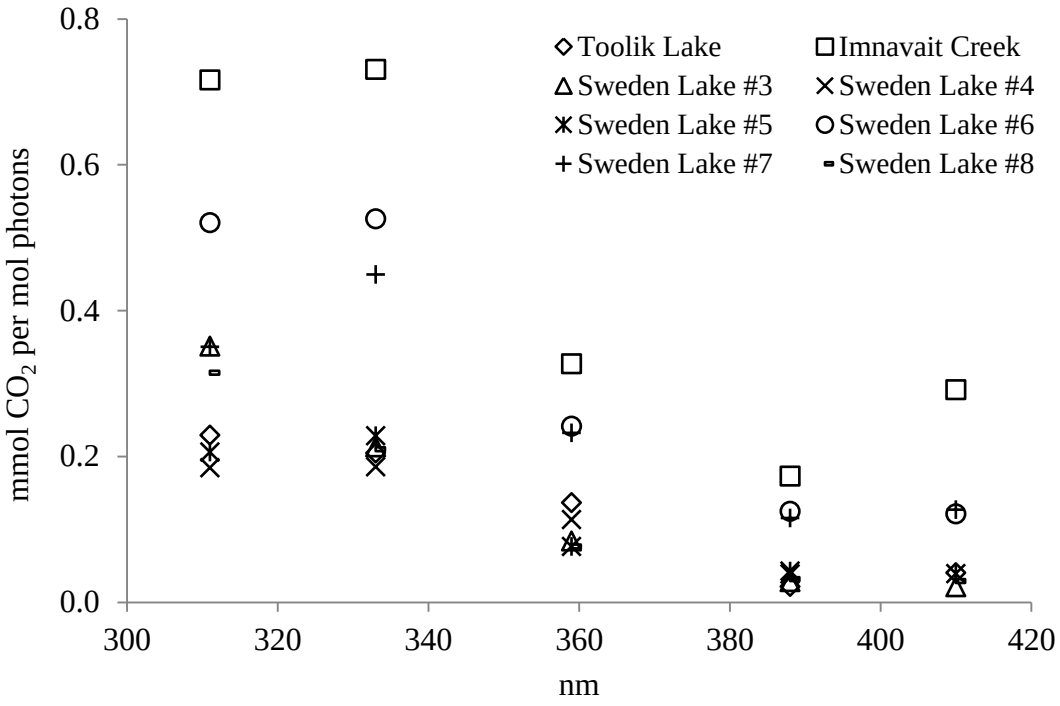

Figure 5.5: Average Φ_λ spectra for all DOM sources.

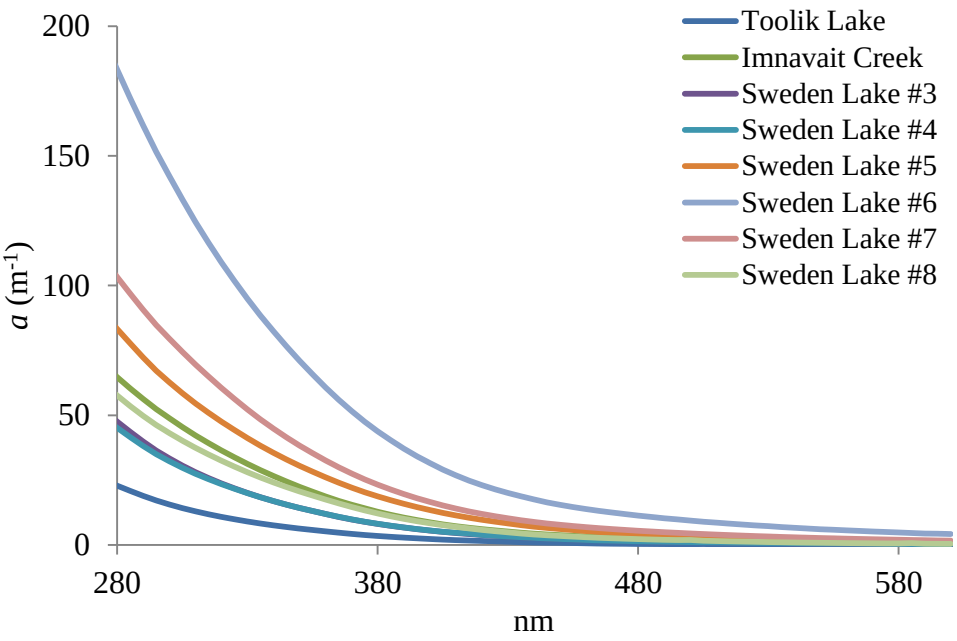

Figure 5.6: Absorption spectra for all DOM sources.

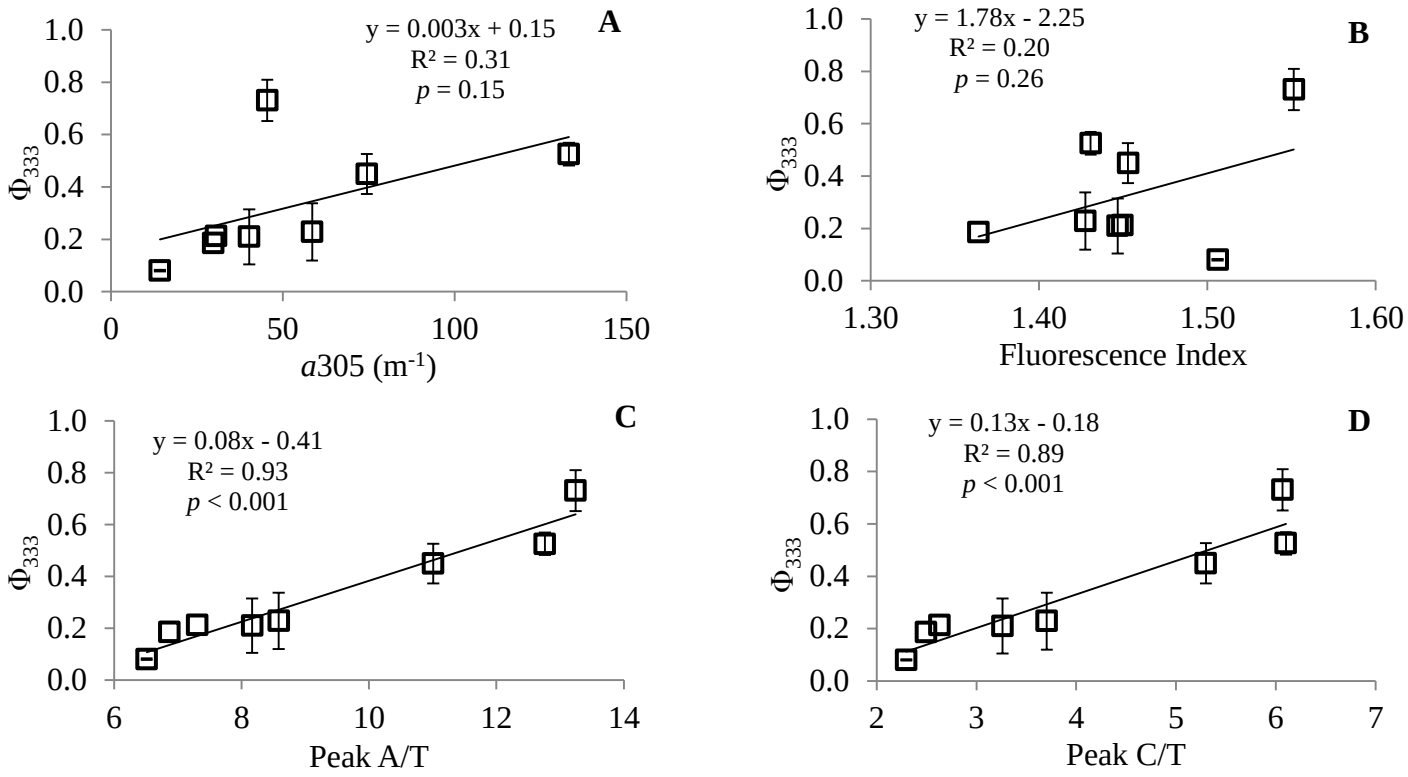

Figure 5.7: Correlations between (**A**) light absorption by CDOM at 305 nm, (**B**) fluorescence index, (**C**) the ratio of FDOM peak A to T, and (**D**) the ratio of FDOM peak C to T, with the apparent quantum yield for photo-mineralization at 333 nm (Φ_{333}; mmol CO_2 per mol photons absorbed at 333 nm).

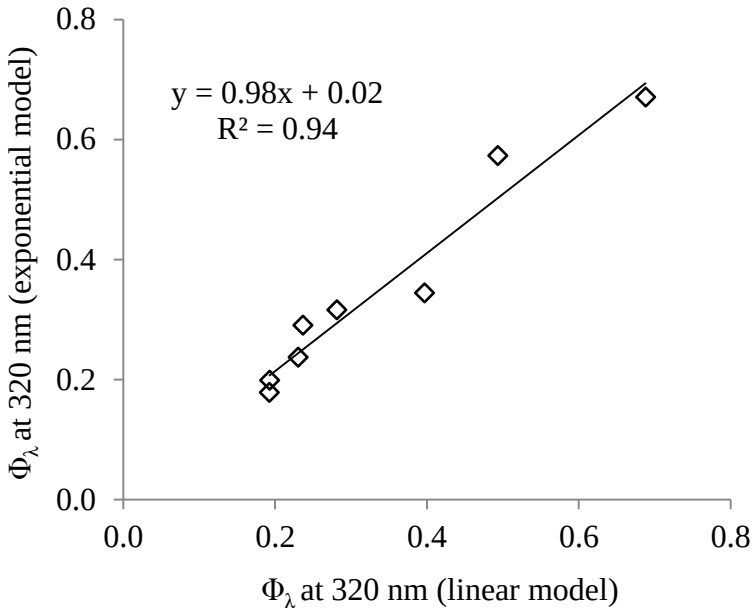

Figure 5.8: Φ_λ for each DOM source at 320 nm calculated using a linear regression model (x-axis) and an exponential decay model (y-axis).

Table 5.1: Summary of light exposure conditions, Φ_λ, and R^2 values for linear and exponential modelled spectrum of each DOM source.

				Avg. Φ_λ (mmol CO_2 per mol photons)					Linear	Exponential
DOM Source	pH	˚C	Time (hrs)	311 nm	333 nm	359 nm	388 nm	410 nm	R^2	R^2
Toolik Lake PM[a]	7.89	21	24	0.22 ± 0.02	0.08 ± 0.002	-	-	-	-	-
Toolik Lake PO	7.89	23	24	0.23 ± 0.05	0.20 ± 0.04	0.14 ± 0.01	0.02 ± 0.008	0.04 ± 0.001	0.92	0.78
Imnavait Creek	6.88	20	6	0.72 ± 0.39	0.73 ± 0.08	0.33 ± 0.17	0.17 ± 0.07	0.29 ± 0.04	0.77	0.71
Sweden Lake 3	7.55	-	24	0.35[b]	0.21[b]	0.08 ± 0.04	0.03 ± 0.001	0.02 ± 0.01	0.89	0.99
Sweden Lake 4	7.48	22	24	0.18 ± 0.09	0.19[b]	0.11[b]	0.04 ± 0.004	-	0.92	0.86
Sweden Lake 5	7.53	18	6	0.21 ± 0.10	0.23 ± 0.11	0.08 ± 0.04	0.04 ± 0.004	0.04 ± 0.01	0.82	0.90
Sweden Lake 6	6.02	17	5	0.52 ± 0.27	0.53 ± 0.04	0.24 ± 0.11	0.12 ± 0.02	0.12 ± 0.03	0.89	0.93
Sweden Lake 7	6.19	16	6	0.35 ± 0.22	0.45 ± 0.1	0.23 ± 0.10	0.12 ± 0.04	0.13 ± 0.02	0.76	0.83
Sweden Lake 8	6.12	19	24	0.31[c]	0.21 ± 0.10	0.08 ± 0.005	0.03 ± 0.01	0.03 ± 0.001	0.89	0.96

[a] Photo-mineralization (PM) in longpass filters > 345 nm was below the LOD of CO_2, so photochemical O_2 consumption (PO) was measured instead. [b] The seal of one replicate vial was compromised during light exposure. [c] One replicate exhibited similar CO_2 production in the 295 and 320 nm filter treatment and was not included in the calculation.

References:

1. J. J. Cole, Y. T. Prairie, N. F. Caraco, W. H. McDowell, L. J. Tranvik, R. G. Striegl, C. M. Duarte, P. Kortelainen, J. A. Downing, J. J. Middelburg, and J. Melack, *Ecosystems*, 2007, **10**, 171–184.

2. P. A. Raymond, J. Hartmann, R. Lauerwald, S. Sobek, C. McDonald, M. Hoover, D. Butman, R. Striegl, E. Mayorga, C. Humborg, P. Kortelainen, H. Dürr, M. Meybeck, P. Ciais, and P. Guth, *Nature*, 2013, **503**, 355–9.

3. G. W. Kling, G. W. Kipphut, and M. C. Miller, *Science*, 1991, **251**, 298–301.

4. R. M. Cory, C. P. Ward, B. C. Crump, and G. W. Kling, *Science*, 2014, **345**, 925–928.

5. A. V. Vähätalo and M. Salkinoja-Salonen, *Limnol. Oceanogr.*, 2000, **45**, 664–676.

6. B. Koehler, T. Landelius, G. A. Weyhenmeyer, N. Machida, and L. J. Tranvik, *Global Biogeochem. Cycles*, 2014, **28**, 696–711.

7. S. C. Johannessen and W. L. Miller, *Mar. Chem.*, 2001, **76**, 271–283.

8. C. P. Ward, R. L. Sleighter, P. G. Hatcher, and R. M. Cory, *Environ. Sci. Process. Impacts*, 2014, 721–731.

9. T. M. Kana, C. Darkangelo, and M. D. Hunt, *Anal. Chem.*, 1994, **66**, 4166–4170.

10. E. M. White, D. J. Kieber, J. Sherrard, W. L. Miller, and K. Mopper, *Mar. Chem.*, 2010, **118**, 11–21.

11. P. G. Coble, *Mar. Chem.*, 1996, **51**, 325–346.

12. D. M. McKnight, E. W. Boyer, P. K. Westerhoff, P. T. Doran, T. Kulbe, and D. T. Andersen, *Limnol. Oceanogr.*, 2001, **46**, 38–48.

13. A. Stubbins, R. G. M. Spencer, H. Chen, P. G. Hatcher, K. Mopper, P. J. Hernes, V. L. Mwamba, A. M. Mangangu, J. N. Wabakanghanzi, and J. Six, *Limnol. Oceanogr.*, 2010, **55**, 1467–1477.

14. A. Stubbins, J. F. Lapierre, M. Berggren, Y. T. Prairie, T. Dittmar, and P. A. del Giorgio, *Environ. Sci. Technol.*, 2014, **48**, 10598 – 10606.

15. A. Stubbins, J. Niggemann, and T. Dittmar, *Biogeosciences*, 2012, **9**, 1661–1670.

Chapter 6

Conclusion

6.1 Controls on the complete and partial photo-oxidation of DOM in arctic surface waters

This dissertation investigated how the chemical composition controlled for the photochemical processing of dissolved organic matter (DOM) in arctic surface waters. By investigating the complete and partial degradation of DOM to CO_2 and other products, I demonstrated that (i) aromatic C has a wide range of susceptibilities to complete photo-oxidation to CO_2 (i.e., photo-mineralization) and partial photo-oxidation, and (ii) photo-decarboxylation is likely an important photo-mineralization pathway. I also provided evidence in support of the hypothesis that phenolics may slow the oxidation of DOM by sunlight.

My results help to revise the conceptual model for how "photo-degradation" transforms DOM (Fig. 6.1, 6.2). The current view of DOM oxidation by sunlight is that condensed, low-oxygen containing DOM is oxidized to less condensed and more oxygen-rich; observed on a van Krevelen diagram as a shift from the lower left (low H/C, low O/C) to the upper right (high H/C, high O/C). This view, however, is not consistent with observations (Figs. 2.5, 4.5). Instead, results from photo-degradation of black carbon, organic mat, and permafrost DOM, as well as those in the literature for aquatic DOM,[2,3] show a preferential loss of highly oxygenated compounds, and the production of lower molecular weight aliphatic, less oxidized compounds (black arrow in Fig. 6.1). These shifts from high O/C to low O/C, high H/C were consistent with

photo-decarboxylation as an important pathway for the photo-mineralization of DOM to CO_2 (Ch. 4).

This evidence for photo-decarboxylation refines our conceptual model for the mineralization of DOM by sunlight. Instead of some subset of moieties within the DOM pool being progressively oxidized by sunlight to more oxidized compounds and then eventually produce CO_2 (dotted red arrow in Fig. 6.1), complete photo-oxidation to CO_2 may occur independently of partial photo-oxidation (solid red arrow in Fig. 6.1), and that there are likely different subsets of moieties involved in complete vs. partial photo-oxidation (Fig. 6.2). When viewed in van Krevelen space, this refined conceptual model of DOM photo-degradation suggests that DOM sources more susceptible to complete photo-oxidation to CO_2 will exhibit more pronounced shift to low O/C, high H/C space, while DOM sources more susceptible to partial photo-oxidation will exhibit a more pronounced shifts to high O/C, high H/C space (assuming all partially oxidized DOM were detectable using FT-ICR MS; Fig. 6.2).

The refined conceptual model for DOM photo-degradation presented here may also help explain why general expectations of DOM lability to degradation by sunlight don't match up well with predictions based on alignment with precursor biomolecules.[4–6] For example, the expectation was that aromatic C should be a good predictor of photochemical conversion of DOM to CO_2. Black carbon represents an 'end-member' fraction of DOM with respect to aromatic C content. The relatively higher susceptibility of black carbon to partial, and not complete photo-oxidation, demonstrated that aromatic C content alone doesn't control for the susceptibility of DOM to complete photo-mineralization to CO_2.[9,10] This is evident when examining Fig. 6.3, which shows that dBC exhibited one of the lowest susceptibilities to photo-mineralization to CO_2, despite that the aromatic C content of dBC was two to three-fold higher

than all other DOM sources. My results challenge the hypothesis that dBC is in important source of CO_2 produced when DOM is exposed to sunlight.[9] However, my results strengthen the hypothesis that although dBC is a trace fraction of aquatic DOM ($\leq$ 10%),[8] it may be an important, photo-reactive fraction of DOM, contributing to observations of loss of chromophoric DOM (i.e., photo-bleaching) and loss of aromatic C, the consumption of dissolved O_2, and the production of partially oxidized compounds that remain in the DOM pool and are exported to the ocean.

My study showing that dBC can be broken down to CO_2 and to aliphatic compounds no longer recognizable as "black carbon" is important for several reasons. First, there is widespread interest in quantifying the photochemical sink for dissolved black carbon because estimates of riverine transport of dBC to the ocean are much higher than required to account for the stock of dBC in the oceans,[7,8] suggesting that DBC delivered from rivers is either degraded during riverine transit or in the coastal ocean prior to reaching the open ocean. Because dBC is resistant to bacterial degradation, and comprised of light-absorbing aromatic C, the expectation is that sunlight breaks down dBC. Consistently, several studies have shown that dBC can be broken down by sunlight, suggesting that photo-degradation of dBC during riverine transport or in the coastal ocean may be an important sink for dBC. However, previous work has equated the "loss of dBC" with the conversion of black carbon to CO_2, suggesting that sunlight is the dominant sink for dBC.[9] My work suggests that a significant fraction of the dBC is not mineralized to CO_2, but rather partially photo-oxidized or degraded to aliphatic compounds that would likely not undergo further (direct) photo-degradation. Thus, the lability of these partially photo-oxidized compounds to further break down by bacteria or other processes must be investigated to refine our understanding of sunlight as sink for black carbon.

My results suggesting that carboxylic acids could account for a significant fraction of the CO_2 produced by the photochemical degradation of DOM (~ 40-90%) helps address the recent calls for a better understanding on what controls whether DOM ends up in the atmosphere as CO_2 or the oceans as DOM.[11,12] Carboxylic acids are a small but ubiquitous component of DOM in inland waters,[13] and further evidence that these moieties may be preferentially mineralized to CO_2 by sunlight may help put bounds on the degree of DOM conversion to CO_2 in inland waters. However, my results suggest it is the composition and arrangement, rather than the initial absolute content of carboxyl moieties that may explain the production of CO_2 when DOM is exposed to sunlight. For instance, permafrost DOM contained less initial carboxyl C than organic mat DOM, yet the loss of carboxyl C via photo-decarboxylation reactions accounted for a larger fraction of CO_2 produced by sunlight in permafrost relative to organic mat DOM (Ch. 4). Thus, the composition and structural arrangement of carboxyl C may help explain the variability of photo-mineralization apparent quantum yields between different DOM sources (i.e., variability on the y-axis in Fig. 6.3).

While carboxyl C may help explain the variability in DOM photo-mineralization yields, the composition and content of phenolics, a subset of the aromatic C, may help explain the variability on the x-axis of Fig. 6.3. A recent study proposed that phenolics within the DOM pool act as "anti-oxidants" by quenching the reactive radicals or oxidants produced by photochemical reactions of DOM (e.g., hydroxyl radical or singlet oxygen). In this study, the susceptibility of DOM to partial photo-oxidation was inversely related to the abundance of phenolics. For instance, dBC was relatively depleted in phenolics and exhibited the second highest ratio of O_2 consumption to CO_2 production, while organic mat DOM was relatively enriched in phenolics and exhibited one of the lowest ratio of O_2 consumption to CO_2 production (Fig. 2.5, 3.5, 6.3).

An additional outcome from this dissertation included a novel approach to simultaneously quantify the complete and partial photo-oxidation of DOM (Ch. 2 and 4). This is important because it allows us to quantitatively compare the two main classes of photo-degradation products while concurrently measuring changes to the chemical composition of DOM after exposure to sunlight. In turn, this allows us to determine the composition of compounds that may be completely photo-oxidized to CO_2 versus partially photo-oxidized to compounds that remain in the DOM pool. In contrast, previous work has measured changes to the chemical composition or the loss of DOM following photo-exposure, and then developed relationships between the fraction of DOM that was degraded by sunlight and the initial chemical composition of DOM.[2,3,10,14] It is likely that this previous approach has confounded the interpretation of the moieties within DOM that may contribute to photochemical production of CO_2.[2,3,10,14]

6.2 Future work: implications for the aquatic C cycling

The findings from this dissertation evoked a number of new questions that could substantially improve our understanding of the controls on carbon cycling in sunlit surface waters:

(i) What fraction of photo-mineralization and partial photo-oxidation in surface waters can be accounted for by dissolved black carbon within the DOM pool?

(ii) What are the dominant production pathways, the chemical composition, and the fate of partially photo-oxidized molecules that remain in the DOM pool?

(iii) What is the role of glacial history on the chemical composition of DOM draining permafrost soils, and how do these potential compositional differences influence the susceptibility of DOM to oxidation by sunlight and bacteria?

(iv) What is the dose dependence of photochemical reactions in surface waters?

Wildfire derived condensed aromatics comprise ~10% of DOC exported through rivers to oceans,[8] exhibit a high rate of light absorption,[15] and are highly susceptible to photo-oxidation,[9,15] raising the possibility that condensed aromatics account for a disproportionate amount of CO_2 and partially oxidized C production in sunlit surface waters. A logical approach towards filling this knowledge gap is to test for the wavelength dependence of the photo-oxidation of a wide range dissolved black carbon sources (e.g., varying vegetation, climate, and age). Once the range in apparent quantum yield spectra for dissolved black carbon photo-oxidation is constrained, these yields could be compared to yields for the photo-oxidation of DOM in a wide range of surface waters. If condensed aromatics were to contribute significantly to the photo-oxidation of DOM in surface waters, it's plausible to expect the overall processing of C in surface waters and relative importance of sunlight driven process to increase over the next 100 years as the sources of condensed aromatics to watersheds rapidly increase.[16]

Partial photo-oxidation is the most important sunlight driven degradation pathway in arctic surface waters, producing compounds that remain in the DOM pool.[17] While not quantified yet, it's likely that partial photo-oxidation is also a key pathway for DOM oxidation in temperature waters. However, our understating of the pathways that control for the partial photo-oxidation of DOM, the chemical composition, and the reactivity of partially oxidized C is poorly constrained. Singlet oxygen has been hypothesized as an important pathway for partial photo-oxidation,[5] but cannot account for all the calculated partial photo-oxidized C. DOM partially

oxidized by singlet oxygen exhibited characteristics similar to carboxylic-rich alicyclic molecules[5] and carbohydrates.[2,18] Given that these partially oxidized compounds are aliphatic, it is unlikely that these molecules are susceptible to direct photochemical pathways, but they could undergo further degradation by indirect photochemical pathways. The labilty of partially photo-oxidized DOM to heterotrophic bacteria varies widely,[5,19–21] potentially due to differences in the chemical composition of oxidized DOM and in the functional potential of the native bacterial community. For instance, DOM chemistry and bacterial community composition jointly control how and how fast DOM is degraded by bacteria in surface waters,[19,22] however we know too little about which metabolic pathways are accelerated or slowed when bacteria respire partially photo-oxidized DOM vs. DOM kept in the dark. Given the importance of partial photo-oxidation to aquatic C cycling, and the predicted increase in rates of partial photo-oxidation in arctic surface waters (Ch. 4), developing a framework for the controls on partial photo-oxidation, and determining the chemical composition and reactivity of partially oxidized C in surface water is critical.

We demonstrated significant differences in the chemical composition of DOM draining shallow and deep layers of soils within the Imnavait Creek watershed (Ch. 3). These differences in composition were consistent with the expected controls on DOM composition at depth in the soil column, including sorption to mineral phases, microbial degradation, and mobilization.[23] The Imnavait Creek watershed was glaciated about 610 - 132 k yr BP (i.e., Sagavanirktok glaciation) and is much older than surrounding land surfaces, including Itkillik-aged surfaces which experienced two glacial advances 115 - 12 k yr BP. Given that factors contributing to the controls on DOM composition at depth in the soil column (e.g., vegetation, soil acidity, and exchangeable iron and aluminum) are highly dependent on land surface ages on the North

Slope,[24] the chemical composition of DOM draining soils of different land surface ages is likely to vary significantly. Soil pH is lowest in older land surfaces due to differences in weathering and vegetation, which in turn increases exchangeable iron and aluminum concentrations and the importance of sorption processes in the soil column. Thus, older land surfaces likely exhibit the largest differences in DOM chemical composition at depth in the soil column, while DOM draining different depths of younger land surface likely exhibit relatively small differences in DOM chemistry. Because the chemical composition of DOM is an important control on its susceptibility to oxidation (Ch. 4), depth-dependent differences in the susceptibility to oxidation are likely large on older surfaces than younger surfaces. Testing these hypotheses will be important as the climate warms, thaw depth increases, and hydrologic flow paths deepen, exporting more permafrost DOM to surface waters, where its susceptibility to oxidized by sunlight and bacteria is unknown.

Finally, every experiment in this dissertation was conducted under the assumption that short-term incubations with sunlight minimize the "bottle effect," offering the best opportunity to capture or mimic the rapid dynamics of photo-oxidation in aquatic systems. However, the time-frame of our experiments was constrained analytically by our limit of detection for changes in dissolved CO_2 or O_2, raising the possibility that our estimates for the yields and rates of photo-oxidation are conservative (low). For example, when quantifying photochemical mineralization, we typically exposed DOM to natural sunlight for 12 - 48 hours in order to produce a detectable amount of dissolved CO_2. Given the strong evidence for chemical composition and light exposure history as a control on the yield of photo-mineralization, as discussed in Chapters 4 and 5, it's likely that a spectrum of compounds with a wide range of susceptibilities to photo-mineralization comprise the DOM pool. In this case, the most susceptible compounds could be

mineralized in a few hours, far quicker than the length of our incubation experiments, suggesting that our estimates for photo-mineralization yields are conservative. Consistently, yields for the photo-mineralization of temperate riverine and coastal DOM determined over a 48 hour sunlight exposure period were ~40% lower than those determined over a 6 - 12 hour exposure period.[25] Thus, the dose dependence of yields for DOM photo-oxidation should be estimated to further constrain the importance of sunlight driven reactions in arctic surface waters.

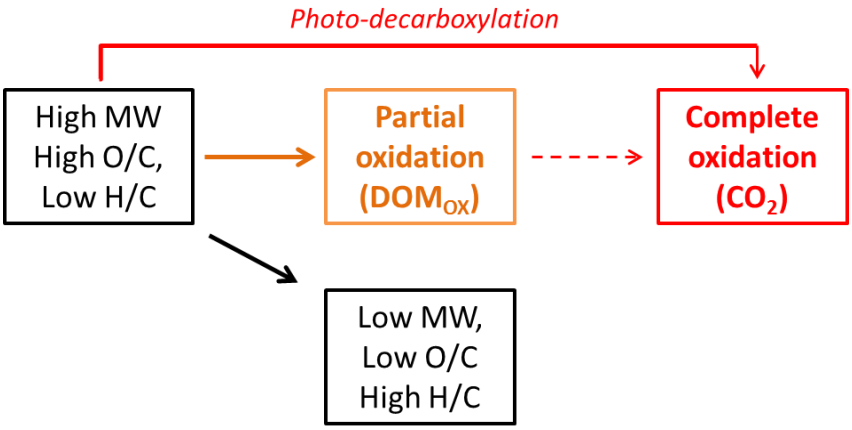

Figure 6.1 Revised conceptual framework for the oxidation of DOM by sunlight.

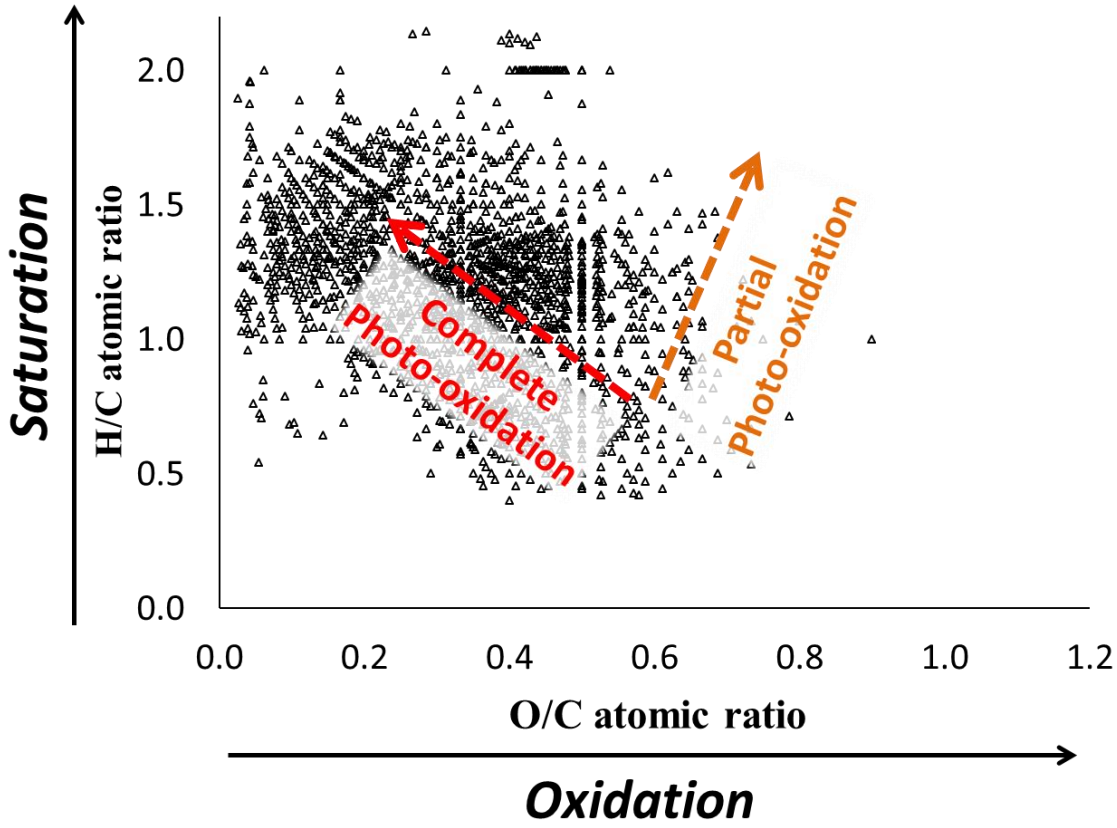

Figure 6.2 Revised model for how complete and partial photo-oxidation change the composition of DOM in van Krevelen space after sunlight exposure.

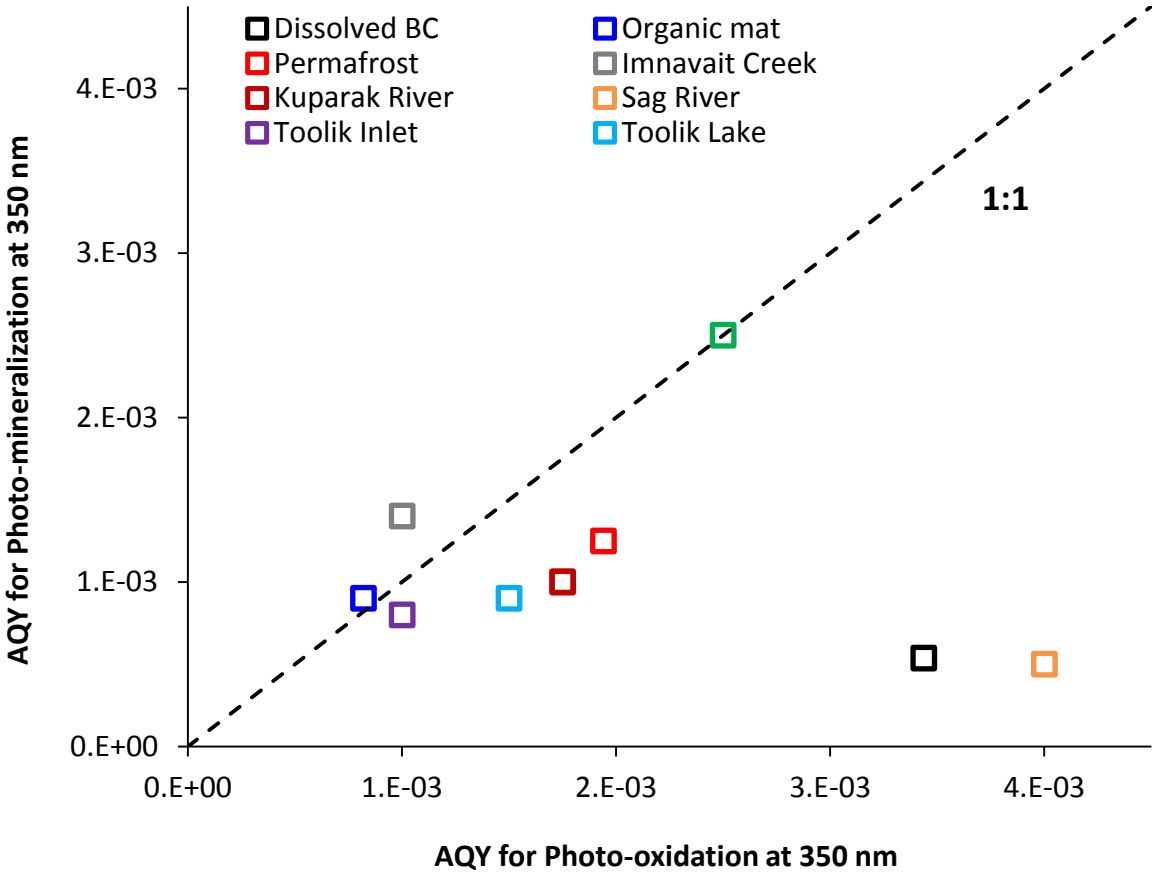

Figure 6.3 Apparent quantum yields for photochemical O_2 consumption (x-axis) and photochemical CO_2 production (y-axis) for multiple DOM sources from the Alaskan Arctic. Imnavait Creek, Kuparuk River, Sag River, Toolik Inlet, Toolik Lake, and Coastal Plain data are from Cory et al., (2014).

References

1. A. V. Vähätalo and R. G. Wetzel, *Limnol. Oceanogr.*, 2008, **53**, 1387–1392.

2. M. Gonsior, N. Hertkorn, M. H. Conte, W. J. Cooper, D. Bastviken, E. Druffel, and P. Schmitt-Kopplin, *Mar. Chem.*, 2014, **163**, 10–18.

3. A. Stubbins, R. G. M. Spencer, H. Chen, P. G. Hatcher, K. Mopper, P. J. Hernes, V. L. Mwamba, A. M. Mangangu, J. N. Wabakanghanzi, and J. Six, *Limnol. Oceanogr.*, 2010, **55**, 1467–1477.

4. R. L. Sleighter, R. M. Cory, L. A. Kaplan, H. A. N. Abdulla, and P. G. Hatcher, *J. Geophys. Res. Biogeosciences*, 2014, **119**, 1520–1537.

5. R. M. Cory, K. McNeill, J. P. Cotner, A. Amado, J. M. Purcell, and A. G. Marshall, *Environ. Sci. Technol.*, 2010, **44**, 3683–9.

6. R. M. Cory and L. A. Kaplan, *Limnol. Oceanogr.*, 2012, **57**, 1347–1360.

7. T. Dittmar and B. P. Koch, *Mar. Chem.*, 2006, **102**, 208–217.

8. R. Jaffé, Y. Ding, J. Niggemann, A. Vähätalo, A. Stubbins, R. G. M. Spencer, J. Campbell, and T. Dittmar, *Science*, 2013, **340**, 345–347.

9. A. Stubbins, J. Niggemann, and T. Dittmar, *Biogeosciences*, 2012, **9**, 1661–1670.

10. P. J. Mann, A. Davydova, N. Zimov, R. G. M. Spencer, S. Davydov, E. Bulygina, S. Zimov, and R. M. Holmes, *J. Geophys. Res.*, 2012, **117**, G01028.

11. J. E. Vonk and Ö. Gustafsson, *Nat. Geosci.*, 2013, **6**, 675–676.

12. P. A. Raymond, J. Hartmann, R. Lauerwald, S. Sobek, C. McDonald, M. Hoover, D. Butman, R. Striegl, E. Mayorga, C. Humborg, P. Kortelainen, H. Dürr, M. Meybeck, P. Ciais, and P. Guth, *Nature*, 2013, **503**, 355–9.

13. R. Jaffé, Y. Yamashita, N. Maie, W. T. Cooper, T. Dittmar, W. K. Dodds, J. B. Jones, T. Myoshi, J. R. Ortiz-Zayas, D. C. Podgorski, and A. Watanabe, *Geochim. Cosmochim. Acta*, 2012, **94**, 95–108.

14. M. Gonsior, B. M. Peake, W. T. Cooper, D. Podgorski, J. D'Andrilli, and W. J. Cooper, *Environ. Sci. Technol.*, 2009, **43**, 698–703.

15. C. P. Ward, R. L. Sleighter, P. G. Hatcher, and R. M. Cory, *Environ. Sci. Process. Impacts*, 2014, 721–731.

16. M. Moritz, M. Parisien, and E. Batllori, *Ecosphere*, 2012, **3**, 1–22.

17. R. M. Cory, C. P. Ward, B. C. Crump, and G. W. Kling, *Science*, 2014, **345**, 925–928.

18. B. M. Peterson, *Probing the Photochemistry of Humic Substances*, Dissertation Thesis. ETH Zurich, 2012.

19. K. E. Judd, B. C. Crump, and G. W. Kling, *Ecology*, 2006, **87**, 2068–79.

20. K. Mopper and W. Stahovec, *Mar. Chem.*, 1986, **19**, 305–321.

21. H. E. Reader and W. L. Miller, *Limnol. Oceanogr.*, 2014, **59**, 182–194.

22. B. Crump, G. Kling, M. Bahr, and J. Hobbie, *Appl. Environ. Microbiol.*, 2003, **69**, 2253–2268.

23. K. Kaiser and K. Kalbitz, *Soil Biol. Biochem.*, 2012, **52**, 29–32.

24. M. D. Walker, T. D. Hamilton, H. A. Maier, A. M. Corinne, and M. K. Raynolds, in *A Changing Arctic: Ecological Consequences for Tundra, Streams, and Lakes.*, eds. J. E. Hobbie and G. W. Kling, Oxford University Press, New York, 2014, vol. 89 (7), pp. 61 – 80.

25. L. C. Powers and W. L. Miller, *Mar. Chem.*, 2015, **171**, 21–35.